

Improving Spectral Efficiency Using Hybrid System Solutions

Von der Fakultät für Elektrotechnik und Informatik
der Gottfried Wilhelm Leibniz Universität Hannover
zur Erlangung des akademischen Grades
Doktor-Ingenieurin/Doktor-Ingenieur
(abgekürzt: Dr.-Ing.)
genehmigte Dissertation

von

M. Sc. Chung Le Thi
geboren am 10. October 1984
in Vietnam

2019

1. Referentin/Referent: Prof. Dr. Jürgen Peissig
 2. Referentin/Referent: Prof. Dr.-Ing. Anja Klein (TU Darmstadt)
- Tag der Promotion: 18 Februar 2019

ABSTRACT

As frequency bands become increasingly crowded, one of the major research challenges for future wireless communication networks is how to use the radio frequency bands more efficiently. In wireless communication networks, spectral efficiency can be improved either through frequency reuse technologies such as cognitive radio and multi-user techniques or by using technologies to increase the data rate. However, in this regard there is still room for further improvements, and thus, development of novel hybrid solution approaches to enhance spectral efficiency for future wireless communication networks is put into the focus of this dissertation.

In this thesis, a multi-tier heterogeneous network with macro cells, small cells and relays is addressed. In order to improve spectral efficiency in a single carrier system, the non-orthogonal transmission scheme Faster-than Nyquist (FTN) signaling is investigated. Furthermore, novel hybrid interference mitigation approaches to achieve a spectral efficiency improvement in multi-user multicarrier Multiple-Input and Multiple-Output (MIMO) systems by using cognitive radio and relay technology are proposed.

FTN signaling is an effective approach to boost the data rate by reducing the symbol period below the Nyquist criterion. In other words, FTN offers higher bandwidth efficiency compared to the Nyquist signaling for a given bandwidth by increasing the data rate and accepting inter-symbol interference. For future FTN applications in 5G wireless communication networks, it is of important to investigate whether FTN signaling delivers higher spectral efficiency compared to the Nyquist signaling under practical conditions of use. Simulation results show that by using FTN, the loss of spectral efficiency due to a guard band between two systems and the excess bandwidth of the pulse shape can be regained through adjustment of the FTN rate, which leads to an efficient use of the radio frequency band.

Cognitive radio is a frequency reuse technology which allows unlicensed users (Secondary Users (SUs)) to use the licensed radio spectrum unoccupied by a licensed user (Primary User (PU)). In addition, using the cognitive radio technique, an SU can simultaneously use the same spectrum with a PU as long as the quality of service of the PU remains unaffected. The existing cognitive radio approaches require either a spectrum sensing process or constraints on the SU transmit power. To overcome this shortcoming, a novel adaptive transmission approach based on Interference Alignment (IA) is proposed in this thesis. The proposed approach applies a modified water filling method to the primary link and a pre-coding approach based on IA and the null-steering method to the secondary link to ensure an interference free coexistence between users. It is shown that utilizing this approach both primary and secondary links can adapt their transmission to improve the spectral efficiency.

The concept of relay node densification within a macro cell is one of the network architectures for 5G networks to improve the spectral and energy efficiency, due to the fact that the edge nodes can transmit at higher rate with lower transmis-

sion power. This in turn poses new challenges regarding interference mitigation techniques. For a multi-user half-duplex amplify-and-forward MIMO relay system, two novel IA schemes are proposed, for which a hybrid optimization approach based on the Zero-Forcing (ZF) and Minimum Mean Square Error (MMSE) criteria is developed to deal with the multi-user interference problem in perfect and imperfect Channel State Information (CSI) cases. In case of perfect CSI, the non-robust IA approach offers benefits in terms of convergence and improvement of the system performance in low to moderate signal-to-noise ratios. Here, the interference mitigation approach based on zeros-forcing criterion is used as a reference. In case of having imperfect CSI, the system performance is significantly improved using the robust IA approach.

Keywords: Interference Alignment, Multi-user MIMO Systems, Linear Pre-coding, Faster-than-Nyquist Signaling, Relays, Cognitive Radio

ZUSAMMENFASSUNG

Spektrale Effizienz ist eine der großen Herausforderungen für drahtlose Kommunikationsnetze und soll aufgrund des begrenzten Funkfrequenzspektrums verbessert werden. Dies gewinnt insbesondere in den zukünftigen Mobilfunknetzen mit dem prognostizierten exponentiellen Wachstum der Anzahl der Mobilfunkgeräte zunehmend an Bedeutung. Eine bessere spektrale Effizienz kann vor allem entweder durch Mehrfachausnutzung der Frequenzbänder, wie z.B. kognitive Funk- und Mehrbenutzertechnologie oder durch Verwendung der Technologien zur Erhöhung der Datenrate erzielt werden. Allerdings besteht hier noch Potential für Verbesserungen. Aus diesem Grund wird die Entwicklung neuer Ansätze zur Steigerung der spektralen Effizienz für 5G-Kommunikationsnetze in den Fokus dieser Dissertation gestellt.

In dieser Arbeit wird ein mehrstufiges heterogenes Netzwerk mit Makrozellen, kleinen Zellen und Relais berücksichtigt, womit eine Erhöhung der Datenrate und Verbesserung der spektralen Effizienz sowie eine Optimierung der Abdeckung in den 5G-Mobilfunknetzen erzielt werden können. Aufgrund der geringen Komplexität und des niedrigen Verhältnis von Spitzen zur mittleren Leistung soll Einträgerverfahren in den 5G-Kommunikationsnetzen verwendet werden. Zur Verbesserung der spektralen Effizienz in einem Einträger-System wird das nicht-orthogonale sogenannte *Faster-than-Nyquist* (FTN) Übertragungsschema untersucht. Darüber hinaus werden hier neue hybride Ansätze zur Interferenzminimierung für Mehrnutzer-Mehrträgersysteme mit mehreren Sende- und Empfangsantennen vorgestellt, um eine effiziente Ausnutzung des Frequenzbands zu erreichen. Hierbei werden kognitive Funk- und Relaisstechnologien eingesetzt.

FTN ist eine aussichtsreiche Technik zur Erhöhung der Übertragungsrate durch Reduzierung der Symbolperiode unter dem Nyquist Kriterium. Es ist hier wichtig zu untersuchen, ob FTN eine höhere Systemleistung hinsichtlich der spektralen Effizienz im Vergleich zum Nyquist-Übertragungsschema ermöglicht. Laut den Untersuchungsergebnissen können unter Verwendung von FTN die aufgrund von Schutzbandern und der für die Pulsformung zusätzlich benötigten Bandbreite entstehenden Kapazitätsverluste durch passende Wahl der Symbolperiode und die zugelassene Intersymbolinterferenz zurückgewonnen werden. Dieses führt zu einer effizienten Nutzung des Frequenzbands.

Funkbasierte Übertragungssysteme mit kognitiven Fähigkeiten (Cognitive Radio (CR)) sind als vielversprechende Technologien zur Erhöhung der spektralen Effizienz in drahtlosen Kommunikationsnetzen bekannt. CR bietet unlizenziierten Benutzern verschiedene Möglichkeiten, ihr Übertragungsverhalten bezüglich der Frequenzbelegung an ihre Betriebsumgebung anzupassen. Unter Verwendung der CR-Technologie können unlizenziierten Benutzern nicht nur das vom lizenzierten Benutzer unbelegte Spektrum, sondern auch gleichzeitig dasselbe Spektrum mit einem lizenzierten Benutzer nutzen, solange die Servicequalität des lizenzierten Benutzers davon nicht beeinträchtigt wird. Die bisherigen CR-Ansätze erfordern

jedoch entweder Spektrum Sensing oder eine Anpassung der Sendeleistung des unlizenzieren Benutzers. Um diesem Nachteil entgegenzuwirken, wird in dieser Arbeit ein neuartiger adaptiver Ansatz, der sowohl auf Water-Filling als auch auf IA-Verfahren basiert, vorgestellt. Dieser Ansatz gewährt einerseits unter Verwendung des modifizierten Water-Filling-Verfahrens eine beständige Übertragung für die unlicenzierte Benutzern. Andererseits ermöglicht ein auf der Interferenzausrichtung basierendes Vordierungsverfahren eine Koexistenz mehrerer unlicenzierten Benutzern. Es wird gezeigt, dass mit diesem Ansatz sowohl der unlicenzierte als auch lizenzierte Benutzer ihre Übertragung anpassen können, sodass eine höhere Ausnutzung des Frequenzbands erreicht wird.

Wie bekannt, bietet das Konzept der Verdichtung von Relaisknoten innerhalb einer Makrozelle zahlreiche Vorteile, wie z.B. höhere spektrale Effizienz, bessere Fairness in der Ressourcenallokation sowie optimale Abdeckung für 5G-Netzwerke. Diese begegnet jedoch verschiedenen Herausforderungen einschließlich Techniken zur Interferenzunterdrückung. In dieser Arbeit werden zwei neuartigen IA-Schemata für ein Mehrnutzer half-duplex Amplify-and-Forward Relaisystem mit mehreren Sende- und Empfangsantennen vorgeschlagen. Für diese wird ein neuer hybrider auf *zero-forcing* und MMSE Optimierungskriterien basierender Ansatz zur Formulierung des Optimierungsproblems entwickelt, um Interferenzen in Anbetracht der perfekten und unvollständigen Kenntnisse des Übertragungskanal zu behandeln. Für den Fall der perfekten Kanalkennntnis, bringt das nicht robuste IA-Ansatz Vorteile hinsichtlich der Konvergenz und Verbesserung der Systemleistung bei niedrigem bis mittleren Signal-Rausch-Verhältnis. Hierbei wird der Ansatz, bei dem alle Filtern ausschließlich basierend auf dem *zero-forcing* Kriterium angepasst werden, als Referenz verwendet. Im Fall der unvollständigen Kanalkennntnis wird eine Steigerung der Systemleistung durch die Verwendung des robusten IA-Verfahren gewährleistet.

Schlagwörter: Inteference Alignment, Mehrnutzer-MIMO Systeme, Lineare Vordierung, Faster-than-Nyquist Signaling, Relaisysteme, Kognitive Funkssysteme

CONTENTS

I	DISSERTATION	xxi
1	INTRODUCTION	1
1.1	Motivation	1
1.2	Thesis Contribution and Outline	2
2	FASTER-THAN-NYQUIST SIGNALING	5
2.1	Introduction	5
2.2	System Model	6
2.3	Pulse Shape Background	7
2.3.1	Root Raised Cosine Pulse Shape	8
2.3.2	PHYDYAS Pulse Shape	8
2.3.3	EGF Pulse Shape	9
2.3.4	Hermite Pulse Shape	9
2.4	Practical Benefits of FTN Signaling	10
2.4.1	PAPR System Performance	10
2.4.2	BER System Performance	14
2.5	Spectral efficiency of FTN Signaling	17
2.5.1	FTN Spectral Efficiency in Single User Scenarios	17
2.5.2	FTN Spectral Efficiency in Coexistence Scenarios	17
2.6	Summary	25
3	MIMO-OFDM TECHNIQUES	27
3.1	Introduction to MIMO Technique	27
3.1.1	Space-Time Block Code	29
3.1.2	Linear Pre-coding	31
3.1.3	Multi-user MIMO Systems	34
3.2	Principle of OFDM Technique	37
3.3	MIMO-OFDM System	39
4	INTERFERENCE ALIGNMENT FOR MU-MIMO SYSTEMS	40
4.1	Introduction	40
4.2	Principle of Interference Alignment Technique	41
4.3	Degrees of Freedom and Maximum Capacity	45
4.4	Interference Alignment Approaches with Perfect CSI	46
4.4.1	Closed-form Solution for Interference Alignment	46
4.4.2	Interference Alignment via Reciprocity	47
4.4.3	MMSE-Based Interference Alignment	50
4.5	AS-MMSE-Based IA with Imperfect CSI	52
4.6	Simulation Results	55
4.7	Summary	57
5	IA IN COGNITIVE RADIO NETWORK	59
5.1	Introduction	59
5.2	Application Scenarios and System Model	61
5.2.1	Macro-Small Cell Coexistences	61

5.2.2	Macrocell-Femtocell Coexistences	62
5.2.3	System Model	64
5.3	Modified WF Algorithm in Primary Network	66
5.4	Linear pre-coding Based on IA in Secondary Network	69
5.4.1	Beamforming for Coexistence Between PU and SUs	69
5.4.2	Beamforming for Coexistence Between SUs	71
5.4.3	Feasibility of IA Condition for Multi-user Broadcast Channel in Underlay CR	72
5.5	Simulation Results	72
5.6	Summary	76
6	IA IN MU-MIMO RELAY NETWORKS	78
6.1	Introduction	78
6.2	Application Scenarios and System Model	78
6.2.1	Relays in Wireless Communication Networks	78
6.2.2	Related Works and Motivation	81
6.2.3	System Model	83
6.3	Joint Estimation for Perfect CSI	86
6.3.1	Optimization Problem	86
6.3.2	Non-Robust IA Approach	89
6.4	Joint Estimation for Imperfect CSI	91
6.4.1	Optimization Problem	91
6.4.2	Robust IA Approach	93
6.5	IA Feasibility Conditions	95
6.5.1	Required Number of Relay Nodes	95
6.5.2	Required Number of Relay Antennas	96
6.6	Simulation Results	96
6.6.1	Convergence Analysis	97
6.6.2	System Performance of the Non-Robust IA Approach	98
6.6.3	System Performance of the Robust IA Approach	100
6.7	Summary	101
7	CONCLUSION AND FUTURE WORK	103
7.1	Conclusions	103
7.2	Future Works	104
II	APPENDIX - PROOF OF EQUATIONS	105
A	APPENDIX	106
A.1	Feasibility Conditions for the IA Technique	106
A.2	Derivation of The Mean-Squared Error (MSE) at User k	108
A.3	The Sum-Interference Leakage	109
A.3.1	Perfect CSI	109
A.3.2	Imperfect CSI	109
A.4	Derivation of the post-processing filter for user k	110
A.5	Derivation of the pre-coding filter for user l	111
A.6	Relation Between MMSE and The Total Interference Leakage	111
	BIBLIOGRAPHY	113

INDEX	122
SCIENTIFIC CAREER	123
LIST OF PUBLICATIONS	125

LIST OF FIGURES

Figure 2.1	The SC-FTN signaling system model	6
Figure 2.2	Time domain representation of the pulse shaping filters . . .	10
Figure 2.3	Frequency domain representation of the pulse shaping filters	11
Figure 2.4	PAPR comparison between FTN and Nyquist signaling using different rRC pulse shapes	12
Figure 2.5	CCDF of PAPR comparison between FTN and the Nyquist sig- naling using the Hermite pulse shape	13
Figure 2.6	CCDF of PAPR comparison between FTN and the Nyquist sig- naling using the EGF pulse shape	14
Figure 2.7	BER performance of FTN signaling using rRC pulse shape with different β and τ	15
Figure 2.8	The uncoded BER performance comparison between FTN and Nyquist signaling	16
Figure 2.9	The coded BER performance comparison between FTN and Nyquist signaling using convolutional coding	16
Figure 2.10	The SE comparison for FTN and Nyquist signaling using con- volutional coding	18
Figure 2.11	Multiple-access channel coexistence scenarios	19
Figure 2.12	Interference power versus frequency distance	21
Figure 2.13	SE of three considered scenarios	23
Figure 2.14	SE of three considered scenarios using a rRC pulse shape . .	25
Figure 3.1	General block diagram of a MIMO system	27
Figure 3.2	Block diagram of a STBC encoder in a MIMO system	31
Figure 3.3	Block diagram of the pre-coding approach based on SVD for a MIMO system	33
Figure 3.4	Single cell MU-MIMO scenarios	35
Figure 3.5	General block diagram of an OFDM system	38
Figure 4.1	The IA concept	42
Figure 4.2	IA system model	43
Figure 4.3	The concept of the IA approach via reciprocity	48
Figure 4.4	The average sum-rate comparison between IA and OFDMA .	55
Figure 4.5	average sum-rate comparison for different number of users	56
Figure 4.6	The comparison of BER performance using different IA ap- proaches	56
Figure 4.7	MSE performance comparison between perfect and imper- fect CSI	57
Figure 5.1	Heterogeneous networks-coexistence of macro and small cells	62
Figure 5.2	Open vs. Closed Access of femtocell in two-tier networks . .	63
Figure 5.3	General system model of multi-user MIMO broadcast chan- nel in underlay CR	64
Figure 5.4	The Waterfilling concept	68

Figure 5.5	Equivalent two interference-free systems	70
Figure 5.6	The capacity of the primary link with different number of antennas versus SNR by employing WF technique	73
Figure 5.7	The DoF of the primary and secondary link versus SNR using the conventional WF for a 3×3 MIMO PU system.	74
Figure 5.8	The DoF of the primary and secondary link versus SNR using the modified WF for a 3×3 MIMO PU system.	75
Figure 5.9	The sum-rate of the secondary link versus SNR using the conventional and modified WF algorithms at the primary link for a 3×3 MIMO PUs and 2-users 5×5 MIMO SU system	76
Figure 5.10	The BER performance of PU and SUs versus SNR a 3×3 MIMO PUs and 2-users 5×5 MIMO SU systems	77
Figure 6.1	Two relay operating modes	80
Figure 6.2	Relay based HetNets architecture	80
Figure 6.3	Multi-user relay MIMO system	84
Figure 6.4	Convergence behavior of the non-robust IA approach	98
Figure 6.5	The effective end-to-end SINR for both single and multi-cell coexistence scenarios	99
Figure 6.6	The average sum-rate for both single and multi-cell coexistence scenarios	100
Figure 6.7	The BER performance comparison for both single and multi-cell coexistence scenarios	100
Figure 6.8	The average sum-rate of the non-robust IA design approach for different number of user in a single cell scenario	101
Figure 6.9	MSE performance comparison for a multi-cell scenario	102

LIST OF TABLES

Table 2.1	The excess bandwidth factors of the considered pulse shapes and corresponding PAPR gains provided by FTN signaling	14
Table 2.2	Benefits of 4-QAM FTN with $\tau = 0.5$ compared to 16-QAM Nyquist signaling system with the same data rate and pulse shape	17
Table 2.3	The frequency distance between MC and SC systems at an interference level of around -22 dB for different pulse shapes	22
Table 2.4	SE loss and related equivalent guard band of coexistence scenarios	24

ACRONYMS

5G	fifth Generation
CCI, ACI	Co- or Adjacent Channel Interference
AF	Amplify-and-Forward
AWGN	Additive White Gaussian Noise
AS-MMSE	Average-Sum Minimum Mean Squared Error
BC	Broadcast Channel
BD	Block Diagonalization
BER	Bit Error Rate
BLER	Block Error Ratio
BS	Base Station
CCDF	Complementary Cumulative Distribution Function
CQI	Channel Quality Indicator
CoMP	Coordinated Multi-Point
CR	Cognitive Radio
CP	Cyclic Prefix
CSI	Channel State Information
CSIT	Channel State Information at Transmitter
DAC	Digital-to-Analog Converter
DF	Decode-and-Forward
DoF	Degree of Freedom
DPC	Dirty Paper Code
DSL	Digital Subscriber Line
DVB-T	Digital Video Broadcasting-Terrestrial
EGC	Equal Gain Combining
EGF	Extended Gaussian Function
FAP	Femtocell Access Point

FBS	Femtocell Base station
FDMA	Frequency-Division Multiple Access
FDD	Frequency-Division Duplex
FFT	Fast Fourier Transformation
FTN	Faster-than Nyquist
FU	Femtocell User
GB	Guard Band
HetNets	Heterogeneous Networks
HFA	High Frequency Amplifier
IA	Interference Alignment
ICI	Inter-carrier Interference
IFFT	Inverse Fast Fourier Transformation
IOTA	Isotropic Orthogonal Transform Algorithm
ISI	Inter-symbol Interference
KKT	Karush-Kuhn-Tucker
LTE	Long-Term Evolution
MC	Multi-carrier
MAI	Multi-Access Interference
MBS	Macro-cell Base Station
MIMO	Multiple-Input and Multiple-Output
MISO	Multiple-Input and Single-Output
MMSE	Minimum Mean Square Error
MRC	Maximal Ratio Combining
MU	Multi-user
MUI	Multi-user Interference
MTC	Machine-Type Communication
MSE	Mean-Squared Error
MS-MSE	Mean Sum-of-Mean-Squared Error
OFDM	Orthogonal Frequency-Division Multiplexing

OFDMA	Orthogonal Frequency-Division Multiple Access
OQAM	Offset Quadrature Amplitude Modulation
OQAM/OFDM	Offset Quadrature Amplitude Modulation/Orthogonal Frequency-Division Multiplexing
PA	Power Amplifier
PAM	Pulse-Amplitude Modulation
PAPR	Peak-to-Average Power Ratio
PMI	Pre-coding Matrix Indicator
PU	Primary User
PSD	Power Spectral Density
QAM	Quadrature Amplitude Modulation
QoS	Quality of Service
RF	Radio Frequency
RI	Rank Indicator
RN	Relay Node
rRC	root Raised Cosine
SC	Single Carrier
SBS	Smallcell Base Station
SDMA	Space-Division Multiple Access
SE	Spectral Efficiency
SIMO	Single-Input and Multiple-Output
SIC	Successive Interference Cancellation
SISO	Single-Input and Single-Output
SINR	Signal-to-Interference-plus-Noise Ratio
SNR	Signal-to-Noise Ratio
STBC	Space-time Block Coding
SU	Secondary User
SVD	Singular Value Decomposition
SS	Spectrum Sensing

STR	Simultaneous Transmit and Receive
TDD	Time-Division Duplex
TDMA	Time-Division Multiple Access
TTR	Time-Division-Transmit and Receive
UE	User Equipment
WF	Water-Filling
WiMAX	Worldwide Interoperability for Microwave Access
WLAN	Wireless Local Area Network
ZF	Zero-Forcing
ZF-BF	Zero-Forcing Beamforming

LIST OF SYMBOLS

Symbol	Description
$A(\mu, \nu)$	Cross-ambiguity function
$\operatorname{argmin}\{\mathbf{X}\}$	The arguments min of \mathbf{X}
B	Bandwidth
β	Excess bandwidth factor of a pulse shape
c	Speed of light
C	Channel capacity
d_k	Number of independent data streams
$d_{k,m}$	Real valued OQAM/OFDM mapped to the k -th sub-carrier at the m -th OQAM/OFDM symbol
d_{RX}	Distance between two receive antennas at each user
d_{TX}	Distance between two transmit antennas at each user
\mathbf{E}_m^F	Channel estimation error matrix of channel matrix \mathbf{F}_m
\mathbf{E}_{km}^G	Channel estimation error matrix of channel matrix \mathbf{G}_{km}
\mathbf{E}_{kl}	Channel estimation error matrix of the channel matrix \mathbf{H}_{kl}
$\mathbb{E}\{\mathbf{X}\}$	Expected value of matrix \mathbf{X}
$\mathbb{E}\{\epsilon\}$	Expected value of the sum MSE
ϵ_k	The MSE at receiver k
$\operatorname{eig}(\mathbf{X})$	The operation to get the eigenvector of a matrix \mathbf{X}
ϵ	The sum MSE over all users
η	Spectral efficiency
f_c	Center frequency
f_{sc}	Center frequency of the SC system
\mathbf{F}_m	Channel matrix from the MBS to relay m
$\widehat{\mathbf{F}}_m$	Estimated channel matrix from the MBS to relay m
f_{sc}	Center frequency of the SC system
\mathbf{G}_{km}	Channel matrix from relay m to destination (user) k
$\widehat{\mathbf{G}}_{km}$	Estimated channel matrix from relay m to user k
\mathbf{H}	Channel matrix
$\overline{\mathbf{H}}$	Channel matrix in the reverse link
\mathbf{H}_{kl}	Channel coefficients from the l -th transmitter to the k -th receiver

$\bar{\mathbf{H}}_{kl}$	Channel coefficients from the l -th transmitter to the k -th receiver in the reverse link
\mathbf{H}_{00}	Channel matrix of the primary link
\mathbf{I}	The identity matrix
\mathbf{I}_k	Total interference leakage at the k -th receiver
$\bar{\mathbf{I}}_l$	Total interference leakage at the l -th receiver in the reverse link
K	Number of users
k	Receiver index
$L(\cdot)$	The Lagrange function
l	Transmitter index
$\lambda_{\mathbf{H}_{00},i}$	The i -th singular values of the matrix \mathbf{H}_{00}
λ_k	The Lagrange multiplier factor of user k
μ	Time or symbol offset
M	Number of RN
m	Relay index
N_e	The total number of equations
\mathbf{n}_k	Noise signal vector at receiver k
\mathbf{n}_m	Additive noise at relay m
N_r	Number of receive antennas
$N_{r,k}$	Number of receive antennas at user k
$N_{r,0}$	Number of receive antennas at the PU receiver
N_t	Number of transmit antennas
$N_{t,0}$	Number of transmit antennas at the MBS in the primary link
N_v	The total variables of system
ν	Frequency offset
$\nu_d(\mathbf{X})$	The d_k smallest eigenvalues of matrix \mathbf{X}
ν_0	The normalized sub-carrier spacing specified for OQAM/OFDM system
P	Oversampling factor of Nyquist signaling
p_i	The optimally allocated power to the i -th sub-channel using the modified WF method
$p_k(n - m\tau_0 K)$	Real valued and even transmit pulse shape modulated to sub-carrier k at the m -th symbol
P_l	Transmit power at transmitter l
Q	Oversampling factor of FTN signaling
\mathbf{Q}_k	Interference covariance matrix at receiver k
$\bar{\mathbf{Q}}_l$	Interference covariance matrix at at receiver k in the reverse link
R_b	Bit rate

R_c	Channel code rate
\mathbf{R}_{nn}	Covariance matrix of noise
$R_{RX}^{(k)}$	Receive antenna correlations matrix at receiver k
$R_{TX}^{(l)}$	Transmit antenna correlations matrix at transmitter l
\mathbf{R}_{00}	Covariance matrix of the PU transmitted signal
$\mathbf{R}_{\omega\omega}$	Covariance matrix of ω_k
$\hat{\mathbf{s}}_k$	Estimated signal at user k
\mathbf{s}_l	Transmitted data vector at transmitter l
σ_n^2	Noise power
$\text{span}(\mathbf{X})$	The space spanned by the column vectors of matrix \mathbf{X}
\mathbf{s}_0	Estimated data streams at the PU receiver
σ_m^2	Noise power at relay m
σ_k^2	Noise power at destination k
$\sigma_{E_{km}^G}^2$	Variance of channel estimated error matrix E_{km}^G
$\sigma_{E_m^F}^2$	Variance of channel estimated error matrix E_m^F
T	Symbol period of Nyquist signaling
τ	FTN signaling factor
τ_0	The normalized symbol duration specified for OQAM/OFDM system
$\text{Tr}(\cdot)$	The trace operation
\mathbf{U}	Post-Processing matrix
$\bar{\mathbf{U}}$	Post-Processing matrix in the reverse link
\mathbf{U}_k	Post-Processing matrix of receiver k
$\bar{\mathbf{U}}_k$	Post-Processing matrix of receiver k in the reverse link
\mathbf{U}_0	Post-processing matrix at the PU receiver
\mathbf{V}	Pre-Coding matrix
$\bar{\mathbf{V}}$	Pre-Coding matrix in the reverse link
\mathbf{V}_l	Pre-Coding matrix at transmitter l
$\bar{\mathbf{V}}_l$	Pre-Coding matrix at transmitter l in the reverse link
\mathbf{V}_0	Pre-coding matrix at the PU transmitter
$\text{vec}(\mathbf{X})$	The vectorization of matrix \mathbf{X}
\mathbf{W}	Relay matrix
\mathbf{W}_m	Relay matrix at relay m
ω_k	Total noise at destination k
$\text{vec}(\mathbf{X})$	Vectorization of matrix \mathbf{X}
\mathbf{x}_l	Transmitted signal vector at transmitter l
\mathbf{x}_0	Transmitted signal vector of the PU
\mathbf{y}_k	Received signal vector at receiver k

\mathbf{z}_m	Received signal at the m -th relay
ζ	Water level
\otimes	The Kronecker product of two matrices

Part I
DISSERTATION

INTRODUCTION

1.1 MOTIVATION

In comparison to the previous generations of wireless communication network, the future/fifth Generation (5G) wireless communication network is expected to achieve the system performance in terms of higher capacity, higher data rate, lower latency, massive device connectivity and higher Spectral Efficiency (SE) [51]. For this purpose, a network architecture consisting of multi-tier heterogeneous networks will be considered. A dense multi-tier heterogeneous network with macro cells and small cells such as relays, femtocells and picocells could provide enhancement in terms of coverage and energy efficiency. In the current situation, most of the available frequency resources have been assigned to the existing communication systems, resulting in the limited frequency resources usability. Therefore, increasing the radio frequency use becomes one of the most important issue for future wireless communication networks, especially when the number of wireless devices increases rapidly. SE can be improved by increasing either or both the frequency reuse and the data rate.

Cognitive Radio (CR) technology is a promising frequency reuse technology which can increase the efficiency of the spectrum use through the intelligent utilization of the licensed spectrum. There are two approaches of CR technology. The first one is called the interweave CR, where an unlicensed user is allowed to use the licensed spectrum if it is not occupied by a licensed user. To accomplish this, interweave CR requires an efficient spectrum sensing process. The second approach of CR is called the underlay CR, which enables an unlicensed user to share the licensed spectrum in the same time with a licensed user as long as the transmission quality of the licensed user remains unaffected. To fulfill this condition, in underlay CR, the unlicensed users have to control their transmit power, so that the interference caused to the licensed user by the unlicensed users does not exceed the interference tolerance level of the licensed user. Due to its sharing capability, the underlay CR technique offers higher SE compared to the interweave CR. Interweave CR has been widely studied in literature, while underlay CR still poses a great challenge and deserves further investigation. For this reason, this thesis focuses on underlay CR technology to improve the radio frequency reuse.

In contrast to the CR techniques which require spectrum sensing process or pose constraints on the transmit power of the unlicensed users, SE can also be improved by using the technique to overlap multiple users in both time and frequency domain. However, this approach requires efficient Multi-user Interference (MUI) mit-

igation/suppression techniques. Accordingly, developing interference mitigation techniques being capable of handling the multi-user interference problem is of a great importance for future wireless communication networks. In this context, a simple linear pre-coding technique called Interference Alignment (IA) is considered in this thesis. Using the IA technique, all interference from other transmitters operating in the same channel will be aligned in the same direction at each receiver. Thus, a receiver can easily decode its desired signal without additional user detection process.

As for increasing the data rate to improve SE, it can be typically achieved by reducing the symbol period, through utilization of the Multiple-Input and Multiple-Output (MIMO) or multi-carrier techniques. According to literature employing the massive MIMO technology in 5G networks can increase the SE by approximately 10 to 20 times [39].

Beside the above mentioned techniques to improve the data rate, Faster-than Nyquist (FTN) signaling is a potential solution to enhance the bandwidth efficiency by increasing the data rate over the Nyquist rate while keeping the bandwidth constant. In FTN, the data rate is boosted through reducing the symbol period. FTN is one of the promising transmission schemes for future wireless communication systems and is suggested to be applied in Long-Term Evolution (LTE)-uplink systems to provide higher bandwidth efficiency [67]. However, the investigations on the practical benefits of FTN in comparison to the Nyquist signaling so far has not been studied in literature. Therefore, this is the scope of our investigation.

Tackling the above mentioned challenges to improve the spectral efficiency in wireless communication networks is the main research topics of this thesis.

1.2 THESIS CONTRIBUTION AND OUTLINE

Within the framework of this thesis, new hybrid approaches based on FTN and IA to improve the SE for a single-user and multi-user system in a multi-tier heterogeneous network using relay and CR technologies are proposed and investigated. The main contributions of this work are summarized as follows:

- *The practical system performance in terms of SE for a non-orthogonal transmission scheme based on FTN signaling is investigated and compared with that of a single carrier Nyquist signaling system. For this purpose, single user Single Carrier (SC) and multiple-access channel scenarios are considered*
- *For an increase of the radio frequency use through overlapping of multi-user in both time and frequency domains, new pre-coding approaches based on IA are proposed and investigated. Here, different conditions; perfect and imperfect of the Channel State Information (CSI) are considered.*
- *In order to improve the spectrum reuse in underlay CR, a novel adaptive transmission scheme is introduced. To this, a pre-coding approach based on IA and the modified Water-Filling (WF) method is proposed and investigated for a multi-user underlay CR system to guarantee a continuous transmission of unlicensed users and achieve an interference-free coexistence of users.*

- *Relays enabled with multi-user technique is a great solution to achieve an enhancement in terms of energy and spectral efficiency as well as coverage in 5G wireless communication networks. In this context, two novel IA approaches are developed to deal with the MUI problem in a multi-user half-duplex Amplify-and-Forward (AF)-MIMO relay system. Here, the IA filters are optimized based on both Zero-Forcing (ZF) and Minimum Mean Square Error (MMSE) optimization criteria for both perfect and imperfect CSI cases.*

The above mentioned contributions are described in detail in the rest of this thesis, which is organized as follows:

In Chapter 2, the FTN signaling is introduced, which is used to increase the data rate in single carrier systems. Here, the FTN system performance in terms of SE, Bit Error Rate (BER) and Peak-to-Average Power Ratio (PAPR) is investigated and compared with that of a single carrier Nyquist signaling system. Furthermore, a multi-access channel is considered, where a single-carrier system using the Nyquist or FTN signaling shares the spectrum with a multi-carrier system. In this regard, the SE of different coexistence scenarios is evaluated and discussed. In order to assess the system performance of FTN signaling, a single user Multi-carrier (MC) system based on Offset Quadrature Amplitude Modulation (OQAM)-Orthogonal Frequency-Division Multiplexing (OFDM) is used as reference.

In Chapter 3, a brief introduction to MIMO and MC-OFDM techniques is given. The MIMO technique is well-known as an approach to increase the data rate in wireless communication systems and has been deployed in several wireless standards. An overview about the pre-coding techniques used in MIMO systems is provided in this chapter. Furthermore, different kinds of multi-user MIMO scenarios are introduced and the interference mitigation approaches to overcome the MUI problem are proposed.

In Chapter 4, IA is investigated to overcome the disadvantages of the interference mitigation techniques introduced in Chapter 3. In this chapter, the principles of the IA technique is derived and different IA approaches under assumption of perfect CSI are evaluated. In addition, the system performance of the proposed IA approaches is investigated and compared with each other and with that of a Orthogonal Frequency-Division Multiple Access (OFDMA) system. In the presence of CSI error, a new robust IA approach based on the average-sum minimum mean squared error is developed and evaluated.

In Chapter 5, a short overview on the coexistence of a macro and multiple small cells in multi-tier Heterogeneous Networks (HetNets) using underlay CR technique is given. For such coexistence scenarios, the ZF-based IA approach introduced in Chapter 4 is extended to handle the MUI problem. Here, a novel adaptive transmission scheme is proposed, in which a pre-coding method based on the IA technique is introduced to guarantee an interference-free coexistence of multiple users. The system performance of the proposed transmission scheme in terms of channel capacity and BER is investigated and discussed.

In Chapter 6, a heterogeneous network architecture is considered, where the edge cell users of a macro cell communicate with the macro base station via relay nodes. Two novel IA schemes based on the extension of two MMSE-based IA approaches introduced in chapter 4 are developed to overcome the problem of

MUI under different CSI conditions. In case of having perfect CSI, the non-robust IA scheme with a hybrid optimization approach based on the ZF and MMSE criteria is proposed. In the presence of CSI error, a robust IA design approach based on minimizing the expected values of cost functions is presented. Here, the system performance of both IA approaches is evaluated and compared with each other and with the reference method.

Finally, the contributions of this dissertation are summarized and future research topics are derived in chapter 7.

FASTER-THAN-NYQUIST SIGNALING

2.1 INTRODUCTION

Faster-than Nyquist (FTN) signaling is a non-orthogonal transmission scheme which is able to boost the system capacity by increasing the data rate while keeping the bandwidth constant. It is considered as a potential solution to improve the bandwidth efficiency of conventional orthogonal modulation schemes in future communication systems. A system is said to be FTN if its information symbols are transmitted at a rate higher than that suggested by the Nyquist theorem, or in other words, the information symbols are transmitted with a shorter period than the Nyquist symbol period. In contrast to the Nyquist signaling scheme, which guarantees Inter-symbol Interference (ISI)-free transmission through orthogonality, in FTN signaling, the pulses are no longer orthogonal, and thus ISI is introduced. Consequently, to address this issue, FTN systems require higher receiver complexity compared to the conventional orthogonal modulation schemes. For this reason, FTN signaling is still far away from practical applications.

The concept of FTN signaling was proposed and evaluated first by Mazo in 1975, [71]. In that study, the minimum Euclidean distance at the receiver of an SC-FTN signaling for the sinc pulse is investigated. Here, an un-coded system based on a binary modulation scheme is considered. It is shown that the information symbols can be transmitted at a rate up to 25% higher than the Nyquist signaling without having any loss in the Euclidean distance resulting in the same BER. Accordingly, a pulse period of $0.802T$ is specified as Mazo limit for the sinc pulse with binary input, where T is the symbol period of the Nyquist signaling. In this context, the Mazo limit is defined as the minimum symbol period, for which the minimum Euclidean distance equals to the theoretical minimum distance. However, since sinc pulses are not suitable for practical applications, further evaluation on the Mazo limit is also performed for root Raised Cosine (rRC) pulses with different excess bandwidth factors β in [66]. As already established in Mazo's work, the study in [66] also confirms that a small reduction of the pulse period below the T -Nyquist orthogonal pulse shape period does not affect the minimum Euclidean distance for binary signaling. Furthermore, that study shows that the Mazo limit decreases as the excess bandwidth increases. It signifies that the loss of excess bandwidth, as in orthogonal pulse shape case, can be regained in FTN signaling by reducing symbol spacing and allowing ISI so that more information can be transmitted. This implies that the SE of FTN signaling is higher than that of the Nyquist signaling. The

study on the constrained Shannon capacity of FTN signaling in [85] confirms this statement. In [85], Rusek and Anderson prove also that the loss in capacity due to the excess bandwidth can be regained using FTN signaling. Therefore, using non-sinc pulse shaping FTN delivers higher capacities compared to the Nyquist signaling. Furthermore, the study in [34] reinforces the results of the FTN capacity presented in [85] and additionally indicates that the asymptotic capacity gain achieved by FTN tends to be equal to the excess bandwidth at high Signal-to-Noise Ratios (SNRs). However, in practice the asymptotic region (for large SNRs) is not of main interest. It is much more important to consider the SNR region (operational SNRs), where a system is able to achieve a given target Block Error Ratio (BLER). Therefore, the goal of this chapter is to investigate the practical benefits of FTN signaling in terms of PAPR, BER and SE in a more realistic system.

In this chapter, the SC-FTN system performance in terms of BER, PAPR, SE is investigated and compared with that of a Nyquist signaling system given that both systems have the same pulse shape and data rate. Here, the question to be answered whether FTN allows for a higher SE, a lower BER and PAPR compared to the Nyquist signaling, since a lower modulation order can be used in FTN signaling to achieve the same rate as the Nyquist signaling. Subsequently, a practical application scenario for FTN signaling is introduced and investigated. For this case, a practical multi-access channel is considered, where an SC system using Nyquist or FTN signaling shares the spectrum with a multi-carrier system. The main interest is to investigate whether FTN signaling can recover loss of SE due to guard bands by adjusting the symbol duration and allowing ISI. This leads to an increase of SE.

2.2 SYSTEM MODEL

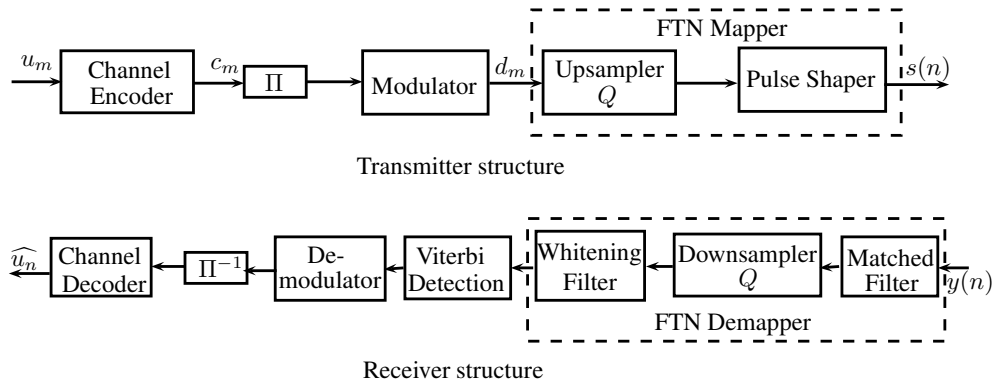


Figure 2.1: The SC-FTN signaling system model

The system model considered for implementing the FTN signaling concept is illustrated in Fig. 2.1. At the transmitter side, u_m and d_m represent uncoded bits and modulated symbols, respectively. After modulation the FTN mapper is applied, which consists of an upsampler with an oversampling factor of Q and a Nyquist pulse shape. If we consider, a comparable system model of Nyquist signaling with an oversampling factor of P , then the FTN rate is defined as P/Q and the FTN factor $\tau = Q/P$. The inherent ISI effect generated by FTN signaling is obtained

through different values of Q and P . The discrete transmit signal for an SC-FTN system is given as follows:

$$s(n) = \sum_m d_m p(n - m\tau P), \quad 0 < \tau \leq 1 \quad (2.1)$$

with $P = TF_s$. Here, F_s is the sampling frequency and $p(n)$ stands for a real-valued discrete pulse shape having unit energy. A system with $\tau = 1$ corresponds to the Nyquist signaling with an orthogonal transmission scheme. In FTN signaling, $\tau < 1$, and thus pulses are no longer orthogonal, i.e.

$$\sum_{n=-\infty}^{\infty} p(n)p(n - m\tau T) \neq \delta(m).$$

The bit rate of an SC-FTN signaling system is given by

$$R_b = \frac{\log_2(M)}{\tau T}, \quad (2.2)$$

where M is the modulation order. In the considered system model, the signal is transmitted through an Additive White Gaussian Noise (AWGN) channel, so that the received signal $y(n)$ is given by

$$y(n) = s(n) + w(n), \quad (2.3)$$

where $w(n)$ is the noise signal. At the receiver side, the received signal $y(n)$ passes through the FTN demapper, which consists of a matched filter $p^*(-n)$ having the same pulse shape used at the transmitter side and a pre-whitening filter applied to decolor noise. To eliminate ISI caused by FTN, a detection based on the Viterbi algorithm is applied after the FTN demapper. Finally, the deinterleaving and channel decoder blocks are deployed. On the contrary, in the Nyquist signaling system over AWGN channel, since it guarantees an FTN free transmission, the pre-whitening process and detection are not required in the receiver side.

2.3 PULSE SHAPE BACKGROUND

In a digital communication system, a pulse $g(n)$ that meets the Nyquist criterion is used for having a minimum ISI. This pulse has the following time domain characteristic

$$g(mT) = \begin{cases} 1 & m = 0 \\ 0 & m = \pm 1, \pm 2, \dots \end{cases} \quad (2.4)$$

where m is the symbol time index. In frequency domain, the Fourier transform of $g(n)$, $G(f)$, meets the following condition [10]

$$\frac{1}{T} \sum_{m=-\infty}^{\infty} G\left(f + \frac{m}{T}\right) = 1. \quad (2.5)$$

In practical implementations, $g(n)$ is the convolution of the transmit pulse shaping filter $p(n)$ and related matched filter at the receiver side $p^*(-n)$, i.e. $g(n) = p(n) * p^*(-n)$.

Designing a pulse shaping filter such that the combined system response of transmit and receive filters satisfies the Nyquist condition in (2.4) is a well-studied problem in digital communication systems. Based on characteristic of the mobile radio channel, pulse shaping filters can be designed and optimized to minimize ISI and Inter-carrier Interference (ICI). In this chapter, to investigate the practical benefits of FTN signaling the Nyquist pulses such as rRC, PHYDYAS, Hermite and Extended Gaussian Functions (EGFs) are considered. These pulse shape filters are currently under discussion for future wireless communication systems.

The excess bandwidth is an important parameter of a pulse shape and indicates how much the spectrum of a pulse shape extends over a given Nyquist bandwidth $W_0 = \frac{1}{T}$. The excess bandwidth is defined as $W - W_0$, whereby W is the bandwidth of the pulse shape. Accordingly, the excess bandwidth factor β can be expressed as follows:

$$\beta = \frac{W - W_0}{W_0}. \quad (2.6)$$

In order to make a valid comparison with the rRC pulse shaping filters, the pulse shape's bandwidth W is determined as the range between the edge points, where the Power Spectral Density (PSD) drops by about 17 dB compared to the center [10]. The excess bandwidth factor is also commonly known as the roll-off factor.

2.3.1 Root Raised Cosine Pulse Shape

The rRC pulse shaping filter family is frequently chosen in a system because it satisfies the Nyquist criterion (2.4) and (2.5). The impulse response of a root raised cosine pulse shaping filter is given as follows [30]:

$$g(t) = \begin{cases} 1 - \beta + 4\frac{\beta}{\pi}, & t = 0 \\ \frac{\beta}{\sqrt{2}} \left[\left(1 + \frac{2}{\pi}\right) \sin\left(\frac{\pi}{4\beta}\right) + \left(1 - \frac{2}{\pi}\right) \cos\left(\frac{\pi}{4\beta}\right) \right], & t = \pm \frac{T}{4\beta} \\ \frac{\sin\left[\pi\frac{t}{T}(1-\beta)\right] + 4\beta\frac{t}{T} \cos\left[\pi\frac{t}{T}(1+\beta)\right]}{\pi\frac{t}{T} \left[1 - \left(4\beta\frac{t}{T}\right)^2\right]}, & \text{otherwise} \end{cases} \quad (2.7)$$

Here, β varies between 0 and 1, and it determines the filter bandwidth $W = (1 + \beta)/(2T)$.

2.3.2 PHYDYAS Pulse Shape

This pulse shape, which has been presented first in [72] and intensively studied within the PHYDYAS project, is a time limited Nyquist filter obtained by frequency sampling and optimized to have a superior stop band attenuation. Due to this property, the PHYDYAS pulse shape is suitable for spectrum sharing scenarios.

The prototype filter function $p(t)$ can be described by a truncated Fourier series with coefficients a_i according to [72],

$$p(t) = \begin{cases} a_0 + 2 \sum_{i=1}^{N-1} a_i \cos\left(\frac{2\pi i t}{NT}\right), & |t| \leq \frac{(N-1)}{2} \\ 0, & \text{otherwise} \end{cases}, \quad (2.8)$$

whereby N is the length of the prototype filter in multiples of the symbol period T . By proper selection of N and a_i , this equation may also be used to describe the well known Hanning, Hamming and Blackman windows. For all investigations in this chapter, the coefficients presented in [72] for $N = 8$ is used, providing the best frequency domain power localization of the available PHYDYAS pulse shape. According to (2.6), the PHYDYAS pulse shape has an equivalent excess bandwidth factor of 0.6.

2.3.3 EGF Pulse Shape

The Gaussian prototype filter has an ideal energy localization in the time-frequency grid, but it is not orthogonal. Therefore, the Isotropic Orthogonal Transform Algorithm (IOTA) is used to transform the non-orthogonal Gaussian function into a prototype filter function which is orthogonal after matched filtering at the receiver side. Thereby, the localization property of the Gaussian function is kept. In the scope of this work, the closed form solution based on EGFs reported in [99] is used, which can be written as

$$p_{\alpha, \nu_0, \tau_0}(t) = \frac{1}{2} \sum_{k=0}^{\infty} d_{k, \alpha, \nu_0} \left[g_{\alpha} \left(t + \frac{k}{\nu_0} \right) + g_{\alpha} \left(t - \frac{k}{\nu_0} \right) \right] \cdot \sum_{l=0}^{\infty} d_{l, 1/\alpha, \tau_0} \cos \left(2\pi l \frac{t}{\tau_0} \right), \quad (2.9)$$

where τ_0 and ν_0 define the applied Gabor frame. α is the spreading factor of the applied Gaussian function g_{α} used to adapt the power spreading in the time-frequency grid and $d_{\{\dots\}}$ are real valued weighting coefficients given in [99]. The given prototype filter function has been truncated, so that $g_{\alpha, \nu_0, \tau_0}(t) = 0$ for $|t| > NT/2$. For a given α , the excess bandwidth factor of the EGF pulse shape is determined according to (2.6) and it increases with rising value of α .

2.3.4 Hermite Pulse Shape

Similar to the IOTA pulse shape, the Hermite prototype filter is derived from the Gaussian function. It has been shown, that it provides a better localization property compared to the IOTA pulse shape, in case both prototype filter functions are truncated to length $L = NT$. For the Hermite pulse shape, the Gaussian function is weighted with isotropic Hermite functions to achieve orthogonality [46]. The Hermite pulse shape is determined according to

$$p(t) = \sum_{k=0}^{N_H-1} H_{4k} h_{4k} (2\sqrt{\pi}t) \quad (2.10)$$

$$p_n(t) = e^{-\frac{t^2}{2}} \frac{d^n}{dt^n} e^{-t^2},$$

with H_{4k} represent the weighting coefficients reported in [46], $\frac{d^n}{dt^n}$ being the n -th derivation with respect to t and $N_H = 4$ is the number of the first isotropic Hermite functions. For all investigations, the given prototype filter function has been truncated, so that $g(t) = 0$ for $|t| > NT/2$. According to (2.6), the Hermite pulse shape has an excess bandwidth factor of 1.5.

Fig. 2.2 and 2.3 depict the representation of the considered pulse shapes in time and frequency domain, respectively. It can be seen that the EGF pulse shape with $\alpha = 3$ has a good time containment property, i.e. the energy of the pulse shape is concentrated in the main lobe. The Hermite and EGF with $\alpha = 2$ pulse shapes have similar characteristics in time and frequency domain. Moreover, both pulse shapes have an equivalent excess bandwidth factor larger than one. The PHYDYAS pulse shape has an equivalent excess bandwidth factor smaller than one and exhibits an excellent stop band attenuation.

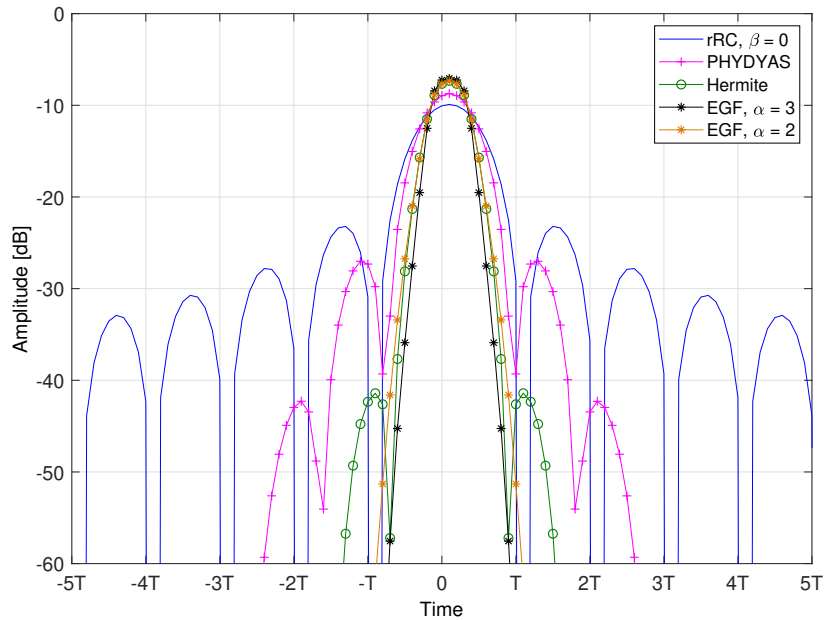


Figure 2.2: Time domain representation of the pulse shaping filters

2.4 PRACTICAL BENEFITS OF FTN SIGNALING

2.4.1 PAPR System Performance

In wireless communication systems, a high PAPR requires higher dynamic ranges of Digital-to-Analog Converter (DAC) and High Frequency Amplifiers (HFAs). Consequently, the system design becomes more complex and the cost increases. Currently, a number of techniques such as clipping, coding and constellation extension as well as selected mapping have been proposed to reduce PAPR in a wireless communication system [98]. It is reported in [98] that for every 1 dB reduction in PAPR

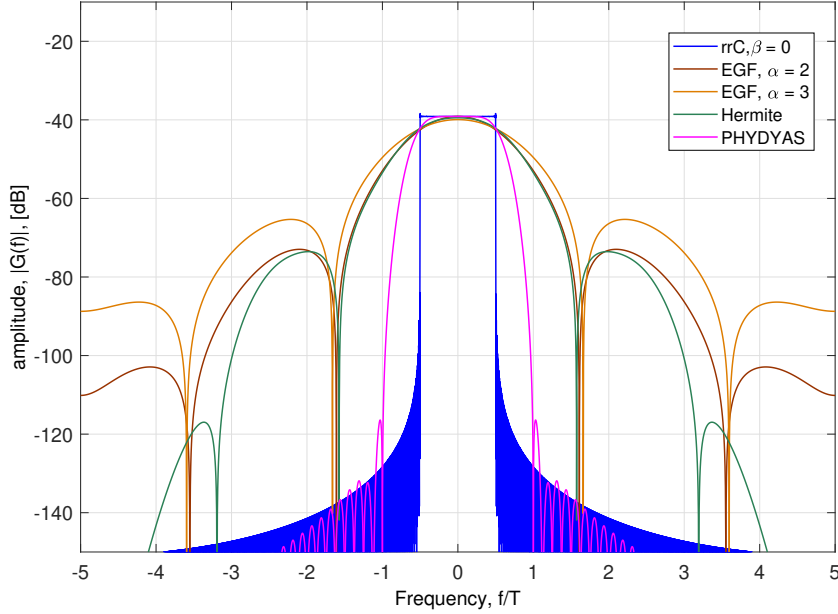


Figure 2.3: Frequency domain representation of the pulse shaping filters

there is more than 9% improvement in the Power Amplifier (PA) efficiency and 6% to 8% reduction in power consumption for the PA and DAC. Therefore, PAPR reduction is an important issue in wireless communication systems. FTN signaling achieves a higher PAPR due to higher transmit power compared to the Nyquist signaling with the same pulse shape and modulation order. However, in this case, FTN signaling offers a higher data rate. Thus, it is of interest to compare the PAPR of both FTN and Nyquist signaling systems under equal achievable rates. Since a lower modulation order can be used in FTN signaling to achieve the same rate as the Nyquist signaling, this raises the question whether FTN allows for lower PAPR compared to the Nyquist signaling.

The PAPR of a transmitted signal $s(n)$ is generally defined as follow:

$$\text{PAPR} = 10 \log_{10} \frac{\max |s(n)|^2}{\mathbb{E} [|s(n)|^2]}, \quad (2.11)$$

where $\max |.|^2$ denotes the peak power of transmitted signal $s(n)$ given in (2.1) and $\mathbb{E} [|.|^2]$ is its average power. In general, the PAPR of an SC system is a function of two components: constellation of the signal and pulse shaping filter. Due to pulse shape filter, PAPR is normally affected by the pulse shaping filter parameters such as the excess bandwidth factor and the number of symbols covered by filter, [98]. In general, PAPR increases with increasing the filter length due to overlapping symbols and with the decreasing of the excess bandwidth factor. Additionally, in FTN signaling, PAPR is dependent on value of τ . By reducing value of the FTN factor τ , the overlap of symbols becomes large and correspondingly PAPR increases. This leads to the conclusion that in FTN signaling the PAPR is a function of τ , M and L : $\text{PAPR} = f(\tau, L, M)$, where L represents the length of pulse shaping filter.

Since the power of the signal in time domain is a random variable and dependent on input symbols, PAPR is also a random variable. Therefore, the Complementary Cumulative Distribution Function (CCDF) is used to describe the probability of the PAPR exceeding a given threshold γ . The CCDF can be described as follows [84]:

$$\text{CCDF} = \Pr(\text{PAPR} > \gamma). \quad (2.12)$$

To evaluate the FTN system performance, all simulations are performed for 1000 frames with each having 10^4 bits, where different pulse shaping filters with an oversampling factor of 8 are considered.

Here, the PAPR of FTN signaling using a rRC pulse shaping filter with different excess bandwidth factors β is investigated. Fig. 2.4 shows the PAPR of both FTN and Nyquist signaling systems, where $\text{CCDF} = 10^{-5}$. In this Figure, the solid curves show the PAPR of the Nyquist signaling and the dash-dotted curves represent the PAPR of FTN signaling systems. As reported in [30], simulation results confirm that by using rRC pulse shape, PAPRs of Nyquist signaling decreases for an excess bandwidth factor from 0 to around 0.4 and is almost constant (with a slight increase) between 0.4 and 1. Moreover, PAPR of FTN signaling increases with decreasing value of τ

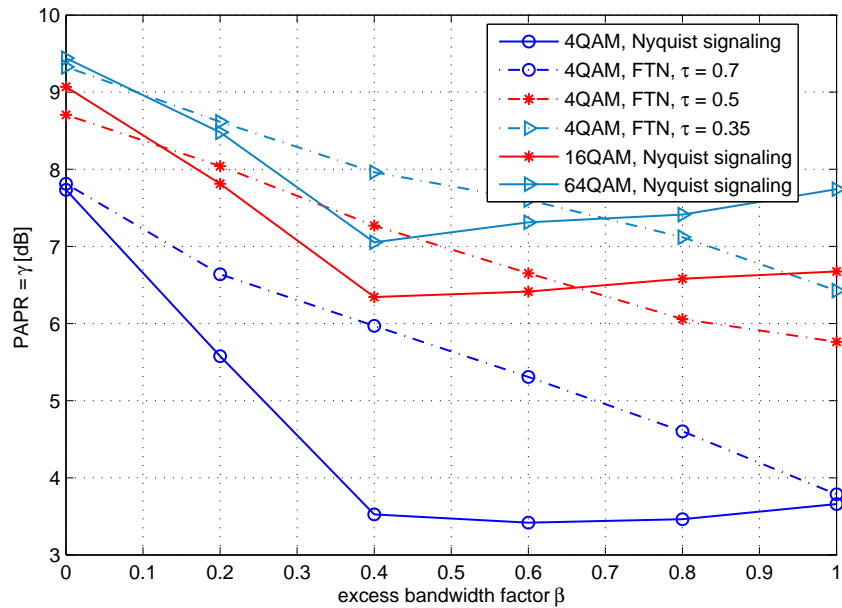


Figure 2.4: PAPR of FTN compared to the Nyquist signaling with the same pulse shape and data rate using different rRC pulse shapes

Now, the PAPR of FTN and Nyquist signaling is compared with each other, as shown in Fig. 2.4. The systems to be compared are represented with the same color and the same symbol marker. Both systems have the same data rate. It can be seen that using a rRC pulse shaping filter with $\beta \leq 0.7$, where the energy of side lobes is large, the SC-FTN signaling achieves PAPRs inferior to the Nyquist signaling systems. However, for $0.7 < \beta \leq 1$ the 4-Quadrature Amplitude Modulation (QAM) FTN signaling with $\tau = 0.5$ provides a PAPR gain up to 1 dB compared to the 16-QAM Nyquist signaling system. Here, both systems have a data rate of 4 bits/symbol.

Similarly, the PAPR of FTN signaling with $\tau = 0.35$ is compared to that given by the 64-QAM Nyquist signaling system, where both systems have the same data rate (6 bits/symbol). For this case, a PAPR gain up to 1.3 dB can be achieved. According to simulation results, it can be seen that PAPR gain of FTN signaling can only be achieved by using the rRC pulse shape with a large excess bandwidth factor β .

Fig. 2.5 depicts the PAPR of SC-FTN signaling using the Hermite pulse shaping filter, where the CCDF is considered. The Hermite and EGF with $\alpha = 2$ pulse shapes have an equivalent excess bandwidth factor of 1.5. In the case of using the Hermite pulse shape, at a CCDF value of 10^{-4} FTN signaling can achieve a PAPR gain of around 2 dB compared to the Nyquist signaling system. In the case of using the EGF pulse shape with $\alpha = 3$ a PAPR gain of around 2.8 dB can be obtained due to its large equivalent excess bandwidth ($\beta = 1.9$), as shown in Fig 2.6.

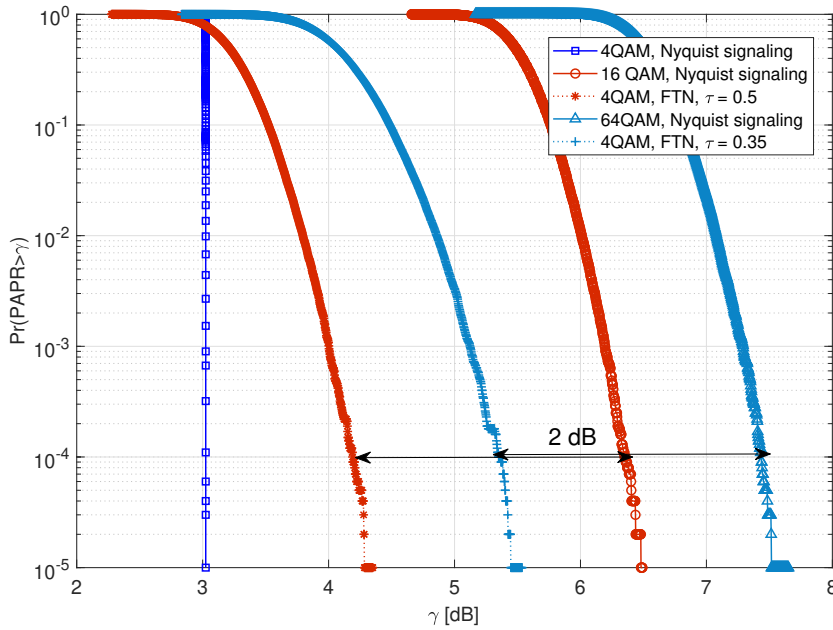


Figure 2.5: CCDF of PAPR comparison between FTN and the Nyquist signaling with the same pulse shaping and data rate using the Hermite pulse shape

Moreover, simulation results related to the equivalent excess bandwidth factor and the PAPR gain achieved by FTN signaling for different pulse shapes are summarized in Table 2.1. Here, it can be seen that the excess bandwidth factor β of the EGF pulse shape increases with the increasing value of α . In addition, these results indicate that the PAPR gain achieved by FTN signaling increases as the excess bandwidth factor of the applied pulse shape rises. Since the PHYDYAS pulse shape has an equivalent excess bandwidth factor of $0.6 < 0.7$, according to statement made in Fig. 2.4, simulation results confirm that using the PHYDYAS pulse shape cannot provide a PAPR gain with FTN signaling.

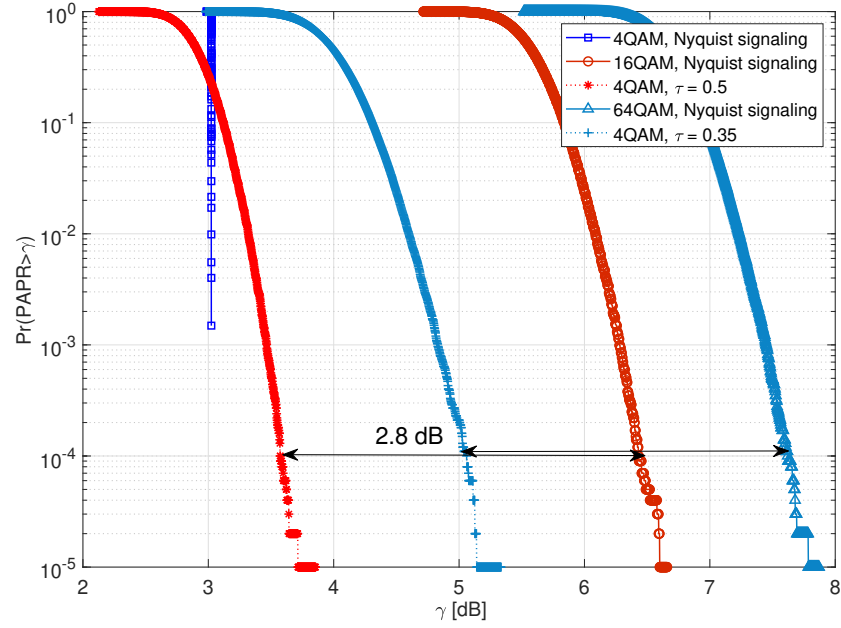


Figure 2.6: CCDF of PAPR comparison between FTN and the Nyquist signaling with the same pulse shape and data rate using the EGF pulse shape with $\alpha = 3$

Pulse Shape		Excess Bandwidth	PAPR-Gain
rRC		0.7-1	0-1 dB
PHYDYAS		0.6	No
Hermite		1.5	≈ 2 dB
EGFs	α		
	0.5	0.3	No
	1	0.8	≈ 0.4 dB
	1.5	1.2	≈ 1.5 dB
	2.0	1.5	≈ 2.0 dB
	2.5	1.7	≈ 2.4 dB
	3.0	1.9	≈ 3.0 dB
	3.5	2.0	≈ 3.2 dB
	4.0	2.1	≈ 3.4 dB
5	2.2	≈ 3.5 dB	

Table 2.1: The excess bandwidth factors of the considered pulse shapes and corresponding PAPR gains provided by FTN signaling

2.4.2 BER System Performance

Fig. 2.7 shows the BER of an SC-FTN signaling system using the rRC pulse shape with $\beta = 0.3$ and $\beta = 0$. These results confirm the Mazo limits reported in [71] and [66].

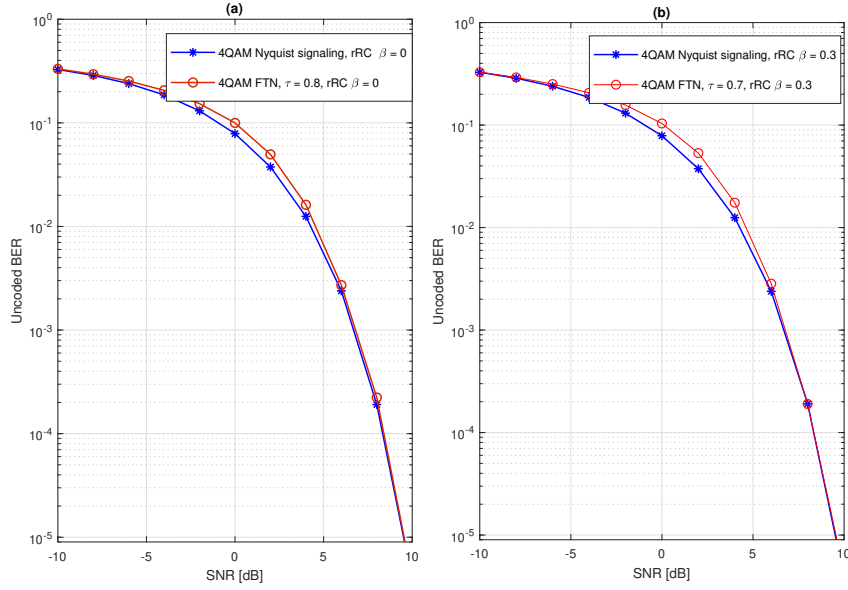


Figure 2.7: (a) BER performance of FTN $\tau = 0.8$ using rRC pulse shape with $\beta = 0$
 (b) BER performance of FTN $\tau = 0.7$ using rRC pulse shape with $\beta = 0.3$

In addition, the 4-QAM FTN system performance in terms of BER for $\tau = 0.5$ is investigated and compared to that of the 4-QAM and 16-QAM Nyquist signaling system. Here, the 4-QAM FTN with $\tau = 0.5$ system has double data rate compared to the 4-QAM Nyquist signaling system. Meanwhile, the 4-QAM FTN with $\tau = 0.5$ and the 16-QAM Nyquist signaling system have the same data rate (4 bits/symbol). It is assumed that all system use the same pulse shape. The uncoded BER curves are shown in Fig. 2.8, where the solid curves show the uncoded BER of the Nyquist signaling systems, remaining curves are for the FTN signaling system using different pulse shapes. It can be seen that the BER performance of the 4-QAM FTN system with $\tau = 0.5$ is worse than that of the 4-QAM Nyquist signaling. Here, the BER increases with decreasing the equivalent excess bandwidth β . However, it is worth mentioning that the BER curves of the FTN systems using the EGF pulse shape with $\{\alpha = 3, \beta = 1.9\}$ and $\{\alpha = 2, \beta = 1.5\}$ are very close to that of the 4-QAM Nyquist signaling. From SNR value of around 5 dB, the BER of the FTN system using the EGF pulse shape with $\{\alpha = 3, \beta = 1.9\}$ is equal to that of the 4-QAM Nyquist signaling with the advantage that the FTN system has double data rate compared to the Nyquist signaling system.

Moreover, in Fig. 2.8, it can be seen that in comparison to the 16-QAM Nyquist signaling system, the 4-QAM FTN with $\tau = 0.5$ system has better BER performance. Here, the BER gain achieved by FTN signaling rises with the increasing value of β . As seen in Fig. 2.8, the BER of FTN signaling using the rRC pulse shapes with $\beta = 0.3$ and $\beta = 0$ are still better than that of the 16-QAM Nyquist system in the high SNR regime (from an SNR value of around 10 dB). In the case of using the EGF pulse shape with $\{\alpha = 3, \beta = 1.9\}$ and $\{\alpha = 2, \beta = 1.5\}$, a BER gain of around 3.5 dB can be achieved at a BER value of 10^{-4} .

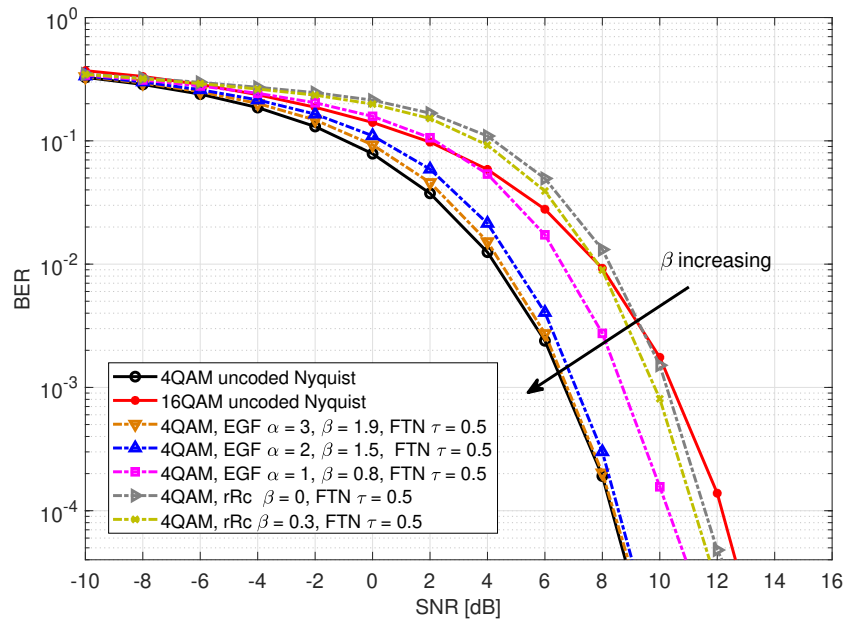


Figure 2.8: The uncoded BER performance comparison between FTN and Nyquist signaling

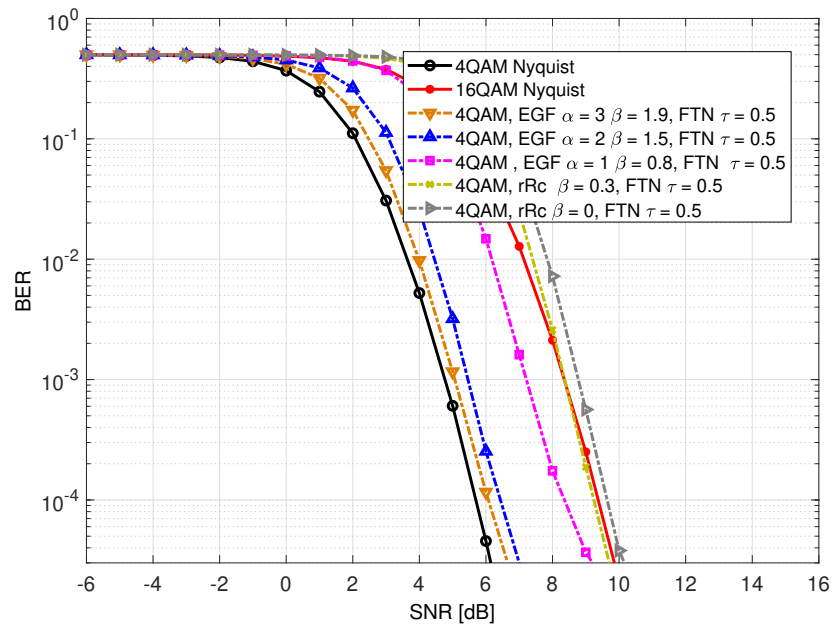


Figure 2.9: The coded BER performance comparison between FTN and Nyquist signaling using convolutional coding with a code rate of $3/4$

Fig. 2.9 shows the coded BER curves of both FTN and Nyquist signaling systems. To this, the convolutional coding with a code rate of $3/4$ is used. Here, all BER curves have the same behavior as in Fig 2.8. However, in the case of using the rRC pulse shapes with $\beta = 0$ and $\beta = 0.3$, the BER of FTN signaling is only close to the 16-QAM Nyquist signaling for high SNRs. Using the EGF pulse shape with $\{\alpha = 3, \beta = 1.9\}$ a coded BER gain of around 3.0 dB can still be achieved at a BER value of 10^{-4} in comparison to the 16-QAM Nyquist signaling with the same pulse shape.

The benefits of FTN signaling using the EGF pulse shape with different values of α are summarized in Table 2.2.

Pulse Shape		Excess Bandwidth	PAPR-Gain	BER-Gain
EGFs	α			
	1	0.8	≈ 0.4 dB	≈ 2 dB
	2.0	1.5	≈ 2.0 dB	≈ 3.5 dB
	3.0	1.9	≈ 3.0 dB	≈ 3.5 dB

Table 2.2: Benefits of 4-QAM FTN with $\tau = 0.5$ compared to 16-QAM Nyquist signaling system with the same data rate and pulse shape

According to simulation results, it can be concluded that FTN has advantages in terms of BER and PAPR in case of using pulse shape with large excess bandwidth factor β . In this case, these gains are proportional to β .

2.5 SPECTRAL EFFICIENCY OF FTN SIGNALING

For the SE evaluations, all considered systems use a convolutional coder (177, 131). Here, the achieved SE is determined by $\eta = (1 - \text{BLER})R_c \log_2 M$.

2.5.1 FTN Spectral Efficiency in Single User Scenarios

In this subsection, the 4-QAM FTN system performance in terms of SE for $\tau = 0.5$ is investigated and compared to that of the 4-QAM and 16-QAM Nyquist signaling system given that all systems use the same pulse shape. Fig. 2.10 shows the SE of all considered coded systems. It can be seen that FTN signaling has higher SE than Nyquist signaling. From an SNR of around 11 dB, the FTN signaling with $\tau = 0.5$ and the 16-QAM Nyquist signaling have the same SE. However, for SNRs < 11 dB, the 4-QAM FTN system with $\tau = 0.5$ delivers better SE performance in comparison to the 16-QAM Nyquist signaling system. At the SE of 2 bits/s/Hz, an SNR gain of around 3 dB and 3.5 dB can be achieved by using the EGF pulse shapes with $\{\alpha = 2, \beta = 1.5\}$ and $\{\alpha = 3, \beta = 1.9\}$, respectively.

2.5.2 FTN Spectral Efficiency in Coexistence Scenarios

Here, a coexistence scenario is considered, where multiple heterogeneous devices communicate with the base station, including mobile services and Machine-Type

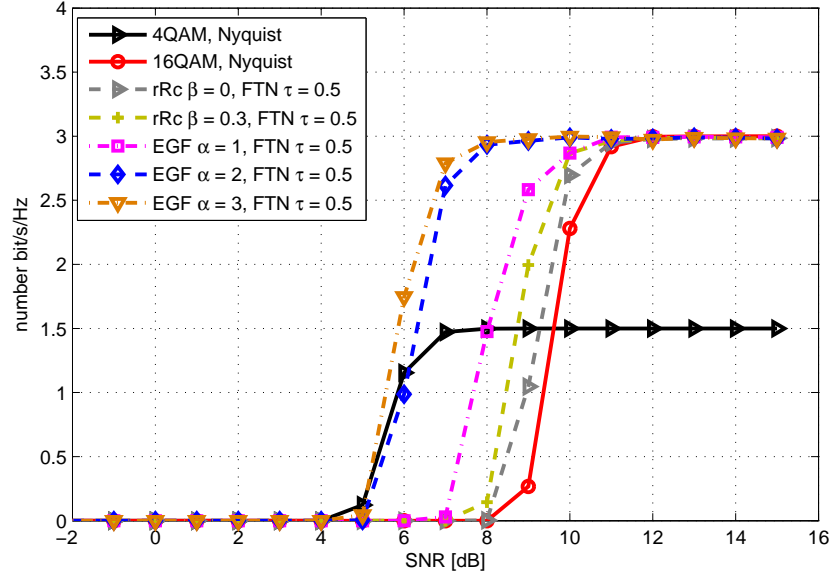


Figure 2.10: The SE comparison for FTN and Nyquist signaling using convolutional coding with a code rate of $3/4$

Communication (MTC). A certain fraction of the frequency band is allocated to each user/service. Due to low complexity and low PAPR, the SC technique is a promising candidate for MTC. As shown in previous subsection, in a single carrier system, FTN delivers higher bandwidth efficiency in comparison to the Nyquist signaling by increasing the data rate while keeping the bandwidth constant. In this subsection, a multiple-access channel is considered, where an SC system based on Nyquist or FTN signaling is operated in a band adjacent to a multi-carrier system. This leads to the question whether FTN signaling can improve spectral/bandwidth efficiency, where a loss in SE is caused by a required guard band needed to keep the co-channel interference under a predefined level. In other words, the main interest is here to show whether FTN can compensate the loss of SE caused by guard bands by adjusting the data rate higher than the rate known from the Nyquist criterion.

The considered coexistence scenario is illustrated in Fig. 2.11, assuming that the multi-carrier system occupies a frequency band of bandwidth W_{MC} . The remaining frequency band of bandwidth $W_{sc} = B - W_{MC}$ is allocated for the SC system including the Guard Band (GB) between two systems. The available frequency band B is divided into K virtual sub-carriers with a carrier spacing of Δf , and K_{ac} sub-carriers are active for the multi-carrier system. The following scenarios are considered:

- Scenario 1: the frequency band B is occupied completely by an Offset Quadrature Amplitude Modulation/Orthogonal Frequency-Division Multiplexing (OQAM/OFDM) system with $K_{ac} = K$
- Scenario 2: the frequency band B is occupied by an OQAM/OFDM and an SC Nyquist signaling system
- Scenario 3: the frequency band B is occupied by an OQAM/OFDM and an SC-FTN signaling system

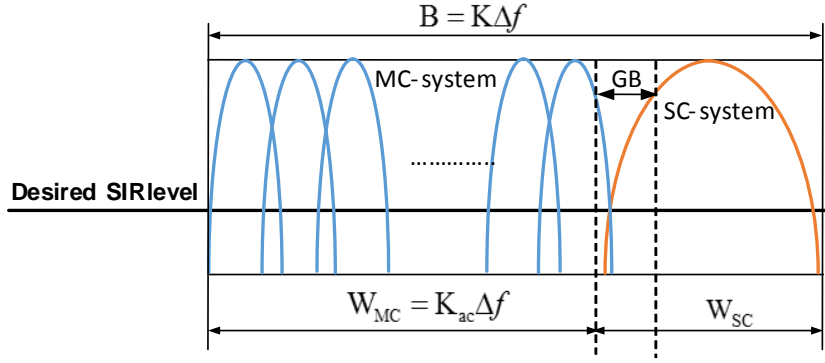


Figure 2.11: Multiple-access channel coexistence scenarios

In scenario 1, it is assumed that the multi-carrier system achieves the maximum SE for a given bandwidth B and it is considered as the reference system. In scenario 2 and 3, a guard band is required between two systems to keep the co-channel interference below a given threshold. As a result, the SE decreases with the increasing of the required guard band. The main aim of this subsection is to show whether FTN can compensate the SE loss, so that scenario 3 achieves the same SE as in scenario 1. In the following, the analysis of the co-channel interference is presented first, followed by the SE analysis of the considered scenarios.

To evaluate the coexistence performance in terms of co-channel interference and SE, all simulations are performed for 1000 frames, each consisting of 10^4 bits, and different modulation pulse shaping filters are used. For SC systems an oversampling factor of 8 is considered for the used pulse shapes. All pulse shapes have an overlapping factor of 4. The whole frequency band B is divided into 128 virtual sub-carriers. It is assumed that the MC and SC systems use the same modulation scheme, channel coding and pulse shape.

2.5.2.1 Interference of Multi-access Channel Analysis

In OQAM/OFDM systems, the discrete transmit signal $s(n)$ can be expressed as

$$s(n) = \sum_{m=-\infty}^{\infty} \sum_{k=-K/2}^{k=K/2-1} j^{m+k} d_{k,m} p_k(n - m\tau_0 K), \quad (2.13)$$

where $d_{k,m}$ is a real valued OQAM/OFDM symbol, which is mapped to the k -th sub-carrier at the m -th OQAM/OFDM symbol. The parameter K represents the total number of sub-carriers and $p_k(n - m\tau_0 K)$ is the real valued and even transmit pulse shape modulated to sub-carrier k at the m -th symbol. In general, the transmit pulse shape $p_k(n)$ is given by

$$p_k(n) = p(n) e^{j2\pi\nu_0 k \frac{n}{K}}. \quad (2.14)$$

Here, the normalized symbol duration $\tau_0 = 0.5$ and the normalized sub-carrier spacing $\nu_0 = 1$ are specified for the OQAM/OFDM system. At the receiver side,

after applying the modulated receiver pulse shape $q_{\tilde{k}}(n) = p_{\tilde{k}}^*(-n)$, the estimated real-valued OQAM symbol $\hat{d}_{\tilde{k},\tilde{m}}$ can be calculated using

$$\hat{d}_{\tilde{k},\tilde{m}} = \Re \left\{ j^{-(\tilde{k}+\tilde{m})} r(n) * q_{\tilde{k}}(n) \Big|_{n=\tilde{m}\tau_0 K} \right\}, \quad (2.15)$$

where $r(n)$ is the received signal. In the coexistence scenarios 2 and 3, the received signal at the OQAM/OFDM receiver for the ideal transmission is given by

$$r_{mc}(n) = s_{mc}(n) + s_{sc}(n) + w(n), \quad (2.16)$$

where $s_{mc}(n)$ and $s_{sc}(n)$ are the OQAM/OFDM and SC transmit signals given by (2.13) and (2.17), respectively. The signal $w(n)$ stands for the noise at the OQAM/OFDM receiver. In order to determine the required guard band between MC and SC systems, it is of interest to investigate the interference caused from the SC system to the edge sub-carrier of the OQAM/OFDM system, which is denoted as the neighbor sub-carrier of the SC system. Assuming that f_{sc} is the center frequency of the SC system and that it corresponds to the l -th sub-carrier in the virtual sub-carrier grid of K carriers and \tilde{k} is the neighbor sub-carrier of the SC system, the transmit signal of the SC system can be expressed as

$$s_{sc}(n) = s_{ftn}(n) e^{j2\pi n \frac{1}{K}}, \quad (2.17)$$

where the signal $s_{ftn}(n)$ is given by (2.1). Inserting (2.13) and (2.17) into (2.16) results in the following general expression for the estimation of the received OQAM/OFDM symbol $d_{\tilde{k},\tilde{m}}$

$$\hat{d}_{\tilde{k},\tilde{m}} = \Re \left\{ j^{-(\tilde{k}+\tilde{m})} r_{mc}(n) * q_{\tilde{k}}(n) \Big|_{n=\tilde{m}\tau_0 K} \right\}. \quad (2.18)$$

Consequently, the interference power caused by the SC system to the estimated real-valued OQAM/OFDM symbol $\hat{d}_{\tilde{k},\tilde{m}}$ is determined using

$$I_{re}(\tilde{m}, \tilde{k}) = \left| \Re \left\{ j^{-(\tilde{k}+\tilde{m})} s_{sc}(n) * q_{\tilde{k}}(n) \Big|_{n=\tilde{m}\tau_0 K} \right\} \right|^2, \quad (2.19)$$

Inserting (2.1) and (2.17) into (2.19) results in

$$I_{re}(\tilde{m}, \tilde{k}) = \left| \Re \left\{ j^{-(\tilde{k}+\tilde{m})} \sum_{n=-\infty}^{\infty} \sum_m d_m p(n-\mu) q(n) e^{-j2\pi n \frac{\nu}{K}} \right\} \right|^2, \quad (2.20)$$

where $\mu = m\tau P - \tilde{m}\tau_0 K$ represents the time or symbol offset between the two systems. $\nu = l - \tilde{k}$ is the sub-carrier offset, which corresponds to the frequency distance between the two coexisting systems. Assuming $\mathbb{E}\{|d_m|^2\} = 1$ and utilizing the cross-ambiguity function $A(\mu, \nu)$ given by

$$A(\mu, \nu) = \sum_{n=-\infty}^{\infty} p(n-\mu) q^*(n) e^{-j2\pi n \frac{\nu}{K}}, \quad (2.21)$$

equation (2.20) can be rewritten as

$$I_{re}(\tilde{m}) = \left| \Re \left\{ j^{-(\tilde{k}+\tilde{m})} A(\mu, \nu) \right\} \right|^2. \quad (2.22)$$

Since transmitted symbols of the SC system are complex and the transmitted Pulse-Amplitude Modulation (PAM) symbol of the OQAM/OFDM system is either in-phase (real part) or the quadrature (imaginary part) components of complex QAM symbols, the interference power is calculated using

$$I(\tilde{m}, \tilde{k}) = \max \{ I_{re}(\tilde{m}), I_{im}(\tilde{m}) \}, \quad (2.23)$$

where $I_{im}(\tilde{m}, \tilde{k}) = \left| \Im \left\{ j^{-(\tilde{k}+\tilde{m})} A(\mu, \nu) \right\} \right|^2$.

As mentioned above, the interference from the SC Nyquist signaling system to the edge sub-carrier of OQAM/OFDM system depending on the frequency distance ν is investigated. Fig. 2.12 depicts the coexistence performance in terms of interference leakage for different pulse shapes, where the frequency distance ν is counted in number of virtual subcarriers. It can be seen that the frequency distance and the required guard band between two systems scale with the excess bandwidth β of the applied pulse shape.

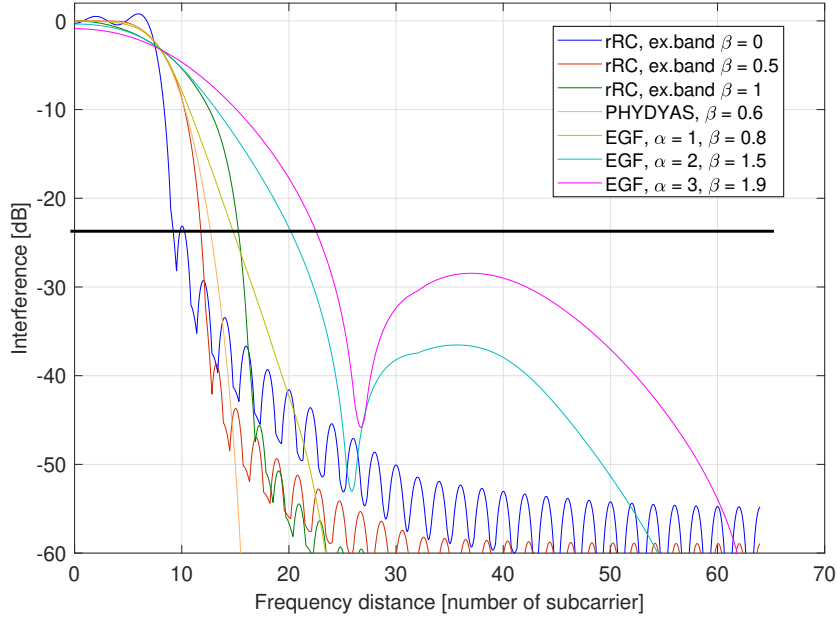


Figure 2.12: Interference power versus frequency distance

The frequency distance between the MC and SC systems for an interference value of around -22 dB is given in Table 2.3. This Table shows that at this interference level for all pulse shapes, the frequency distance ν is equivalent to $\frac{(1+\beta)K}{2P}$ [number of subcarrier]. In general, W_{sc} in Fig. 2.11 is defined as

$$W_{sc} = W_{puls} + GB, \quad (2.24)$$

where W_{puls} is the bandwidth of the pulse shape used in SC system and it is given by

$$W_{puls} = \frac{1 + \beta}{P}. \quad (2.25)$$

Here, the equivalent subcarrier allocated to the SC system can be determined by

$$W_{\text{puls}} = \frac{(1 + \beta) K}{P} [\text{number of subcarrier}]. \quad (2.26)$$

According to (2.26), we have $v = W_{\text{puls}}$. This mean that in this case, $GB = 0$ and the loss in the SE only caused by the excess bandwidth of the pulse shape used in SC system.

Pulse shape	Frequency distance (Eq. number of subcarriers)
rRC $\beta = 0$	≈ 8
rRC $\beta = 0.5$	≈ 12
rRC $\beta = 1$	≈ 16
PHYDYAS $\beta = 0.6$	≈ 13
EGF, $\beta = 0.8$	≈ 15
EGF, $\beta = 1.5$	≈ 20
EGF, $\beta = 1.9$	≈ 23

Table 2.3: The frequency distance between MC and SC systems at an interference level of around -22 dB for different pulse shapes

2.5.2.2 Spectral Efficiency Analysis

For a given allocated bandwidth $[-W, W]$, the optimal Nyquist pulse shape is a sinc pulse shape with a symbol duration of $T = \frac{1}{2W}$. However, a sinc pulse shape is impractical, and thus a typically rRC pulse shape with the excess bandwidth factor β is used. If a rRC pulse occupies the same bandwidth $[-W, W]$, a symbol duration of $T = \frac{1+\beta}{2W}$ can be chosen for having ISI-free transmission. Thus, in comparison to the sinc pulse, a rRC pulse suffers a loss in SE of $\frac{1}{1+\beta}$. In FTN signaling, by setting $\tau T < \frac{1+\beta}{2W}$ the loss can be reduced. For a given bandwidth B , the achieved SE (the normalized data rate) η , at high SNRs is calculated according to

$$\eta = \frac{R}{B} = \frac{R_c \log_2 M}{TB}, \quad (2.27)$$

where R stands for the achieved sum rate and R_c represents the channel code rate. The parameters M and T are the modulation order and symbol duration, respectively. In scenario 1, where only an OQAM/OFDM system operates in the whole frequency band B , the SE of this scenario is given as

$$\eta_1 = \frac{KR_c \log_2 M}{T_{\text{oqam}} B}. \quad (2.28)$$

Here, T_{oqam} is the OQAM/OFDM symbol duration. Assuming that $B = \frac{K}{T_{\text{oqam}}}$ and $\Delta f = \frac{B}{K}$ results in

$$\eta_1 = R_c \log_2 M. \quad (2.29)$$

In the coexistence scenario 2 and 3, it is assumed that both MC and SC systems have the same code rate and modulation order, the achieved sum rate at high SNRs is calculated using

$$R = \underbrace{\left(K - \frac{KW_{sc}}{B} \right) R_c \log_2 M}_{\text{Rate of OQAM/OFDM system}} + \underbrace{\frac{R_c \log_2 M}{\tau T_{sc}}}_{\text{Rate of SC system}}. \quad (2.30)$$

where $W_{sc} = B - W_{MC}$ is the allocated bandwidth for the SC system including the required guard band, and T_{sc} is the Nyquist symbol duration of the SC system. Inserting (2.30) into (2.27) with $B = F_s$ and $T_{sc} = PF_s$ results in

$$\eta_C = \left(1 - \frac{W_{sc}}{B} + \frac{1}{\tau P} \right) R_c \log_2 M, \quad (2.31)$$

where η_C with $\tau = 1$ and $\tau < 1$ stands for the SE of scenario 2 and 3, respectively.

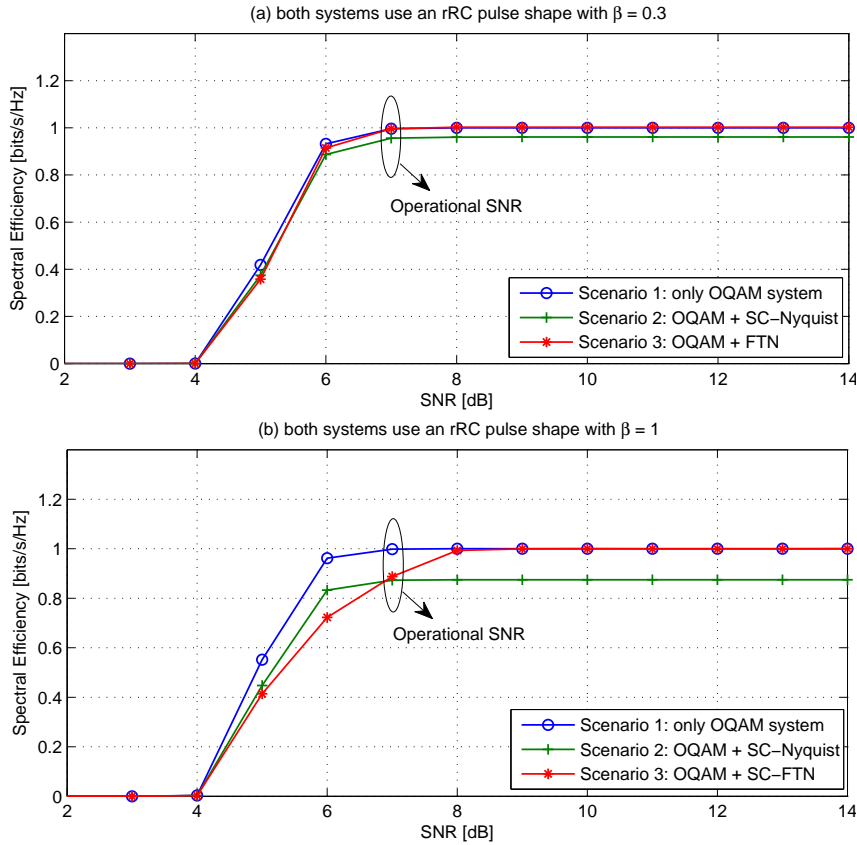


Figure 2.13: SE of three considered scenarios at an interference power of -22 dB with a code rate of 1/2

According to (2.31), it can be seen that in the considered multiple-access channel a loss in SE is incurred due to the guard band between two systems. In scenario 2, the loss in SE increases with the increasing of the guard band. Furthermore, in the SC system the excess bandwidth of used pulse shape also results in a SE loss. In scenario 3, by choosing an appropriate FTN factor τ , the loss in SE can be compensated.

Here, in order to assess the FTN system performance in terms of SE, a single user OQAM/OFDM system is considered as the reference system (scenario 1). Assuming that in scenario 1, the OQAM/OFDM system achieves the maximum SE. Note that for any W_{SC} , in order to compensate the SE loss in coexistence scenarios 2 and 3, we have to adjust the FTN factor τ according to (2.31). To keep the interference power below -22 dB and to recover the SE loss we have to set the FTN factor $\tau = 0.7692 \approx 0.75$ and $\tau = 0.5$ for the case of using an rRC pulse shape with $\beta = 0.3$ and $\beta = 1$, respectively.

Fig. 2.13 illustrates the SE for the cases that both MC and SC systems use a rRC pulse shape of $\beta = 0.3$ and $\beta = 1$. Here, a code rate of $1/2$ is used. Fig. 2.13 indicates that SE of coexistence scenario 2 is smaller than that of scenario 1. Furthermore, in scenario 3, FTN signaling can recover completely the loss in SE at high SNRs. An interesting observation is that FTN signaling can start to recover the SE loss from an SNR value of 6 dB and 7 dB for the case of $\beta = 0.3$ and $\beta = 1$, respectively. For large SNR values, the SE loss is completely recovered. It can be seen, that in the case of $\beta = 0.3$, due to small guard band the SE curve of scenario 3 is very close to that of scenario 1, and from an SNR value of 7 dB, where the OQAM/OFDM system starts to achieve the maximum SE (operational SNR), the loss is already recovered.

The SE loss and the corresponding equivalent guard band at an SNR value of (6 and 7 dB) and (7 and 8 dB) for the case of $\beta = 0.3$ and $\beta = 1$ are given in Table 2.4, respectively. Here, in case of $\beta = 1$, at an SNR value of 7 dB only 1% SE loss can be recovered using FTN. This can be explained by the large guard band and excess bandwidth. For a large guard band/excess bandwidth, in order to recover the SE loss we have to set a smaller value for τ , which leads to a poor BLER performance of the system due to high ISI in FTN system.

Pulse shape	Performance	Scenario 2		Scenario 3			
		SNR	SE loss	Eq.Guard band (nCarr)	SNR	SE loss	Eq.Guard band (nCarr)
rRC $\beta = 0.3$	SNR	6 dB	7 dB	6 dB	7 dB		
	SE loss	$\approx 4\%$	4%	0%	0%		
	Eq.Guard band (nCarr)	≈ 6	≈ 6	0	0		
rRC $\beta = 1$	SNR	7 dB	8 dB	7 dB	8 dB		
	SE loss	13%	12.5%	12%	0.6%		
	Eq.Guard band (nCarr)	≈ 17	≈ 16	≈ 15	≈ 1		

Table 2.4: SE loss and related equivalent guard band of coexistence scenarios

For a small guard band, the SE performance at an interference power of -15 dB is considered. At this interference level, the frequency distance ν is about 13 virtual subcarriers (see Fig. 2.12) corresponding to $W_{SC} \approx 29$ sub-carriers. According to (2.31), in order to recover the SE loss we have to set the FTN signaling factor $\tau = 0.552 \approx 0.6$. The SE for this case is shown in Fig. 2.14. It can be seen that due to the smaller guard band correspondingly a larger τ is needed, thus the SE curve of scenario 3 is close to that of scenario 1. However, due to the rounding applied for factor $\tau = 0.6 > 0.552$, FTN does not fully achieve the maximum SE.

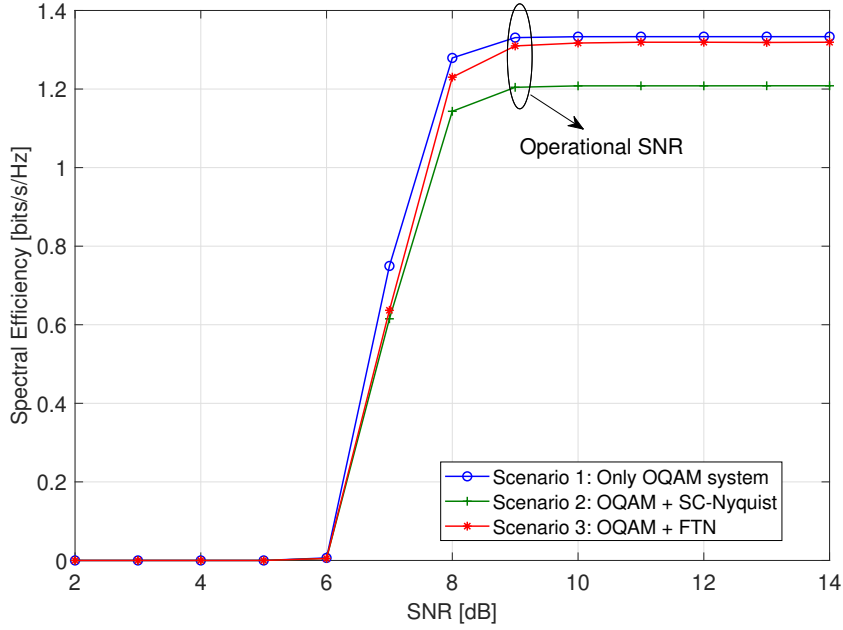


Figure 2.14: SE of three considered scenarios at an interference power of -15 dB using a rRC pulse shape $\beta = 1$ with a code rate of $2/3$

2.6 SUMMARY

As mentioned above, FTN signaling can improve the bandwidth efficiency by increasing the data rate over the Nyquist rate while keeping the bandwidth constant. However, the cost for this is high receiver complexity due to ISI caused by FTN signaling. In this chapter, the practical benefits of FTN signaling is investigated and discussed. To this, an introduction to FTN signaling is given in Sections 2.1 and 2.2. An overview of the considered pulse shapes is presented in Section 2.3.

In Section 2.4, the SC-FTN system performance in terms of BER, PAPR and SE is investigated and compared to that of the SC Nyquist signaling given that both systems use the same pulse shape. In the case that both systems have the same modulation scheme, simulation results confirm that the BER and PAPR of FTN signaling increase with the decreasing value of τ . However, in this case, FTN has an advantage of higher data rate in comparison to the Nyquist signaling. In addition, it is shown that FTN provides benefits in terms of SE, BER and PAPR in comparison to the Nyquist signaling with the same data rate by using a pulse shape with a large excess bandwidth factor. In this case, the gains achieved by FTN increase with the rising of the excess bandwidth factor β .

In Section 2.5, the SE of two coexistence scenarios is evaluated and discussed, where a single-carrier system using the Nyquist or FTN signaling shares spectrum with a multi-carrier system. The simulation results show that FTN signaling can recover completely the loss of SE due to guard bands between systems and excess bandwidth of the applied pulse shape at high SNRs. For any other operational SNR, the SE loss can be regained by choosing an appropriate FTN rate. In coexistence scenarios with small guard band and excess bandwidth, by using FTN signaling the SE curve is close to that of the single-user reference system. This leads to the

conclusion that FTN signaling technique is able to improve the SE in wireless communication systems.

3

MIMO-OFDM TECHNIQUES

3.1 INTRODUCTION TO MIMO TECHNIQUE

In the chapter 2, we discussed about the FTN signaling, which can increase the data rate by reducing the symbol period T below the Nyquist criterion. This approach seems to be simple but suffers disadvantage of very high system complexity as a result of the associated ISI. In general, the data rate can also be boosted by increasing the bandwidth or the SNR power. However, increasing the signal power leads to another problem such as decreasing the battery lifetime and requiring a expensive Radio Frequency (RF) amplifier. In addition, it is difficult to increase the bandwidth in practice due to the fact that frequency resource is expensive and almost always bound to certain applications. To overcome these problems, MIMO transmission technique is employed. It is a well-known fact that using MIMO technology, SE is much higher than that of the conventional Single-Input and Single-Output (SISO) transmission scheme. Nowadays, MIMO systems are already widely implemented in several modern wireless standards such as IEEE 802.11n, LTE and mobile Worldwide Interoperability for Microwave Access (WiMAX). The particular benefits of MIMO technology are boosting the system capacity without increasing the bandwidth and the signal power, robustness and enhancing the reliability of the communication link.

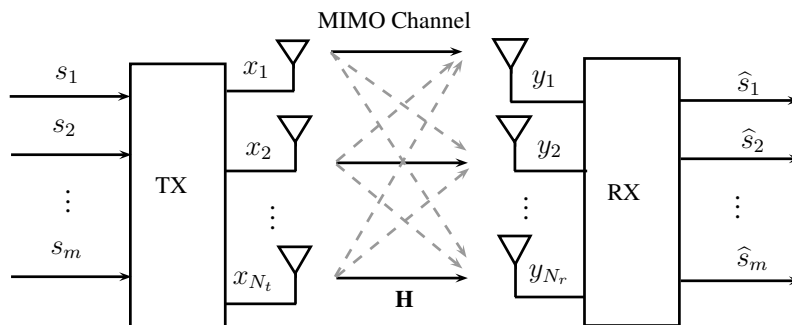


Figure 3.1: General block diagram of a MIMO system

A MIMO system with N_t transmit and N_r receive antennas is depicted in Fig. 3.1, where x_k and y_l are the transmitted and received signal at the k -th transmit and l -th receive antenna, respectively. Assuming a flat fading MIMO channel results in

$$\mathbf{y} = \mathbf{H}\mathbf{x} + \mathbf{n}, \quad (3.1)$$

where \mathbf{H} stands for a $N_t \times N_r$ complex channel matrix and given by

$$\mathbf{H} = \begin{pmatrix} h_{11} & h_{12} & \cdots & h_{1N_t} \\ h_{21} & h_{22} & \cdots & h_{2N_t} \\ \vdots & \vdots & \ddots & \vdots \\ h_{N_r1} & h_{N_r2} & \cdots & h_{N_rN_t} \end{pmatrix}. \quad (3.2)$$

Here, $h_{lk} \forall l, k$ represents the complex channel coefficients from transmit antenna k to receive antenna l . $\mathbf{x} = [x_1, x_2, \dots, x_{N_t}]^T$ and $\mathbf{y} = [y_1, y_2, \dots, y_{N_r}]^T$ are the $N_t \times 1$ complex transmitted and $N_r \times 1$ received signal vector, respectively. The additive noise vector is denoted by $\mathbf{n} = [n_1, n_2, \dots, n_{N_r}]^T$ with $\mathbf{R}_{nn} = \mathbb{E}[\mathbf{n}_k \mathbf{n}_k^H] = \sigma_n^2 \mathbf{I}_{N_r}$, where \mathbf{I}_{N_r} is an $N_r \times N_r$ identity matrix. Considering a time-invariant flat fading MIMO channel with perfect CSI, the MIMO channel capacity can be expressed as below [32]:

$$C = \max_{\mathbf{Q}_x: \text{Tr}\{\mathbf{Q}_x\} \leq P_0} \mathbb{E} \left\{ \log_2 \det \left(\mathbf{I}_{N_r} + \frac{1}{\sigma_n^2} \mathbf{H} \mathbf{Q}_x \mathbf{H}^H \right) \right\} \quad (3.3)$$

with $\mathbf{Q}_x = \mathbb{E} \{ \mathbf{x} \mathbf{x}^H \}$ the covariance matrix of \mathbf{x} . Here $\det(\cdot)$ stands for the determinant operation. The transmit power constraints is denoted by $\text{Tr}\{\mathbf{Q}_x\} \leq P_0$, where P_0 is the maximum transmit power. If no CSI is available at the transmitter side, the MIMO channel capacity can be expressed as [32]

$$C_{\text{no-CSI}} = \mathbb{E} \left\{ \log_2 \det \left(\mathbf{I}_{N_r} + \frac{P_0}{N_t \sigma_n^2} \mathbf{H} \mathbf{H}^H \right) \right\}. \quad (3.4)$$

Here, it is assumed that all transmit antennas have the same transmit power and it leads to

$$\mathbf{Q}_x = \frac{P_0}{N_t} \mathbf{I}_{N_t}. \quad (3.5)$$

In comparison to the conventional SISO systems, MIMO systems provide a number of advantages such as array gain, spatial diversity gain and spatial multiplexing gain as well as interference reduction.

The array gain is an SNR improvement at the receiver, which can be achieved in a Single-Input and Multiple-Output (SIMO), Multiple-Input and Single-Output (MISO) as well as in a MIMO system. In a system with multiple receive antennas, the receive signal power is enhanced through a coherent combining of the received signals, which results in an increase of SNR. In a system with multiple transmit antennas, if Channel State Information at Transmitter (CSIT) is available, the array gain can be obtained by using beamforming technique. This means that the transmitter will weight its transmission with different factors depending on the channel quality. In general, the array gain depends on the number of transmit and receive antennas.

The spatial multiplexing gain denotes an improvement of the data rate in a MIMO system with the same bandwidth and transmit power as in a SISO system. In this case, the spatial diversity gain is achieved by transmitting multiple parallel independent data streams over the same time-frequency resources. This also leads to an enhancement of the channel capacity.

Through providing multiple independent copies of the same transmitted signal at the receiver, the MIMO technique delivers spatial diversity, which is used to combat the effects of a multi-path fading channel. In this way, the probability that all signals fade simultaneously is reduced resulting in a significant improvement of the quality and reliability of reception. The full spatial diversity gain can only be achieved if the antenna spacing is large enough (more than 10λ) to ensure the statistical independence of different fading channels. A MIMO system with N_t and N_r transmit and receive antennas offers a spatial diversity order (maximum diversity) of $(N_t N_r)$ due to having $(N_t N_r)$ independent fading channels [14]. Generally, the space diversity is divided into two groups: transmit and receive diversity. The receive diversity is obtained by combining the received signals from different receive antennas. The existing combining techniques reported in literature are selection combining, Maximal Ratio Combining (MRC) and Equal Gain Combining (EGC). Transmit diversity can be provided by beamforming in case of having CSIT or by Space-time Block Coding (STBC) if channel knowledge is not available at the transmitter side.

Interference in wireless communication networks is normally resulted by overlapping of multiple different transmitted signals in time and frequency dimensions. Interference can be mitigated using the MIMO technique by exploiting space dimensions to separate the signals. In this case, the array gain can improve the Signal-to-Interference-plus-Noise Ratio (SINR) by increasing the tolerance to noise and interference power. In addition, the space dimension can help to forward the signal energy to the desired receiver and minimize the interference to other receivers. This leads to an improvement in terms of SE and coverage.

3.1.1 Space-Time Block Code

STBC is a simple transmit diversity technique in MIMO systems provided by mapping input symbols across time and space. This approach can maximize the transmitted information rate and minimize the error probability by adding proper redundancy in both spatial and time domains, which introduces correlation into the transmitted signal.

The first studied STBC scheme is the Alamouti code scheme, which was developed by Alamouti in [4] and is a complex orthogonal space-time code specified for a system with two transmit antennas. The first investigation of the Alamouti scheme was for a 2×1 MISO system. In this case, the encoder takes a block of two complex modulated symbols x_1 and x_2 to generate a code matrix \mathbf{A} with

$$\mathbf{A} = \begin{bmatrix} x_1 & -x_2^* \\ x_2 & x_1^* \end{bmatrix}. \quad (3.6)$$

The first and second columns of \mathbf{A} represent the first and second transmission period, respectively. Here, the first row of \mathbf{A} corresponds to the symbols transmitted from the first antenna. The second row stands for the symbols transmitted from the second antenna. In other words, at a given symbol period symbols x_1 and x_2 are simultaneously transmitted from the first and second antenna, respectively.

During the next symbol period, the first antenna transmits symbol $-x_2^*$ and the second antenna transmits symbol x_1^* , where x_1^* and x_2^* are the complex conjugate of x_1 and x_2 , respectively. This leads to

$$\begin{aligned}\mathbf{A}_1 &= [x_1, -x_2^*] \\ \mathbf{A}_2 &= [x_2, x_1^*],\end{aligned}\quad (3.7)$$

where \mathbf{A}_1 and \mathbf{A}_2 are the information sequences from antenna 1 and 2, respectively. It can be seen that the symbol sequences \mathbf{A}_1 and \mathbf{A}_2 are orthogonal to each other. It is assumed that the channel coefficients are constant within two consecutive symbol transmission periods, which means that

$$h_i(t) = h_i(t+T) = h_i, \quad \forall i = 1, 2. \quad (3.8)$$

Here T is the symbol duration and h_i is the channel coefficient between receive and transmit antenna i . Accordingly, the received signals for both time slots are given by

$$\begin{aligned}y(t) &= y_1 = h_1x_1 + h_2x_2 + n_1 \\ y(t+T) &= y_2 = -h_1x_2^* + h_2x_1^* + n_2,\end{aligned}\quad (3.9)$$

where y_1 and y_2 are the received signals at time t and $t+T$, respectively and n_1, n_2 are additive white Gaussian noise. Assuming perfect knowledge of the channel information at the receiver side, the received signals can be combined as follows

$$\begin{aligned}\tilde{x}_1 &= h_1^*y_1 + h_2y_2^* \\ \tilde{x}_2 &= h_2^*y_1 - h_1y_2^*.\end{aligned}\quad (3.10)$$

Substituting (3.9) into (3.10) results in

$$\begin{aligned}\tilde{x}_1 &= (|h_1|^2 + |h_2|^2)x_1 + h_1^*n_1 + h_2n_2^* \\ \tilde{x}_2 &= (|h_1|^2 + |h_2|^2)x_2 + h_2^*n_1 - h_1n_2^*\end{aligned}\quad (3.11)$$

In (3.11), it can be seen that transmitted symbol x_1, x_2 can be estimated from the combined signal \tilde{x}_1 and \tilde{x}_2 using the maximum likelihood detector.

The Alamouti principle can also be applied for a 2×2 MIMO system. The concept of the Alamouti scheme has been extended for an arbitrary number of transmit antennas. The objective of this orthogonal space-time coding scheme is to achieve the full diversity order of $N_t N_r$ and minimize the BER of the transmission. The general concept of STBC is illustrated in Fig. 3.2, where N is number of symbol in each STBC block, and L stands for the length of a STBC block. In this regard, the encoder matrix \mathbf{A} has a dimension of $N_t \times L$. Here, the code rate is defined as $R = \frac{N}{L}$. For the cases of having $N_t = 3$ and $N_t = 4$ and $R = 1/2$, the corresponding code matrices \mathbf{A}_3 and \mathbf{A}_4 are given as below [105]:

$$\mathbf{A}_3 = \begin{bmatrix} x_1 & -x_2 & -x_3 & -x_4 & x_1^* & -x_2^* & -x_3^* & -x_4^* \\ x_2 & x_1 & x_4 & -x_3 & x_2^* & x_1^* & x_4^* & -x_3^* \\ x_3 & -x_4 & x_1 & x_2 & x_3^* & -x_4^* & x_1^* & x_2^* \end{bmatrix}, \quad (3.12)$$

$$\mathbf{A}_4 = \begin{bmatrix} x_1 & -x_2 & -x_3 & -x_4 & x_1^* & -x_2^* & -x_3^* & -x_4^* \\ x_2 & x_1 & x_4 & -x_3 & x_2^* & x_1^* & x_4^* & -x_3^* \\ x_3 & -x_4 & x_1 & x_2 & x_3^* & -x_4^* & x_1^* & x_2^* \\ x_4 & -x_3 & -x_2 & x_1 & x_4^* & x_3^* & -x_2^* & x_1^* \end{bmatrix}. \quad (3.13)$$

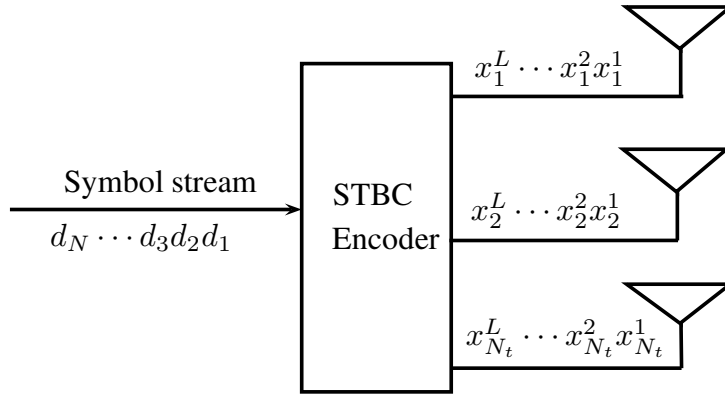


Figure 3.2: Block diagram of a STBC encoder in a MIMO system

3.1.2 Linear Pre-coding

Linear pre-coding is a beamforming technique applied in MIMO systems, which exploits the CSI to improve the system performance by splitting the transmitted signal into orthogonal spatial eigen-beams. These beams are assigned with different power, namely; high power for the beams where the channel is strong and low or no power for the beams with the weak channels. At the transmitter side, the CSI can be available partially, completely, perfect or imperfect. Therefore, there are various pre-coding design methods proposed in literature depending on the type of CSI and the system performance criterion. In the framework of this thesis, different linear pre-coding schemes are considered under the assumption of having different CSI conditions. In the following, an overview about the methods to acquire CSI at the transmitter and the existing pre-coding techniques applied in MIMO systems is given.

3.1.2.1 Channel Acquisition Methods

In wireless communication systems, by using pilot technique the channel can be estimated at the receiver side. Then, the transmitter can acquire the information about the channel by using either the reciprocity principle of the network or feedback from the receiver. The reciprocity principle is that the channel from antenna A to antenna B is identical to the transpose of the channel from antenna B to antenna A, i.e. $\mathbf{H}_{A \rightarrow B} = \mathbf{H}_{B \rightarrow A}^T$. This reciprocity relation can only be achieved if both forward and reverse links operate at the same time in the same frequency band

and with the same antenna locations, which do not hold in most practical systems. In practice, the channel acquisition based on reciprocity is also known as the open-loop method and it is usually applied in Time-Division Duplex (TDD) systems. In TDD systems, although forward and reverse links use the same frequency band and antennas, the reciprocity can only be achieved when the time lag between the forward and reverse link is much smaller than the channel coherence time. Consequently, this method requires transmit-receive chain calibration due to the fact that transmitter and receiver have different radio frequency hardware chains [14].

Another approach to obtain CSIT is by using feedback from the receiver to the transmitter. This means that first the receiver measures channels, and then sends these channel measurements on the reverse link back to the transmitter. This approach is normally referred to as the closed-loop method and it is often used in Frequency-Division Duplex (FDD) systems [14]. Although this channel acquisition method does not require any hardware calibration, it introduces limited feedback problem such as feedback delay and feedback overhead. Therefore, the methods such as quantizing feedback information is very important and necessary in wireless communication systems to overcome these problems. In practice, the following CSI feedback approaches are considered [32];

1. Direct CSI feedback: in this case, the receiver quantizes all elements in a measured channel matrix and then sends them back to the transmitter, [35] [32]. As an alternative, the receiver can analogously modulate all elements in a channel matrix and then sends them back to the transmitter. Furthermore, the study in [88] reports that the receiver can also apply the vector quantization technique on the channel matrix column by column and then sends the indication of the vector back to the transmitter. As a result, the transmitter can reconstruct the channel matrix from the quantized CSI feedback. This CSI feedback method delivers the best performance, but it is difficult to realize in practical systems due to very high feedback overhead [88].
2. Statistical CSI feedback: in some applications, a full CSI is not required at the transmitter, but some statistical CSI is sufficient to manage the interference. In this case, the receiver extracts some statistical information from the channel such as covariance matrix, quantizes these parameters and then sends them back to the transmitter [32].
3. Feedback of transmission based on codebook searching [37], [82]: in some applications, a finite set of transmission recommendations is predefined by a codebook, which is available at both transmitter and receiver sides. Normally, codebook contains information such as channel Rank Indicator (RI), Precoding Matrix Indicator (PMI) and Channel Quality Indicator (CQI). While RI indicates the number of parallel sub-channels for a single or multiple stream transmission, PMI carries the spatial domain transmission information, and CQI measures the channel quality in terms of achievable payload size. In this case, depending on the information needed at the transmitter, the receiver searches corresponding information in codebook and sends the corresponding content back to the transmitter. This CSI feedback has numerous advan-

tages, for example low feedback overhead, simple implementation and low complexity (the CSI can be typically quantized within a few bits) [32].

3.1.2.2 Pre-coding with Perfect CSI

Given perfect CSIT, the channel matrix \mathbf{H} of a single user $N_r \times N_t$ MIMO system can be disassembled into m independent parallel sub-channels determined by the Singular Value Decomposition (SVD) of \mathbf{H} with

$$m = \text{rank}(\mathbf{H}) \leq \min(N_t, N_r). \quad (3.14)$$

Consequently, the SVD of \mathbf{H} results in

$$\mathbf{H} = \mathbf{U}_H \mathbf{\Lambda} \mathbf{V}_H^H, \quad (3.15)$$

where \mathbf{U}_H and \mathbf{V}_H are a $(N_r \times N_r)$ and $(N_t \times N_t)$ unitary matrix, respectively. $\mathbf{\Lambda}$ is a $(N_r \times N_t)$ diagonal matrix and its diagonal elements represent the singular values of matrix \mathbf{H} being square roots of eigenvalues of $\mathbf{H}\mathbf{H}^H$.

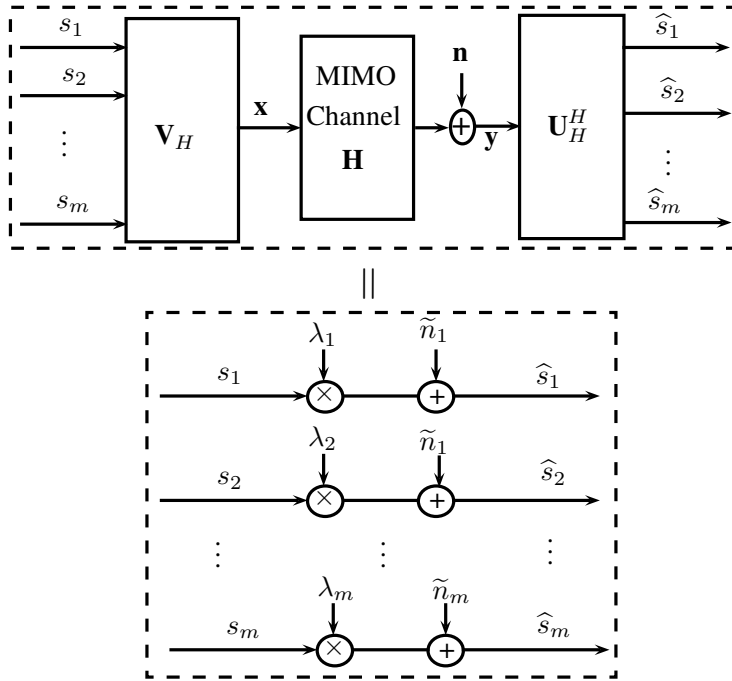


Figure 3.3: Block diagram of the pre-coding approach based on SVD for a MIMO system

The block diagram of the pre-coding approach based on SVD is depicted in Fig. 3.3, where m orthogonal sub-channels (SISO channels) are resulted by multiplying the transmitted signal with pre-coding matrix \mathbf{V}_H and the received signal with post-processing matrix \mathbf{U}_H^H . By doing so, the received signal after the post-processing matrix can be expressed as follow:

$$\begin{aligned} \hat{\mathbf{s}} &= \mathbf{U}_H^H \mathbf{H} \mathbf{V}_H \mathbf{s} + \mathbf{U}_H^H \mathbf{n} \\ &= \mathbf{\Lambda} \mathbf{s} + \mathbf{U}_H^H \mathbf{n} \end{aligned} \quad (3.16)$$

with

$$\hat{\mathbf{s}}_i = \begin{cases} \lambda_i s_i + \tilde{n}_i & 1 \leq i \leq m \\ 0 & m < i \leq N_r \end{cases} \quad (3.17)$$

where $\lambda_i^2 \forall i = 1, 2, \dots, m$ denotes the i -th eigenvalue of $\mathbf{H}\mathbf{H}^H$. Using this approach, the MIMO channel capacity in (3.3) can be reformulated as [32]

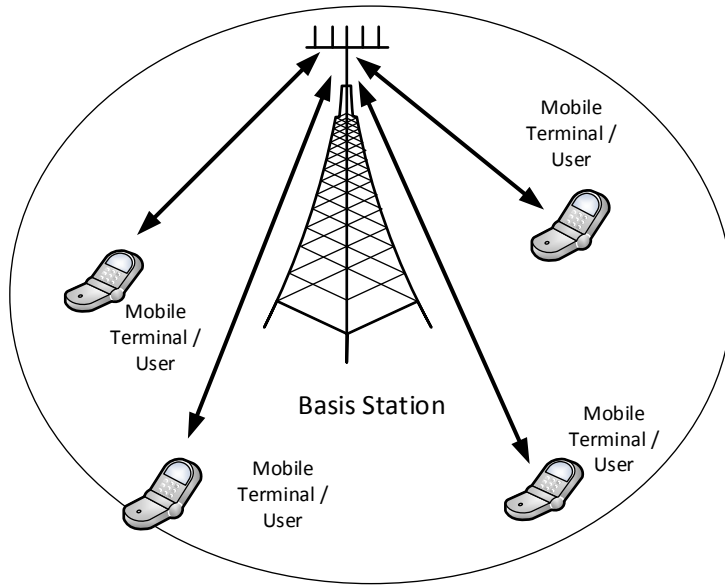
$$C = \sum_{i=1}^m \log_2 \left(1 + \frac{\lambda_i^2 P_i}{\sigma_n^2} \right) \text{ with respect to } \sum_{i=1}^m P_i = P. \quad (3.18)$$

Here, P_i stands for the transmit power allocated on the i -th sub-channel. Using the pre-coding based on SVD, the same transmit power is assigned into all sub-channels independent on the quality of each sub-channel. In this case, the maximum channel capacity can only be reached in high SNRs. To overcome this problem, the power allocation scheme based on the WF approach has been proposed in literature [55]. Using this approach, the optimal power allocation is guaranteed and the maximal channel capacity can be achieved. The concept of the WF principle is that higher power is allocated to the strong sub-channel and low or no power to the weak sub-channels. More detail about the WF approach will be given in chapter 5.

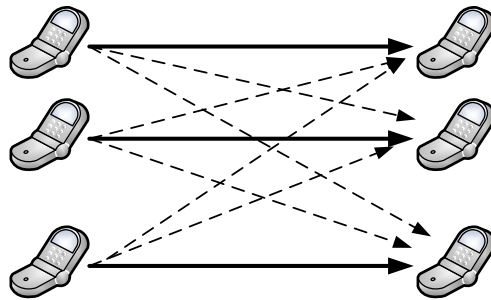
Besides the above-mentioned methods, different sub-optimal pre-coding methods can also be employed, whereby the pre-coding and post-processing filter matrices, \mathbf{V} and \mathbf{U} are optimized based on different optimization criterion such as the ZF, MMSE, maximum information rate, Quality of Service (QoS) or the maximum SNR. The pre-coding techniques applied in a single user MIMO system can also be extended to a multi-user MIMO system.

3.1.3 Multi-user MIMO Systems

As already mentioned above, the MIMO technique is one of the key solutions to achieve high SE, enhanced coverage and link reliability of a wireless communication system in fading environments. An extended concept to enhance the benefits of the MIMO technique, particularly SE, is the overlapping of Multi-user (MU)-MIMO transmission in both time and frequency resources. In contrast to a single-user MIMO system, a MU-MIMO system suffers not only the co-channel interference incurred by the MIMO technique, but also the MUI, which is a major problem in MU networks. To deal with this problem, several interference mitigation approaches have been proposed in literature [48], [103] [26],[102], [25]. Most of these approaches are based on beamforming or pre-coding techniques, which require the channel knowledge at both transmit and receiver sides. The typical MU-MIMO system scenarios are depicted in Fig. 3.4. In Fig. 3.4-a, a Base Station (BS) in a cellular network communicates simultaneously with multiple mobile stations (users). This communication can be established in both uplink and downlink channels. In this case, each user can be equipped with a single or multiple antennas. With assumption of no coordination among the users the MUI can normally be mitigated at the BS. In the uplink, where users transmit the signals to the same BS at the same time and in the same frequency, the signals are usually detected at the BS by



a) Downlink and Uplink MU-MIMO communication system



b) MU-MIMO Point-to-Point communication system

Figure 3.4: Single cell MU-MIMO scenarios

using multi-user detection methods. In the downlink, where the BS transmits the signal to the users simultaneously over the same channel, the interference can be mitigated either at each user or at the BS. However, the multi-user detection at the User Equipment (UE) is often costly for users. Thus, if the CSI is available at the BS, the interference has to be mitigated at the BS using the beamforming or pre-coding technique such as the channel inversion, block diagonalization and Dirty Paper Code (DPC), [25].

Channel inversion is a simple way to mitigate the MUI in downlink transmission schemes. In this case, the transmitted data streams are first pre-processed with the pseudo-inverse of the channel matrix \mathbf{H} . By doing this, an interference-free transmission is guaranteed. However, this approach is a good solution only for the MISO case at high SNRs. The drawbacks of this approach is that the channel matrix is not always invertible and the SNR at the receiver has to be reduced due to power constraints. Although, the channel inversion approach can also be extended to the case of having multiple receiver antennas, it is not an efficient solution due to large channel matrix. For this case, block diagonalization method can be employed,

which can be seen as a channel inversion scheme for MU-MIMO broadcast channels [25].

Unlike the conventional channel inversion method, by using the Block Diagonalization (BD) method MUI can be eliminated by the decomposition of a MU-MIMO broadcast channel into multiple single-user MIMO channels. In this case, the inter-channel interference for each MIMO user has to be mitigated using signal detection methods. Using the BD method, the received signal at user k can be expressed as follows [25]

$$\mathbf{y}_k = \mathbf{H}_k \mathbf{W}_k \mathbf{s}_k + \mathbf{H}_k \sum_{l=1, l \neq k}^K \mathbf{W}_l \mathbf{s}_l + \mathbf{n}_k, \quad (3.19)$$

where \mathbf{H}_k is the channel matrix between the BS and the k -th user and \mathbf{W}_k stands for the pre-coding matrix for user k . The matrix $\mathbf{W}_l \forall l = 1, \dots, K$ has to be designed so that $\mathbf{H}_k \mathbf{W}_l = 0$ for $l \neq k$. For this purpose, \mathbf{W}_l must lie in the null-space of the matrix

$$\mathbf{H}_{\text{block}}^k = [(\mathbf{H}_1)^H \cdots (\mathbf{H}_{l-1})^H \mathbf{H}_{l+1} \cdots (\mathbf{H}_K)^H]^H$$

[25]. By doing so, (3.19) can be reformulated as [25]

$$\begin{pmatrix} y_1 \\ y_2 \\ \vdots \\ y_K \end{pmatrix} = \begin{pmatrix} \mathbf{H}_1 \mathbf{W}_1 & 0 & \cdots & 0 \\ 0 & \mathbf{H}_2 \mathbf{W}_2 & \cdots & 0 \\ \vdots & \vdots & \ddots & \vdots \\ 0 & 0 & \cdots & \mathbf{H}_K \mathbf{W}_K \end{pmatrix} \begin{pmatrix} s_1 \\ s_2 \\ \vdots \\ s_K \end{pmatrix} + \begin{pmatrix} n_1 \\ n_2 \\ \vdots \\ n_K \end{pmatrix}. \quad (3.20)$$

(3.20) indicates that, by using the BD approach, parallel transmission of independent streams can be achieved. However, the eigenvalue decomposition of MU-MIMO broadcast channel requires high computational effort [56].

DPC technique is a pre-coding method that can cancel the MUI at the transmitter before transmission. The idea of the DPC technique is that due to having CSIT, the BS knows the interference introduced to user k . Thus, the transmitted signal for user k can be determined as follows [25]

$$\mathbf{s}_k^{\text{DPC}} = \mathbf{s}_k - \mathbf{I}_k, \quad (3.21)$$

where \mathbf{I}_k is interference caused by other users to user k . The best-known DPC method for downlink communication system is based on \mathbf{RQ} decomposition of the channel matrix \mathbf{H} [103]. In this case, the channel matrix \mathbf{H} can be \mathbf{RQ} -decomposed as [25]

$$\mathbf{H} = \underbrace{\begin{pmatrix} l_{11} & 0 & \cdots & 0 \\ l_{21} & l_{22} & \cdots & 0 \\ \vdots & \vdots & \ddots & \vdots \\ l_{K1} & l_{K2} & \cdots & l_{KK} \end{pmatrix}}_{\mathbf{L}} \underbrace{\begin{pmatrix} q_1 \\ q_2 \\ \vdots \\ q_K \end{pmatrix}}_{\mathbf{Q}} \quad (3.22)$$

Multiplication of the transmitted signal with matrix \mathbf{Q}^H results in

$$\mathbf{y} = \mathbf{H}\mathbf{Q}^H \mathbf{s} + \mathbf{n} \quad (3.23)$$

$$= \begin{pmatrix} l_{11} & 0 & \cdots & 0 \\ l_{21} & l_{22} & \cdots & 0 \\ \vdots & \vdots & \ddots & \vdots \\ l_{K1} & l_{K2} & \cdots & l_{KK} \end{pmatrix} \begin{pmatrix} s_1 \\ s_2 \\ \vdots \\ s_K \end{pmatrix} + \begin{pmatrix} n_1 \\ n_2 \\ \vdots \\ n_K \end{pmatrix}.$$

It can be seen that after pre-coding, the first user does not suffer any interference from others users and the particular user suffers interference only from previous users. However, these interferences are known at the BS, thus this interference can be canceled for user k . In this regard, cancellation of all interferences (3.23) can be reformulated as [25]

$$\begin{aligned} \mathbf{y} &= \begin{pmatrix} l_{11} & 0 & \cdots & 0 \\ l_{21} & l_{22} & \cdots & 0 \\ \vdots & \vdots & \ddots & \vdots \\ l_{K1} & l_{K2} & \cdots & l_{KK} \end{pmatrix} \begin{pmatrix} 1 & 0 & \cdots & 0 \\ -\frac{l_{21}}{l_{22}} & 1 & \cdots & 0 \\ \vdots & \vdots & \ddots & \vdots \\ -\frac{l_{K1}}{l_{KK}} & \frac{l_{K2}}{l_{KK}} & \cdots & 1 \end{pmatrix} \begin{pmatrix} s_1 \\ s_2 \\ \vdots \\ s_K \end{pmatrix} + \begin{pmatrix} n_1 \\ n_2 \\ \vdots \\ n_K \end{pmatrix} \quad (3.24) \\ &= \begin{pmatrix} l_{11} & 0 & \cdots & 0 \\ 0 & l_{22} & \cdots & 0 \\ \vdots & \vdots & \ddots & \vdots \\ 0 & 0 & \cdots & l_{KK} \end{pmatrix} \begin{pmatrix} s_1 \\ s_2 \\ \vdots \\ s_K \end{pmatrix} + \begin{pmatrix} n_1 \\ n_2 \\ \vdots \\ n_K \end{pmatrix} \end{aligned}$$

(3.24) indicates that by using the DPC technique, the interference-free detection is guaranteed for each user. DPC provides the maximum channel capacity, but suffers very high complexity of the transmitter [25], [62].

MU-MIMO systems have been also successfully applied in wireless communication networks including multi-cell networks. In this case, the edge cell users suffer more co-channel interference from adjacent cells. In order to improve the system performance for the edge-cell users, Coordinated Multi-Point (CoMP) transmission can be employed by exploiting the coordination among basis station. In this context, using CoMP joint transmission approach, where the edge-cell users are served by multi-basis station, the inter-cell interference can be mitigated. Besides CoMP, others interference mitigation approach such as IA can be employed. Using the IA technique, all interferences are aligned with the same direction in a subspace, and thus the interference signal dimension observed at user is reduced. Consequently, a simple signal detection can be used at user. IA can be applied in single, multi-cell multi-user MIMO systems or in MU-MIMO point-to-point communication systems (see Fig. 3.4-b). Due to having many benefits as opposed to other MUI mitigation methods, IA is chosen as the main research topic in this thesis.

3.2 PRINCIPLE OF OFDM TECHNIQUE

It is very difficult to handle the effects of a multi-path fading channel in SC systems. In this case, in order to combat the multi-path fading problem, a broadband equalization approach can be used in SC system, but then the receiver becomes more complex. To overcome this problem, a multi-carrier transmission scheme called

OFDM is employed. In contrast to an SC modulation scheme, in the OFDM technique, the available frequency band is divided into multiple orthogonal narrow-band sub-channels, in which the channel is considered as flat fading. As a result, a simple equalizer can be applied in each sub-channel to remove the effects of the multi-path fading channel. Furthermore, OFDM allows overlapping in spectrum of multiple sub-carrier signal leading to high spectral efficiency. In OFDM, an ICI and ISI-free transmission is guaranteed due to the orthogonality among sub-carriers and the insertion of a guard interval called Cyclic Prefix (CP) between OFDM symbols, respectively. CP is the copy of the last few samples of an OFDM symbol, which is inserted into its front and is normally longer than or equal to the maximum delay of the multi-path fading channel. The CP is directly removed at the receiver side after the time synchronization and before the demodulation procedure. By doing so, the ISI can be eliminated and the orthogonality of all sub-carrier signals is maintained. The rectangular pulse shape is used in an OFDM system, and thus the OFDM modulation and demodulation can be easily implemented using Inverse Fast Fourier Transformation (IFFT) and Fast Fourier Transformation (FFT) techniques, respectively. Accordingly, a general block diagram of an OFDM system is illustrated in Fig. 3.5.

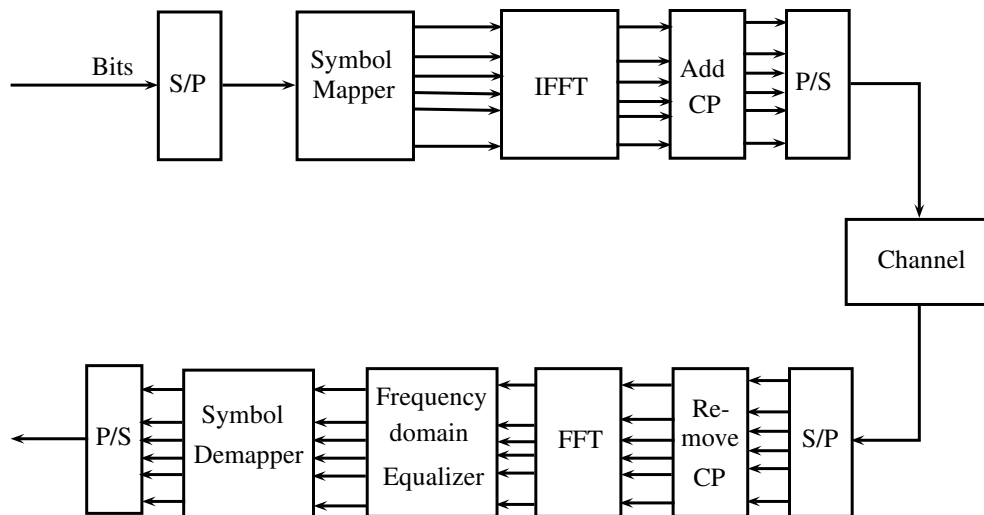


Figure 3.5: General block diagram of an OFDM system

The advantages of the OFDM technology described so far can be summarized as follows:

- High spectral efficiency,
- Low receiver complexity,
- Simple implementation by using IFFT and FFT,
- Robustness for high data rate transmission over multi-path channel,
- High flexibility in terms of link adaptation.

Because of these advantages, OFDM is a promising technique for wireless communication systems and has been employed in several wireless standard technologies such as Wireless Local Area Network (WLAN), Digital Video Broadcasting-Terrestrial (DVB-T), WiMAX, LTE.

3.3 MIMO-OFDM SYSTEM

MIMO in combination with the OFDM technology is a promising solution for wireless communication systems related to high data rate, high SE and link reliability improvement. In MIMO-OFDM systems, parallel transmission is performed in both space and frequency domains, leading to an enhancement of data rate and SE. Literature shows that a data rate up to several hundreds of Mbits/s and an spectral efficiencies of several tens of bits/Hz/s can be achieved for indoor wireless MIMO-OFDM communication systems [47]. The main advantage of a MIMO-OFDM system is that OFDM splits frequency-selective MIMO channel into a set of parallel frequency-flat MIMO channels, and thus all MIMO process can be performed in each sub-channel. This leads to a reduction of the system complexity and all gain provided by the MIMO technique can be achieved in a MIMO-OFDM system. The MIMO-OFDM technique has been adopted in several of wireless standard such as IEEE 802.11n for WLAN, IEEE 802.16a for WiMAX, LTE/LTE-Advanced for high data rate transmission technologies. The IEEE 802.11n standards for WLAN including the MIMO-OFDM technology can provide a throughput of up to 600 Mbps [54]. In a WiMAX system, a combination of the OFDM and MIMO can offer a data rate of more than 155 Mbps. The MIMO technique has been also successfully employed in OFDM based- LTE/LTE-Advanced systems. A 2×2 MIMO LTE-Advanced system (category 6) can achieve a peak data rate of 300 Mbps for downlink and 51 Mbps for uplink communication [107]. In an 8×8 MIMO LTE-Advanced system (category 8), a data rate up to 3 Gbps in downlink and 1.5 Gbps in uplink communication can be obtained [107].

INTERFERENCE ALIGNMENT FOR MU-MIMO SYSTEMS

4.1 INTRODUCTION

Frequency reuse is an effective approach to improve the system capacity and the Spectral Efficiency (SE) in wireless communication systems. However, this approach requires an efficient interference management scheme, mostly due to the fact that the interference is caused by overlapping of multi-user transmissions. In this context, the interference can be classified into Multi-Access Interference (MAI), Co- or Adjacent Channel Interference (CCI, ACI) and MUI. Depending on the interference type, different interference management techniques can be applied. Power control is one of the promising interference management approaches used in wireless communication networks. Here, the interference power is controlled so that the interference lies within the noise floor and can be treated as noise. Thus, a normal single user encoding/decoding strategy can be used, [95, 6]. Due to the implementation simplicity, this approach is of wide-spread use in practice. If the interference power is higher than both noise floor and desired signal power, it is possible to decode the desired signal using the Successive Interference Cancellation (SIC) technique. Using this approach, the interference is first decoded, and then it is subtracted from the received signal. The SIC method is mostly used in applications, where the receiver is of high signal processing capability, for example a BS in cellular networks. However, due to high complexity of the multi-user detection process this method is generally not used frequently in practice, [89, 106]. One common approach to deal with strong interferences is to orthogonalize the channels. Using this interference management scheme, the transmitted signals are chosen to be non-overlapping in the time, frequency or space domain, which corresponds to the Frequency-Division Multiple Access (FDMA), Time-Division Multiple Access (TDMA) or Space-Division Multiple Access (SDMA) transmission scheme, respectively. Although these orthogonalization approaches can effectively eliminate the MUI in wireless communication networks, these orthogonalities may not be given in some cases due to practical issues such as synchronization errors, RF circuitry non-idealities and the effects of wireless propagation channel. Furthermore, using the traditional orthogonal transmission schemes leads to inefficient spectrum utilization, and thus the maximum SE can be not achieved. For example, in FDMA-based wireless communication systems, an SE loss is incurred due to guard bands between systems, which is normally required to eliminate the adjacent band interferences.

Another approach of the frequency reuse techniques proposed to significantly improve the spectrum usage is overlapping of multi-user in both time and frequency dimensions. This frequency reuse method can be used in both uplink and downlink channels, in multi-user point-to-point coexistence scenarios and in cognitive radio, as well as in multi-tier heterogeneous networks.

In cellular networks, if the base station has a sufficient number of antennas, the multi-user transmission can be separated at the BS in spatial domain using beamforming techniques for both uplink and downlink communications [31, 93]. In MU downlink channels, where the BS sends signals to several users on the same time and frequency band, by exploiting the knowledge of CSIT the transmission can be pre-coded at the BS, so that interference can be eliminated at each user [114]. For this purpose, the pre-coding technique based on DPC is known as the best solution when the perfect CSI is available at the BS. The DPC technique uses the successive interference cancellation method at the BS, which employs again a complex encoding structure. Even though DPC provides advantages in terms of SE and high network capacity, this method is of high complexity and requires perfect or nearly perfect channel knowledge and the full information about the transmitted signals. As a result, this method is still far from practical applications, as discussed in Section 3.1.3. Moreover, low-complexity linear pre-coding schemes such as Zero-Forcing Beamforming (ZF-BF) [31], BD [102] were proposed for a MU Broadcast Channel (BC) scenario, where the UE is equipped with single and multiple antenna, respectively. Using ZF-BF and BD precoding techniques, each user signal is transmitted in the null space spanned by other user channel matrix, so that the multi-user interference can be completely mitigated. However, as discussed in Section 3.1.3, these pre-coding techniques suffer several disadvantages such as poor system performance in low SNRs and high computationally effort. To overcome this problem, an interference management approach based on linear pre-coding technique, so-called Interference Alignment (IA) is seen as a promising solution to deal with the MUI problem in a multi-user system. In this way, the fairness among users is guaranteed and the maximum spatial diversity gain is achieved, provided perfect CSI is available at the transmitters. The IA technique can also be applied in cellular wireless communication networks, in multi-user CR systems and ad-hoc networks.

An overview about the IA technique is given in this chapter. First, the principles of the IA technique and the maximum diversity gain are introduced in 4.2 and 4.3, respectively. Three existing IA approaches under the assumption of having perfect CSIT are presented in 4.4. In 4.5, a novel IA approach to deal with the imperfection of CSI in multi-user point-to-point communication systems is proposed. Finally, simulation results are given in 4.6.

4.2 PRINCIPLE OF INTERFERENCE ALIGNMENT TECHNIQUE

The first concept of the IA technique is proposed by Cadambe and Jafar in [17, 16], whereas the Degree of Freedom (DoF) or the maximum spatial multiplexing gain for a K-user interference channel was analyzed. These studies show that using the IA technique the full multiplexing gain in a K-multi-user MIMO system can be achieved at high SNRs. The main idea here is to design a linear pre-coding

filter at each transmitter, so that each receiver can align all interference from undesired transmitters in the interference subspace by exploiting knowledge of CSI of all transmission links. In other words, this approach guarantees that the received signal at each receiver is divided only in two orthogonal subspaces, namely desired and interference signal subspaces. This enables an interference-free decoding of the desired signal.

The principle of the IA technique for three users MIMO system is illustrated in Fig. 4.1, where \mathbf{V}_1 , \mathbf{V}_2 and \mathbf{V}_3 represent the IA pre-coding filters for user 1, 2 and 3, respectively. In this considered scenario, it can be seen that each receiver observes a desired signal and two interference signals, each of which is represented as a vector in three-dimensional space. For example, if the first transmission pair (black) is considered, the blue and orange signal are interfering signals for user 1. Similarly, the black and blue, black and orange signals are interfering signals for user 2 and 3, respectively. Since two interference signals will occupy two difference signal dimensions at each receiver, without the IA technique, it is difficult to successfully decode the desired signal. In contrast to that, by using the IA technique the pre-coding filters matrix $\mathbf{V} = [\mathbf{V}_1, \mathbf{V}_2, \mathbf{V}_3]^T$ is determined, so that after the pre-coding process the interference signals are overlapped and aligned to the same direction also in the interference subspace, and hence the desired signal is placed undisturbed in the another subspace. As a result, each receiver can suppress all interferences by projecting the interference signal onto the orthogonal space of the desired signal subspace.

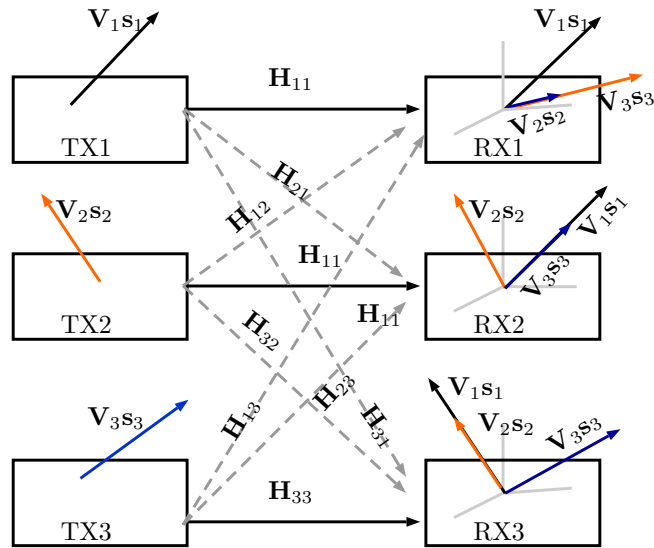


Figure 4.1: The IA concept

Fig. 4.2 shows a K -user MIMO system using the IA technique, where each transmitter and receiver are equipped with N_t and N_r antennas, respectively. Here, the matrix \mathbf{V}_k describes the pre-coding filter at transmitter k and \mathbf{U}_k stands for the interference suppression/post-processing filter at receiver k . d_{TX} represents the distance between two transmit antennas and d_{RX} denotes the distance between two receive antennas at each user. In the considered system, it is assumed that each

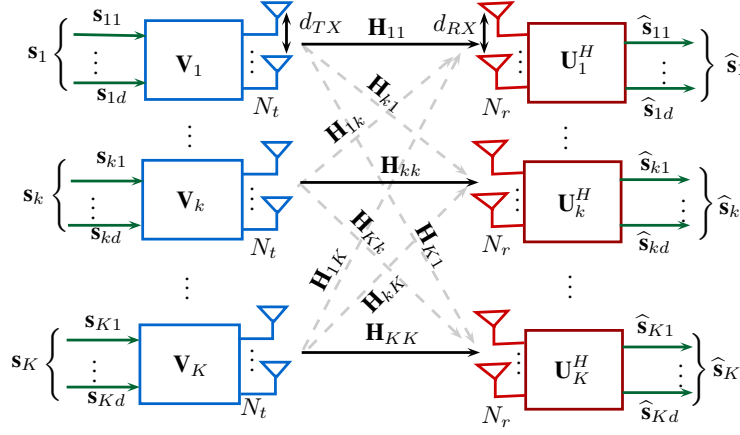


Figure 4.2: IA system model

user sends d independent data streams, $\mathbf{s}_k = [s_{k1}, s_{k2}, \dots, s_{kd}]^T$. The received signal at receiver k can be expressed as

$$\mathbf{y}_k = \mathbf{H}_{kk} \mathbf{x}_k + \sum_{l=1, l \neq k}^K \mathbf{H}_{kl} \mathbf{x}_l + \mathbf{n}_k, \quad (4.1)$$

where $\mathbf{x}_k = \mathbf{V}_k \mathbf{s}_k$ is the $N_t \times 1$ transmitted signal vector and \mathbf{n}_k is the $N_r \times 1$ noise signal vector at receiver k . The additive noise \mathbf{n}_k is assumed to be white Gaussian with covariance matrix $\mathbf{R}_{n_n} = \mathbb{E}[\mathbf{n}_k \mathbf{n}_k^H] = \sigma_n^2 \mathbf{I}_{N_r}$, where σ_n^2 is the noise power. The channel matrix \mathbf{H}_{kl} contains the channel coefficients from the l -th transmitter to the k -th receiver. At the receiver side, the received signal is linearly processed by the receive filter \mathbf{U}_k to reconstruct d desired transmitted data streams. As a result, the estimated data streams $\hat{\mathbf{s}}_k$ at receiver k can be defined as

$$\begin{aligned} \hat{\mathbf{s}}_k &= \mathbf{U}_k^H \mathbf{y}_k \\ &= \underbrace{\mathbf{U}_k^H \mathbf{H}_{kk} \mathbf{V}_k \mathbf{s}_k}_{\text{Desired signal}} + \underbrace{\sum_{l=1, l \neq k}^K \mathbf{U}_k^H \mathbf{H}_{kl} \mathbf{V}_l \mathbf{s}_l}_{\text{Interference signals}} + \underbrace{\mathbf{U}_k^H \mathbf{n}_k}_{\text{Noise}}. \end{aligned} \quad (4.2)$$

In this work, it is assumed that each transmitter sends independent data streams, i.e. $\mathbb{E}[\mathbf{s}_k \mathbf{s}_l^T] = 0$ for $k \neq l$. In addition, all transmitted data streams and noise are statistically independent, $\mathbb{E}\{\mathbf{s}_k \mathbf{n}_l^T\} = 0, \forall (k, l) \in \{1, 2, \dots, K\}$. As aforementioned, IA is a simple linear pre-coding technique for a multi-user system, and it guarantees that after applying a simple linear receiver \mathbf{U}_k all interferences can be completely canceled at receiver k . This leads to the following condition, which has to be fulfilled by determining the IA filters

$$\text{rank}(\mathbf{U}_k^H \mathbf{H}_k \mathbf{V}_k) = d, \forall k = 1, \dots, K \quad (4.3)$$

$$\sum_{l=1, l \neq k}^K \mathbf{U}_k^H \mathbf{H}_k \mathbf{V}_l = 0 \quad \forall l, k = 1, \dots, K, l \neq k, \quad (4.4)$$

where $d \leq \min(N_t, N_r)$. The condition in (4.3) states that the desired signal space has dimension of d , while (4.4) implies that after applying the receiver filter \mathbf{U}_k , all interference signals at receiver k lie in the subspace orthogonal to the desired signal subspace. In other words, the conditions in (4.3) and (4.4) guarantee that each transmitter k can use a linear pre-coding strategy to transmit d interference-free independent data streams to receiver k . Additionally, early works on IA showed that in order to ensure an IA solution, beside the IA conditions in (4.3) and (4.4) certain dimensionality constraints need to be satisfied [117]. For example, IA will only be feasible for a given number of users if there is a sufficient number of transmit and receive antennas. In other words, the flexibility in a IA system increases with the increasing of the number of coding dimensions. The feasibility of the IA technique has been studied extensively in [15, 33, 76, 74, 117]. According to these studies, the following feasibility conditions have to be fulfilled

$$\begin{aligned}
N_t + N_r &\geq (K + 1)d \\
(N_t - d) &\geq [Kd - N_r]_+ \\
[2d - N_r]_+ &\leq [N_t - N_r]_+ \\
d &\leq \min(N_r, N_t) \\
d &\geq (K - 1)[2d - N_r],
\end{aligned} \tag{4.5}$$

with $[x]_+ = \max(0, x)$. The first condition in (4.5) indicates that in order to achieve d DoF at each user, the total number of transmit and receive antennas for each user has to be greater than or equal to $(K + 1)d$ [117]. The second condition in (4.5) shows that a solution for the IA problem will be feasible only if the total number of variables is larger than or equal to the total number of constraints that needs to be fulfilled [76, 74]. The third condition describes the lower and upper bound of the number of streams at each transmitter, which can be aligned by each transmitter to its orthogonal complement of the interference channel matrix. In the IA technique, the total number of streams that each transmitter can align, needs to be bounded by the rank of its pre-coding matrix. This is shown in the last condition in (4.5), [76, 74]. The derivation for these conditions is given in Appendix A.1.

After the interference suppression process, the effective channel $\bar{\mathbf{H}}_{kk}$ for user k can be expressed as

$$\bar{\mathbf{H}}_{kk} = \mathbf{U}_k^H \mathbf{H}_{kk} \mathbf{V}_k. \tag{4.6}$$

For a perfect IA solution at receiver k , all other effective interference channels should be zero, i.e. $\bar{\mathbf{H}}_{kl} = 0$ for $\forall l \neq k$. To diagonalize the effective channel $\bar{\mathbf{H}}_{kk}$ the SVD is applied as follows

$$\bar{\mathbf{H}}_{kk} = \mathbf{Z} \mathbf{D} \mathbf{W}^H, \tag{4.7}$$

where \mathbf{Z} and \mathbf{W} are unitary matrices and \mathbf{D} is a diagonal matrix which contains the d non-zero singular values, $\lambda_1, \lambda_2, \dots, \lambda_d$. Thus, the pre-coding matrix \mathbf{V}_k and the interference suppression matrix \mathbf{U}_k is determined as follows

$$\begin{aligned}
\mathbf{V}_k^{\text{opt}} &= \mathbf{V}_k \mathbf{W} \mathbf{D}^{-1} \\
\mathbf{U}_k^{\text{opt}} &= \mathbf{U}_k \mathbf{Z} \mathbf{D}^{-1}.
\end{aligned} \tag{4.8}$$

4.3 DEGREES OF FREEDOM AND MAXIMUM CAPACITY

The DoF is an important parameter in wireless communication systems, which is usually used to demonstrate the advantages of a MIMO system in comparison to a SISO system. In this case, the DoF is normally used to approximate the maximum MIMO channel capacity. Furthermore, the DoF can be considered as the number of independent signal space dimensions, and thus is also known as the maximum spatial multiplexing gain provided by a MIMO system at high SNRs [52].

A single user SISO system has 1 DoF and its system capacity with a bandwidth $B = 1$ is expressed by

$$C = \log_2 (1 + \text{SNR}). \quad (4.9)$$

At high SNRs, the system capacity of a SISO system can be approximated as

$$C = \log_2 (\text{SNR}). \quad (4.10)$$

In a K -user SISO system, where an orthogonal multiple access scheme is used, the 1 DoF is divided to K users, so that each user gets $1/K$ DoF. In this case, each SISO system has the capacity of $C = \frac{1}{K} \log_2 (\text{SNR})$.

With assumption of equal power at each transmit antenna, the channel capacity of a single user MIMO system with N_t transmit and N_r receiver antennas is given by [32, 111]

$$C_{\text{MIMO}} = \mathbb{E} \left\{ \log_2 \det \left(\mathbf{I}_{N_r} + \frac{P_0}{N_t \sigma_n^2} \mathbf{H} \mathbf{H}^H \right) \right\} \quad (4.11)$$

$$= \mathbb{E} \left\{ \sum_{i=1}^m \log_2 \left(1 + \frac{\text{SNR}}{N_t} \lambda_i^2 \right) \right\}. \quad (4.12)$$

Here $\text{SNR} = P_0/\sigma_n^2$ is the SNR at each receive antenna. λ_i stands for singular values of \mathbf{H} and $m = \min(N_r, N_t)$ is the number of non-zero singular values. Using Jensen's inequality condition results in

$$\sum_{i=1}^m \log_2 \left(1 + \frac{\text{SNR}}{N_t} \lambda_i^2 \right) \leq m \log_2 \left(1 + \frac{\text{SNR}}{N_t} \frac{1}{m} \sum_{i=1}^m \lambda_i^2 \right). \quad (4.13)$$

According to (4.11) and (4.13), in very high SNRs we obtain [111]

$$C_{\text{MIMO}} \leq m \log_2 \left(1 + \frac{\text{SNR}}{N_t} \frac{1}{m} \sum_{i=1}^m \mathbb{E} \{ \lambda_i^2 \} \right) \quad (4.14)$$

$$\leq m \log_2 \frac{\text{SNR}}{N_t} \quad (4.15)$$

It is shown in [111, 52] that in the very high SNR regime, for the case of N_t and N_r smaller than 8, the maximum MIMO capacity scales with $m \log_2 (\text{SNR})$.

The DoF d can be defined as below [53]:

$$d = \lim_{\text{SNR} \rightarrow \infty} \frac{C_{\text{MIMO}}}{\log_2 (\text{SNR})}. \quad (4.16)$$

In other words, the DoF corresponds to the parallel channels that can be isolated using the SVD technique, which means

$$d = m = \min(N_t, N_r). \quad (4.17)$$

Consequently, the maximum MIMO capacity in (4.14) can be expressed as

$$C_{\text{MIMO}} \approx d \log_2(\text{SNR}). \quad (4.18)$$

In [17], Cadambe proved that using the IA technique the channel capacity can reach the maximum capacity at high SNRs. Here, a K-user SISO system with symbol extension was considered. For this system, Cadambe and Jafar showed in [17] that the system capacity using the IA technique at high SNRs grows linearly with K and is given by

$$C = \frac{K}{2} \log_2(\text{SNR}) + O(\log_2(\text{SNR})). \quad (4.19)$$

This can be mainly explained by functionality of the IA-based pre-coding method. In the IA technique, each receiver is able to divide its observed signal space into two subspaces of equal size namely: desired and interference signal spaces. Thus, each user can achieve approximately one half of the interference-free capacity. In this regard, the system has totally $\frac{K}{2}$ DoF. It can be seen that in contrast to the conventional interference mitigation approaches, by using the IA technique the system capacity is increased with the increasing of number of active user pairs. In addition, [17] shows that a K-user MIMO system, where each node is equipped with N antennas, has a DoF of $\frac{KN}{2}$. If user k has $N_{t,k}$ transmitter and $N_{r,k}$ receiver antennas, the total number of DoF is given by

$$d = \sum_{k=1}^K d_k \geq \frac{1}{2} \sum_{k=1}^K \min(N_{t,k}, N_{r,k}). \quad (4.20)$$

This implies that in a K-user MIMO system by using the IA pre-coding technique not more than half of the DoF is lost.

4.4 INTERFERENCE ALIGNMENT APPROACHES WITH PERFECT CSI

4.4.1 Closed-form Solution for Interference Alignment

The IA approach with a closed-form expression for the pre-coding filter matrix \mathbf{V}_k is presented in [17, 16]. In this case, at each receiver the interference can be perfectly aligned into the interference subspace, which is orthogonal to the desired signal subspace by applying pre-coding filters at each transmitter. Therefore, it is simple to decode the desired signal at the receiver side. Unfortunately, this closed-form solution for IA exists only for the case of three users. As shown in Fig. 4.1, the k-th transmitter encodes its signal \mathbf{s}_k using the pre-coding vector \mathbf{V}_k , $\forall k = \{1, 2, 3\}$. It should be noted that

- The interference from transmitter 2 and 3 to receiver 1 can be perfectly aligned in the same direction if

$$\text{span}(\mathbf{H}_{12}\mathbf{V}_2) = \text{span}(\mathbf{H}_{13}\mathbf{V}_3) \quad (4.21)$$

- This also applies true for receiver 2 and 3 as below:

$$\text{span}(\mathbf{H}_{21}\mathbf{V}_1) = \text{span}(\mathbf{H}_{23}\mathbf{V}_3), \quad (4.22)$$

$$\text{span}(\mathbf{H}_{31}\mathbf{V}_1) = \text{span}(\mathbf{H}_{32}\mathbf{V}_2). \quad (4.23)$$

It means that for three users case, to align all interferences into the interference subspace at each receiver each pre-coder has to be designed to fulfilled the conditions given in (4.21), (4.22) and (4.23), where $\text{span}(\mathbf{X})$ denotes the space spanned by the column vectors of the matrix \mathbf{X} . As reported in [16], we have

$$\text{span}(\mathbf{H}_{13}\mathbf{H}_{23}^{-1}\mathbf{H}_{21}\mathbf{V}_1) = \text{span}(\mathbf{H}_{12}\mathbf{H}_{32}^{-1}\mathbf{H}_{31}\mathbf{V}_1). \quad (4.24)$$

By solving this equation, \mathbf{V}_1 can be determined using

$$\mathbf{V}_1 = \text{eig}((\mathbf{H}_{31})^{-1}\mathbf{H}_{32}(\mathbf{H}_{12})^{-1}\mathbf{H}_{21}(\mathbf{H}_{23})^{-1}\mathbf{H}_{31}), \quad (4.25)$$

where $\text{eig}(\mathbf{X})$ denotes the operation to get the eigenvector of the matrix \mathbf{X} . Consequently, to satisfy above conditions the pre-coding vectors \mathbf{V}_2 and \mathbf{V}_3 can be chosen as follows:

$$\mathbf{V}_2 = (\mathbf{H}_{32})^{-1}\mathbf{H}_{31}\mathbf{V}_1, \quad (4.26)$$

$$\mathbf{V}_3 = (\mathbf{H}_{23})^{-1}\mathbf{H}_{21}\mathbf{V}_1. \quad (4.27)$$

It should be mentioned that the closed-form solution is easy to implement and requires less computational effort. However, this method requires global CSI at the transmitter side, which is impractical. Furthermore, this solution is only optimal in high SNR regime. Thus, this IA approach is not considered in this thesis.

4.4.2 Interference Alignment via Reciprocity

The IA closed-form solution presented in Subsection 4.4.1 suffers from many drawbacks. One of them is the requirement of global channel knowledge at each node, which is not practicable. To overcome this problem, [42] proposed an iterative IA approach to design IA filters requiring only local channel knowledge at each node. Furthermore, this approach deals with arbitrary number of users. In other words, using this approach the number of users is not limited to three. However, for a given number of users, the number of antennas at each node has to fulfill the conditions in (4.5). The idea of this approach is to exploit the duality relationships enabled by the reciprocity of the propagation channel to adjust the IA filter coefficients. In principle, the reciprocity property of a channel can be obtained in two-way communication networks based on TDD. In this context, [118] shows that the capacity remains constant if: i) in both links the transmitter and receiver are interchangeable, ii) the channel matrix is transposable, and iii) the same transmit power constraint is used to the reciprocal network.

Recent literature shows that in TDD-based systems, where transmissions on both links overlap in frequency and are minimally separated in time, the propagation channel in both directions can be considered as being identical [8]. In this case, the channels are said to be reciprocal and this enables the build up of a dual

network. In a dual network for a multi-user MIMO system with linear beamformers, the same SINR performance for each user can be achieved in both original and reciprocal links if the total transmit power is equal in both links. Accordingly, this dual network can be employed to solve the MUI problem [101, 111]. In this regard, the following rules are applied for a multi-user MIMO system in a dual network

- reverse the communication direction of all links
- replace any MIMO complex channel matrix \mathbf{H}_{kl} by its conjugate transpose \mathbf{H}_{kl}^H
- use precoding vectors as post-processing vectors and vice versa.

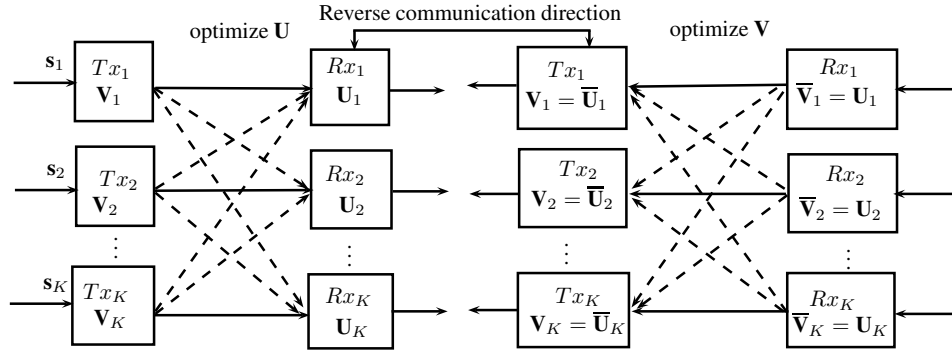


Figure 4.3: The concept of the IA approach via reciprocity

[42] proposed a distributed IA approach based on the reciprocity. In that study, the pre-coding and post-processing filter matrix is optimized based on the minimization of the interference leakage in both forward and reverse links. The main concept of this IA approach is illustrated in Fig. 4.3. In the forward/original link, the estimated signal at user k is given by

$$\hat{\mathbf{s}}_k = \underbrace{\mathbf{U}_k^H \mathbf{H}_{kk} \mathbf{V}_k \mathbf{s}_k}_{\text{Desired Signal}} + \underbrace{\sum_{l=1, l \neq k}^K \mathbf{U}_k^H \mathbf{H}_{kl} \mathbf{V}_l \mathbf{s}_l}_{\text{Interference Signal}} + \underbrace{\mathbf{U}_k^H \mathbf{n}_k}_{\text{Noise}}. \quad (4.28)$$

Because of the reversal role between a transmitter and a receiver in the reciprocal/reverse link), the estimated signal of the k -th user in reverse link can be determined as follows

$$\hat{\bar{\mathbf{s}}}_k = \underbrace{\bar{\mathbf{U}}_k^H \bar{\mathbf{H}}_{kk} \bar{\mathbf{V}}_k \bar{\mathbf{s}}_k}_{\text{Desired Signal}} + \underbrace{\sum_{l=1, l \neq k}^K \bar{\mathbf{U}}_k^H \bar{\mathbf{H}}_{kl} \bar{\mathbf{V}}_l \bar{\mathbf{s}}_l}_{\text{Interference Signal}} + \underbrace{\bar{\mathbf{U}}_k^H \bar{\mathbf{n}}_k}_{\text{Noise}}, \quad (4.29)$$

where the transmit and receive filter matrices $\bar{\mathbf{V}}_l, \bar{\mathbf{U}}_k$ as well as the channel matrix $\bar{\mathbf{H}}_{kl}$ from the k -th receiver to the l -th transmitter in the reciprocal link are defined as

$$\bar{\mathbf{U}}_k = \mathbf{V}_k, \quad (4.30)$$

$$\bar{\mathbf{V}}_l = \mathbf{U}_l \quad (4.31)$$

$$\bar{\mathbf{H}}_{kl} = \mathbf{H}_{kl}^H. \quad (4.32)$$

Note that the IA conditions are equal for both links. As a result, the interference received at a user in the forward link is the same as that caused by this user to other users in the reverse link. Therefore, the total interference leakage is unchanged in both links. Consequently, the pre-coding and interference suppression filter matrices can be optimized by minimizing the interference leakage in both links [42]. In forward link, the total interference leakage at the k -th receiver is determined as follows:

$$I_k = \text{Tr}(\mathbf{U}_k^H \mathbf{Q}_k \mathbf{U}_k), \quad (4.33)$$

where $\mathbf{Q}_k = \sum_{l=1, l \neq k}^K \mathbf{H}_{kl} \mathbf{V}_l \mathbf{V}_l^H \mathbf{H}_{kl}^H$ represents the interference covariance matrix at receiver k . Similarly, \bar{I}_l and $\bar{\mathbf{Q}}_l$ are the total interference leakage and interference covariance matrix at user l in the reciprocal link, respectively. This results in

$$\bar{I}_l = \text{Tr}(\bar{\mathbf{U}}_l^H \bar{\mathbf{Q}}_l \bar{\mathbf{U}}_l), \quad (4.34)$$

with $\bar{\mathbf{Q}}_l = \sum_{k=1, k \neq l}^K \bar{\mathbf{H}}_{lk} \bar{\mathbf{V}}_k \bar{\mathbf{V}}_k^H \bar{\mathbf{H}}_{lk}^H$.

As presented in [42], this IA approach is performed iteratively, so that within each link the interference suppression filter coefficients are updated to minimize their total interference, i.e.

$$\begin{aligned} \mathbf{U}_k^{ZF} &= \underset{\mathbf{U}_k}{\text{argmin}} \{I_k\}, \\ \bar{\mathbf{U}}_l^{ZF} &= \underset{\bar{\mathbf{U}}_l}{\text{argmin}} \{\bar{I}_l\}. \end{aligned} \quad (4.35)$$

At the k -th receiver, the received signal subspace with the least interference is the space spanned by the eigenvectors, which correspond to the d_k smallest eigenvalues of the interference covariance matrix \mathbf{Q}_k . Thus, the d_k columns of \mathbf{U}_k^{ZF} are given by

$$\mathbf{U}_{k,d_k}^{ZF} = \mathbf{v}_d(\mathbf{Q}_k), \quad d = 1, 2, \dots, d_k, \quad (4.36)$$

where $\mathbf{v}_d(\mathbf{Q}_k)$ is the eigenvector corresponding to the d -th smallest eigenvalue of \mathbf{Q}_k . Similarly, in the reciprocal link it results in

$$\bar{\mathbf{U}}_{k,d}^{ZF} = \mathbf{v}_d(\bar{\mathbf{Q}}_k), \quad d = 1, 2, \dots, d_k. \quad (4.37)$$

Due to the reciprocal relationship, the pre-coding filter matrix in the forward link is updated in the reverse link with $\mathbf{V}_k^{ZF} = \bar{\mathbf{U}}_k^{ZF}$. In this context, the iterative procedure for solving the minimization problem consists of following steps:

- Step 1: arbitrarily initialize the pre-coding matrices $\mathbf{V}_k, \forall k = 1, 2, \dots, K$.
- Step 2: compute the interference covariance matrix \mathbf{Q}_k at the receivers in the forward link.

- Step 3: compute post-processing matrix \mathbf{U}_k at each receiver according to equation (4.36) in the forward link.
- Step 4: reverse the communication direction and set $\bar{\mathbf{V}}_k = \mathbf{U}_k$.
- Step 5: compute the interference covariance matrix $\bar{\mathbf{Q}}_k$ at the new k-th receiver in the reverse link.
- Step 6: compute post-processing matrix $\bar{\mathbf{U}}_k$ at each new receiver according to equation (4.37) in the reverse link.
- Step 7: reverse the communication direction and set $\mathbf{V}_k = \bar{\mathbf{U}}_k$.
- Step 8: repeat from step 2 until convergence.

The general frame work of this IA approach via reciprocity can be summarized as follow:

- In the forward link: first arbitrary pre-coding filters $\mathbf{V}_1, \mathbf{V}_2, \dots, \mathbf{V}_K$ are initialized. Transmitters send pre-coded pilot symbols using a set of above initial pre-coding filters. Receivers estimate the channel parameters and compute the post-processing filter coefficients.
- In the reverse link: Receivers send pre-coded pilot symbols using the post-processing filter from above step as transmit pre-coders ($\bar{\mathbf{U}}_k = \mathbf{V}_k$). Transmitters in turn optimize the pre-coders with $\mathbf{V}_k = \bar{\mathbf{U}}_k$ and initiate a second training phase with the updated pre-coders.
- Communication pairs iterate the previous step until convergence.

The convergence of the proposed IA scheme is confirmed in [42].

4.4.3 MMSE-Based Interference Alignment

The iterative IA algorithms based on the reciprocity alleviates the problem of the IA approach-based closed-form solution in terms of the global knowledge of CSI problem and the limitation of the user number. However, the proposed scheme has some drawbacks due to exploiting the reciprocal network to solve the IA problem. In practice, due the fact of pilot overhead and calibration of Radio Frequency (RF) devices, it is difficult to achieve the reciprocal channel. Furthermore, by using the IA approaches presented in Subsections 4.4.1 and 4.4.2, all IA filters are designed without concerning the noise. As a result, both approaches are only optimal in the high SNR regime. In order to avoid this disadvantage, [90] proposed a MMSE-based IA approach, which requires no additional requirements, e.g. the reciprocal channel or global channel knowledge at each node. Moreover, by using this IA approach, the system performance can be improved in the low and moderate SNR regimes by considering noise to adjust the IA filter coefficients.

In the described multi-user system with time invariant channels as shown in Fig. 4.2, the Mean-Squared Error (MSE) at receiver k is defined as

$$\epsilon_k = \mathbb{E} \left[\|\hat{\mathbf{s}}_k - \mathbf{s}_k\|^2 \right] \quad (4.38)$$

$$\begin{aligned}
 &= \|\mathbf{U}_k^H \mathbf{H}_{kk} \mathbf{V}_k - \mathbf{I}_d\|^2 + \sum_{l=1, l \neq k}^K \|\mathbf{U}_k^H \mathbf{H}_{kl} \mathbf{V}_l\|^2 \\
 &\quad + \|\mathbf{U}_k^H\|^2 \mathbf{R}_{nn}.
 \end{aligned} \tag{4.39}$$

Using the IA approach proposed in [90], the pre-coding filter \mathbf{V}_k and the interference suppression filter matrix \mathbf{U}_k can be optimized with respect to the minimization of the total MSE subject to the transmit power constraints. Therefore, the optimization problem can be formulated as follows

$$\mathbf{U}_k^{\text{MMSE}}, \mathbf{V}_k^{\text{MMSE}} = \underset{\mathbf{U}_k, \mathbf{V}_k}{\text{argmin}} \sum_{k=1}^K \epsilon_k, \quad \text{subject to } \|\mathbf{V}_l\|^2 \leq P_l, \tag{4.40}$$

where P_l is the transmit power at transmitter l . This optimization problem can be solved by using the Karush-Kuhn-Tucker (KKT) conditions at each step [90]. In this context, the Lagrange function can be defined as below:

$$L^{\text{MMSE}}(\lambda_l, \mathbf{U}_k, \mathbf{V}_l) = \epsilon_k + \lambda_l (\text{Tr}(\mathbf{V}_l \mathbf{V}_l^H) - P_l), \tag{4.41}$$

where λ_l is the Lagrange multiplier, which is chosen to meet the transmit power constraints $\|\mathbf{V}_l\|^2 \leq P_l$. The KKT conditions are specified by

$$\begin{aligned}
 \nabla_{\mathbf{V}_l} L^{\text{MMSE}} &= 0, \\
 \nabla_{\mathbf{U}_k} L^{\text{MMSE}} &= 0, \\
 \lambda_l (\text{Tr}(\mathbf{V}_l^H \mathbf{V}_l) - P_l) &= 0, \quad \forall k, \\
 \text{Tr}(\mathbf{V}_l^H \mathbf{V}_l) &\leq P_l \quad \forall k.
 \end{aligned} \tag{4.42}$$

In this case, the optimal interference suppression filter matrix $\mathbf{U}_k^{\text{MMSE}}$ can be found by solving the equation $\nabla_{\mathbf{U}_k} L^{\text{MMSE}} = 0$ for fixed \mathbf{V}_l and λ_l as follows:

$$\mathbf{U}_k^{\text{MMSE}} = \left(\sum_{l=1}^K \mathbf{H}_{kl} \mathbf{V}_l \mathbf{V}_l^H \mathbf{H}_{kl}^H + \sigma_n^2 \mathbf{I}_{N_r} \right)^{-1} \mathbf{H}_{kk} \mathbf{V}_k. \tag{4.43}$$

Similarly, the optimal pre-coding filter matrix $\mathbf{V}_l^{\text{MMSE}}$ is obtained by solving the equation $\nabla_{\mathbf{V}_l} L^{\text{MMSE}} = 0$ for fixed \mathbf{U}_k according to

$$\mathbf{V}_l^{\text{MMSE}} = \left(\sum_{k=1}^K \mathbf{H}_{kl} \mathbf{U}_k \mathbf{U}_k^H \mathbf{H}_{kl} + \lambda_l \mathbf{I}_{N_t} \right)^{-1} \mathbf{H}_{ll}^H \mathbf{U}_l. \tag{4.44}$$

An iterative procedure to solve the equation in (4.40) was proposed in [90] and is performed in the following steps:

- Step 1: initialize arbitrarily the pre-coding filter matrices $\mathbf{V}_k, \forall k = 1, 2, \dots, K$, so that $\text{Tr}(\mathbf{V}_l \mathbf{V}_l^H) \leq P_l$
- Step 2: optimize the interference suppression filter matrix \mathbf{U}_k for a fixed pre-coding filter matrix \mathbf{V}_l according to equation (4.43),

- Step 3: optimize the pre-coding filter matrix \mathbf{V}_l for a fixed interference suppression filter matrix \mathbf{U}_k according to equation (4.44),
- Step 4: repeat from step 2 until convergence.

Convergence of this approach has been proven in [90, 79].

4.5 AS-MMSE-BASED IA WITH IMPERFECT CSI

As mentioned, the IA technique provides the maximum spatial multiplexing gain and high system performance in terms of the average sum-rate. However, this technique requires perfect knowledge of the CSI at both transmitter and receiver sides. Furthermore, as shown in our study [60], the IA system performance is degraded with the increasing of the correlation between the channels. In practice, the problem of the channel correlation can be solved by antenna design, antenna positioning and antenna selection. The main problem of IA lies mostly in the accuracy of CSIT. Since it is very difficult to have perfect CSI at the transmitter, developing a robust IA approach to deal with the imperfection of CSI plays an important role in realization of the IA technique in practical applications. Based on the methods to acquire the CSI, the CSI error is often caused by the channel estimation error, feedback delay and the channel quantization error. In fact, the receiver has a better knowledge of the CSI compared to the transmitter. Thus, it is more practical when all IA filters are determined at the receiver side and then receiver sends the pre-coding filters back to the transmitter.

In this section, the CSI error caused by the channel estimation error is considered. For this case, the actual channel matrix \mathbf{H}_{kl} can be modeled as

$$\mathbf{H}_{kl} = \hat{\mathbf{H}}_{kl} + \mathbf{E}_{kl}, \quad \forall k, l = 1, 2, \dots, K \quad (4.45)$$

where \mathbf{E}_{kl} is the channel estimation error and the estimated channel is denoted by $\hat{\mathbf{H}}_{kl}$, which is available at both receiver and transmitter sides. In this CSI model, the channel estimation error matrix is assumed to be complex Gaussian distributed with zero mean and $\mathbb{E} \left\{ \text{vec}(\mathbf{E}_{kl}) \text{vec}(\mathbf{E}_{kl})^H \right\} = \sigma_{\mathbf{E}_{kl}}^2 \mathbf{I}$. Here, $\text{vec}(\mathbf{X})$ represents the vectorization of matrix \mathbf{X} . Based on this assumption, a robust IA approach based on the Average-Sum Minimum Mean Squared Error (AS-MMSE) is proposed to determine the IA filters in the case of having imperfect CSI

Inserting (4.45) into (4.38), the expected value of the sum MSE can be formulated as

$$\begin{aligned} \bar{\epsilon} \{ \mathbf{U}_k, \mathbf{V}_l \} = \mathbb{E} \{ \epsilon \} = & \mathbb{E} \left\{ \sum_{k=1}^K \sum_{l=1}^K \text{Tr} \left(\mathbf{U}_k^H \left(\hat{\mathbf{H}}_{kl} + \mathbf{E}_{kl} \right) \mathbf{V}_l \mathbf{V}_l^H \left(\hat{\mathbf{H}}_{kl}^H + \mathbf{E}_{kl}^H \right) \mathbf{U}_k \right) \right\} \\ & - \mathbb{E} \left\{ \sum_{k=1}^K \text{Tr} \left(\mathbf{U}_k^H \left(\hat{\mathbf{H}}_{kk} + \mathbf{E}_{kk} \right) \mathbf{V}_k + \mathbf{V}_k^H \left(\hat{\mathbf{H}}_{kk} + \mathbf{E}_{kk} \right)^H \mathbf{U}_k \right) \right\} \\ & + d + \mathbb{E} \left\{ \sum_{k=1}^K \left\| \mathbf{U}_k^H \right\|^2 \mathbf{R}_{nn} \right\} \end{aligned} \quad (4.46)$$

Using the property of the $\text{Tr}(\cdot)$ operation $\text{Tr}(\mathbf{AB}) = \text{Tr}(\mathbf{BA})$ and $\mathbb{E}\{\mathbf{E}_{kl}\} = 0 \forall k, l$, we obtain

$$\begin{aligned} \bar{\epsilon}\{\mathbf{U}_k, \mathbf{V}_l\} &= \frac{1}{K} \sum_{k=1}^K \sum_{l=1}^K \text{Tr} \left(\mathbf{U}_k^H \widehat{\mathbf{H}}_{kl} \mathbf{V}_l \mathbf{V}_l^H \widehat{\mathbf{H}}_{kl}^H \mathbf{U}_k \right) \\ &+ \frac{1}{K} \sum_{k=1}^K \sum_{l=1}^K \text{Tr} \left(\mathbf{U}_k^H \mathbf{E}_{kl} \mathbf{V}_l \mathbf{V}_l^H \mathbf{E}_{kl}^H \mathbf{U}_k \right) \\ &- \frac{1}{K} \sum_{k=1}^K \text{Tr} \left(\mathbf{U}_k^H \widehat{\mathbf{H}}_{kk} \mathbf{V}_k + \mathbf{V}_k^H \widehat{\mathbf{H}}_{kk}^H \mathbf{U}_k \right) + d + \frac{1}{K} \sum_{k=1}^K \sigma^2 \text{Tr} \left(\mathbf{U}_k \mathbf{U}_k^H \right) \end{aligned} \quad (4.47)$$

Lemma I: Let \mathbf{X} be $L \times L$ random matrix, then $\text{Tr}\{\mathbf{XAX}^H\mathbf{B}\} = \text{vec}(\mathbf{X})^H (\mathbf{B}^T \otimes \mathbf{A}) \text{vec}(\mathbf{X})$.

Proof: Using the following properties of $\text{vec}(\cdot)$ and $\text{Tr}(\cdot)$ operations for any matrices \mathbf{A} , \mathbf{B} and \mathbf{C}

1. $\text{Tr}(\mathbf{AB}) = \text{vec}(\mathbf{A}^H)^H \text{vec}(\mathbf{B})$
2. $\text{vec}(\mathbf{ABC}) = (\mathbf{C}^T \otimes \mathbf{A}) \text{vec}(\mathbf{B})$,

we obtain

$$\begin{aligned} \text{Tr}(\mathbf{XAX}^H\mathbf{B}) &= \text{Tr}(\mathbf{X}^H\mathbf{BXA}) \\ &= \text{vec}(\mathbf{X})^H \text{vec}(\mathbf{BXA}) \\ &= \text{vec}(\mathbf{X})^H (\mathbf{A}^T \otimes \mathbf{B}) \text{vec}(\mathbf{X}). \end{aligned}$$

Lemma II: Let \mathbf{X} be $n \times n$ random matrix with $\mathbb{E}\{\text{vec}(\mathbf{X})^H \text{vec}(\mathbf{X})\} = \sigma_X^2 \mathbf{I}$, then $\mathbb{E}\{\text{Tr}\{\mathbf{X}^H\mathbf{BXA}\}\} = \sigma_X^2 \text{Tr}(\mathbf{A})\text{Tr}(\mathbf{B})$.

Proof: Utilizing Lemma I and the following properties of $\text{Tr}(\cdot)$ operations for both matrices \mathbf{A} and \mathbf{B}

1. $\text{Tr}(\mathbf{A} \otimes \mathbf{B}) = \text{Tr}(\mathbf{A})\text{Tr}(\mathbf{B})$
2. $\text{Tr}(\mathbf{A}^T) = \text{Tr}(\mathbf{A})$,

result in

$$\begin{aligned} \mathbb{E}\{\text{Tr}(\mathbf{X}^H\mathbf{BXA})\} &= \mathbb{E}\{\text{vec}(\mathbf{X})^H (\mathbf{A}^T \otimes \mathbf{B}) \text{vec}(\mathbf{X})\} \\ &= \text{Tr}(\mathbf{A}^T \otimes \mathbf{B}) \mathbb{E}\{\text{vec}(\mathbf{X})^H \text{vec}(\mathbf{X})\} \\ &= \sigma_X^2 \text{Tr}(\mathbf{A}) \text{Tr}(\mathbf{B}) \end{aligned}$$

Applying Lemma II with $\mathbb{E}\{\text{vec}(\mathbf{E}_{kl}) \text{vec}(\mathbf{E}_{k'l'})^H\} = 0 \forall k \neq k', l \neq l'$ to (4.46), this equation can be rewritten as

$$\begin{aligned} \bar{\epsilon}\{\mathbf{U}_k, \mathbf{V}_l\} &= \frac{1}{K} \sum_{k=1}^K \sum_{l=1}^K \text{Tr} \left(\mathbf{U}_k^H \widehat{\mathbf{H}}_{kl} \mathbf{V}_l \mathbf{V}_l^H \widehat{\mathbf{H}}_{kl}^H \mathbf{U}_k \right) \\ &+ \frac{1}{K} \sum_{k=1}^K \sum_{l=1}^K \sigma_{\mathbf{E}_{kl}}^2 \text{Tr}(\mathbf{V}_l^H \mathbf{V}_l) \text{Tr}(\mathbf{U}_k \mathbf{U}_k^H) \\ &- \frac{1}{K} \sum_{k=1}^K \text{Tr} \left(\mathbf{U}_k^H \widehat{\mathbf{H}}_{kk} \mathbf{V}_k + \mathbf{V}_k^H \widehat{\mathbf{H}}_{kk}^H \mathbf{U}_k \right) + d + \frac{1}{K} \sum_{k=1}^K \sigma_n^2 \text{Tr}(\mathbf{U}_k \mathbf{U}_k^H). \end{aligned} \quad (4.48)$$

Consequently, the optimization problem described in (4.40) can be reformulated as

$$\mathbf{U}_k^{\text{ASMSE}}, \mathbf{V}_l^{\text{ASMSE}} = \underset{\mathbf{U}_k, \mathbf{V}_l}{\text{argmin}} (\bar{\epsilon}\{\mathbf{U}_k, \mathbf{V}_l\}), \text{ subject to } \|\mathbf{V}_l\|^2 \leq P_l, \quad (4.49)$$

As discussed in Subsection 4.4.3 the optimization problem in (4.49) can be solved by using the Lagrange duality and the KKT method, where the Lagrange function is given by

$$\begin{aligned} L^{\text{ASMSE}}(\lambda_l, \mathbf{U}_k, \mathbf{V}_l) &= \bar{\epsilon}\{\mathbf{U}_k, \mathbf{V}_l\} + \lambda_l(\text{Tr}(\mathbf{V}_l \mathbf{V}_l^H) - P_l) \\ &= \frac{1}{K} \sum_{k=1}^K \sum_{l=1}^K \text{Tr}(\mathbf{U}_k^H \hat{\mathbf{H}}_{kl} \mathbf{V}_l \mathbf{V}_l^H \hat{\mathbf{H}}_{kl}^H \mathbf{U}_k) \\ &\quad + \frac{1}{K} \sum_{k=1}^K \sum_{l=1}^K \sigma_{E_{kl}}^2 \text{Tr}(\mathbf{V}_l^H \mathbf{V}_l) \text{Tr}(\mathbf{U}_k \mathbf{U}_k^H) \\ &\quad - \frac{1}{K} \sum_{k=1}^K \text{Tr}(\mathbf{U}_k^H \hat{\mathbf{H}}_{kk} \mathbf{V}_k + \mathbf{V}_k^H \hat{\mathbf{H}}_{kk}^H \mathbf{U}_k) \\ &\quad + d + \frac{1}{K} \sum_{k=1}^K \sigma_n^2 \text{Tr}(\mathbf{U}_k \mathbf{U}_k^H) + \lambda_l(\text{Tr}(\mathbf{V}_l \mathbf{V}_l^H) - P_l) \end{aligned}$$

Using the KKT conditions described in (4.42), for a fixed pre-coding filter matrix \mathbf{V}_l , post-processing filter matrix \mathbf{U}_k can be determined by solving equation $\nabla_{\mathbf{U}_k^H} L^{\text{ASMSE}} = 0$. This leads to

$$\mathbf{U}_k^{\text{ASMSE}} = \left(\sum_{l=1}^K \hat{\mathbf{H}}_{kl} \mathbf{V}_l \mathbf{V}_l^H \hat{\mathbf{H}}_{kl}^H + \sum_{l=1}^K \sigma_{E_{kl}}^2 \text{Tr}(\mathbf{V}_l \mathbf{V}_l^H) \mathbf{I}_{N_r} + \sigma_n^2 \mathbf{I}_{N_r} \right)^{-1} \hat{\mathbf{H}}_{kk} \mathbf{V}_k. \quad (4.50)$$

Similarly, for a fixed pre-coding filter matrix \mathbf{U}_k , by solving equation $\nabla_{\mathbf{V}_l^H} L^{\text{ASMSE}} = 0$, we get

$$\mathbf{V}_l^{\text{ASMSE}} = \left(\sum_{k=1}^K \hat{\mathbf{H}}_{kl} \mathbf{U}_k \mathbf{U}_k^H \hat{\mathbf{H}}_{kl}^H + \sum_{l=1}^K \sigma_{E_{kl}}^2 \text{Tr}(\mathbf{U}_k \mathbf{U}_k^H) \mathbf{I}_{N_t} + \lambda_l \mathbf{I}_{N_t} \right)^{-1} \hat{\mathbf{H}}_{ll}^H \mathbf{U}_l. \quad (4.51)$$

The proposed robust IA approach can be summarized as follows

1. initialize the pre-coding and post-processing filters $\mathbf{V}_l, \forall l = 1, \dots, K$, so that $\text{Tr}(\mathbf{V}_l \mathbf{V}_l^H) \leq P_l$.
2. determine the post-processing filter matrix \mathbf{U}_k according to (4.50) for a given pre-coding filter matrix \mathbf{V}_l .
3. optimize the pre-coding filter matrix \mathbf{V}_l according to (4.51) for a given post-processing filter matrix \mathbf{U}_k .
4. repeat from step 2 until convergence.

4.6 SIMULATION RESULTS

In this subsection, the system performance of above considered IA approaches in terms of the average sum-rate and BER is evaluated for a multi-user MIMO OFDM system. For a given set of $\{K, d\}$, the number of transmit and receive antennas is determined according to (4.5). All simulations were conducted using the 4-QAM modulation scheme and a statistical multi-path fading channel model. The noise is assumed to be statistically independent, zero-mean complex Gaussian random variables. Furthermore, each transmitter has the same transmission power P , i.e. $P_l = P$ for $\{\forall l = 1, 2, \dots, K\}$, which is further equally divided among the N_t transmit antennas. The average sum-rate and BER performance are averaged over 100 channel realizations.

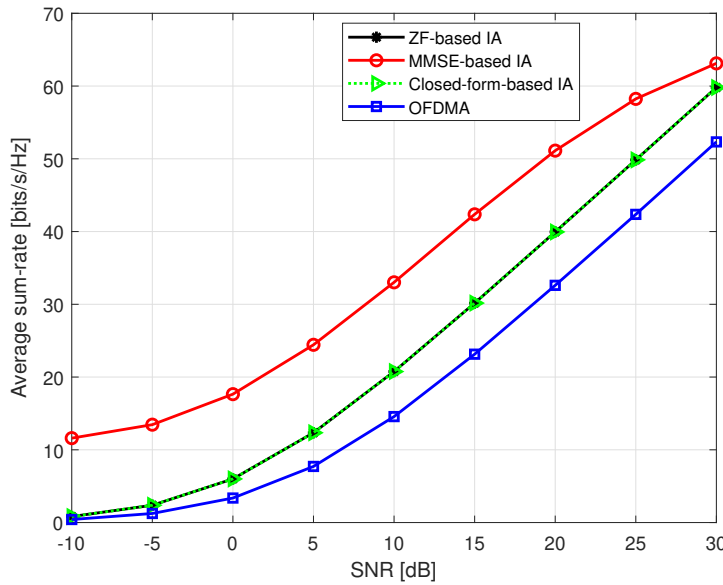


Figure 4.4: The average sum-rate comparison for 3 users 6×6 MIMO OFDM system

First, the system capacity achieved by three existing IA approaches is compared to that using the OFDMA technique for the case of $\{K = 3, N_r = N_t = 4, d = 2\}$. Fig. 4.4 shows that the IA schemes outperforms the OFDMA scheme. It can be explained that by using the OFDMA technique, the total bandwidth is equally divided over K users, i.e. each user has less bandwidth. Consequently, the OFDMA approach achieves inferior capacity in comparison to the considered IA approaches. Furthermore, simulation results confirm that, due to IA filters optimization by taking the noise into consideration, the MMSE-based IA approach delivers the best system performance in term of the average sum-rate. Moreover, it can be seen that using the ZF- and closed form-based IA approaches, the pre-coding filter \mathbf{V}_l and post-processing filter \mathbf{U}_k are optimized based on the ZF criterion, and thus both IA approaches deliver the same average sum-rate. However, the closed-form based IA approach works only for the case of three users.

Subsequently, the system performance of the ZF- and MMSE-based IA approaches is investigated for different number of users. For the case $\{d = 2, N_r = N_t = 7\}$, according to the conditions in (4.5) this configuration can only support from 3 up

to 5 users. As seen in Fig. 4.5, the average sum-rate is increased with the increasing of number of users.

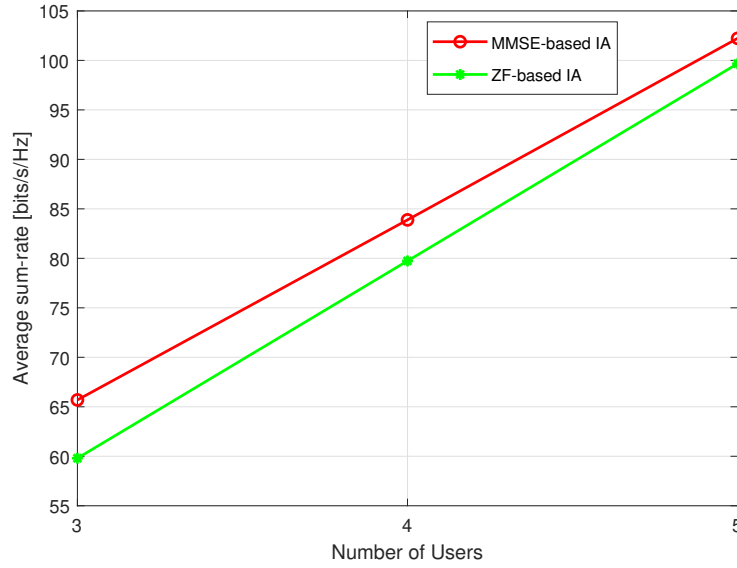


Figure 4.5: average sum-rate comparison for different number of users

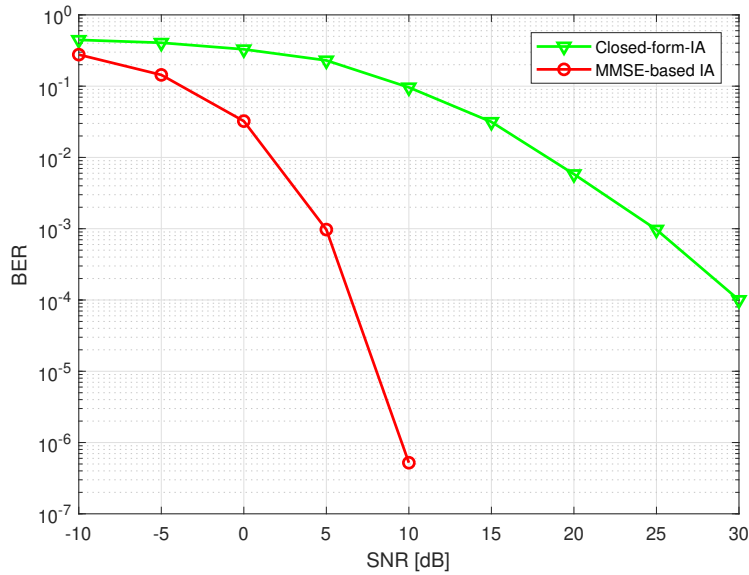


Figure 4.6: The comparison of BER performance using different IA approaches

Fig. 4.6 illustrates the BER performance vs. SNR of the three existing IA approaches for the case of $\{K = 3, N_r = N_t = 4, d = 2\}$. This Figure indicates that the MMSE-based IA scheme provides superior BER performance compared to the closed-form-based IA scheme over all SNR regimes.

In the case of imperfect CSI, the AS-MMSE-based IA system performance in terms of MSE is investigated with different values of CSI errors. Here, the system performance of the conventional MMSE-based IA approach serves as the reference system. For this purpose, the average MSE as a function of SNR for the case of

$\{K = 3, N_t = N_r = 6, d = 2\}$ is depicted in Fig. 4.7. It can be seen that the MSE of the MMSE-based IA approach decreases with the increasing of the inaccuracy of CSI. However, by concerning the CSI error to determine the IA filters, the AS-MMSE-based IA approach delivers better performance compared to the conventional MMSE-based approach. Using this IA approach the MSE is significantly reduced.

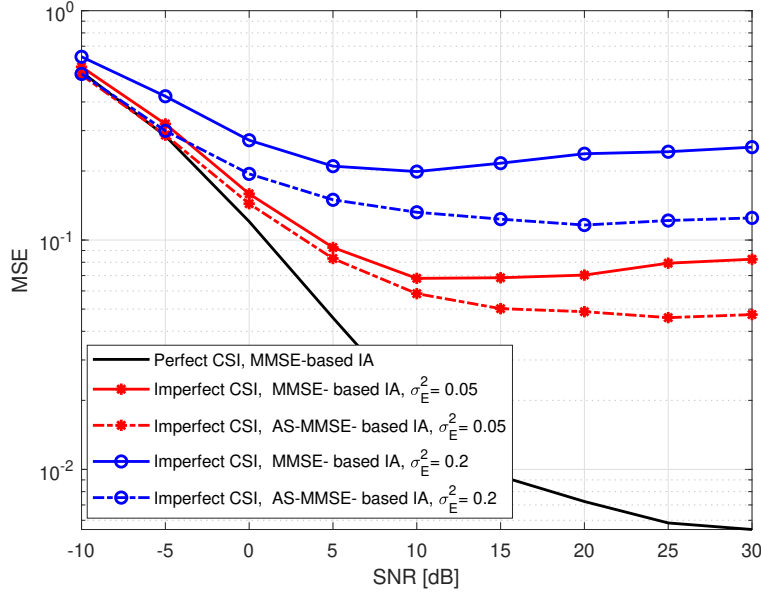


Figure 4.7: MSE performance comparison between perfect and imperfect CSI

4.7 SUMMARY

In this chapter, an overview about the IA technique is given. Here, three conventional IA approaches having perfect CSI are introduced. In addition, a novel IA approach based on the AS-MMSE optimization criterion is proposed to deal with the imperfection of CSI.

First, the motivation for using the IA technique to deal with the MUI problem in a multi-user MIMO system is illustrated in Section 4.1. It is explained that IA is one of the most promising frequency reuse techniques used in wireless communication systems to achieve an SE improvement. Using the IA technique, the maximum spatial diversity can be achieved. Moreover, the concept and the system model of IA are described in Section 4.2. In case of having perfect CSI, three conventional IA approaches are introduced in Section 4.4. The first approach is the IA approach based on the closed-form solution. The second approach is the ZF-based IA approach using the reciprocity of the propagation channel. Using these approaches the IA problem is solved by minimizing the total interference leakage at each receiver without considering the noise. Thus, the main drawback of the first and second IA approach is that both approaches are only optimal in the high SNR regime. Therefore, the MMSE-based IA approach is proposed to improve the system performance in the low and moderate SNR regimes. *In order to overcome the imperfection of CSI*

problem caused by the channel estimation error, a novel IA approach based on the AS-MMSE criterion is proposed and evaluated in Section 4.5. Simulation results in Section 4.5 show that three conventional IA approaches provide better average sum-rate compared to the OFDMA scheme. Furthermore, simulation results confirm that due to IA filters optimization by taking the noise into consideration, the MMSE based IA approach delivers the best system performance in term of the average sum-rate and BER. In the case of imperfect CSI, it is shown that the IA system performance in terms of MSE decreases with the increasing of the inaccuracy of CSI. In this case, by using the novel IA approach based on the AS-MMSE criterion the MSE is significantly reduced.

In the next chapters, the IA approaches based on the ZF, MMSE and AS-MMSE are extended for the cases of a multi-user underlay CR and a multi-user relay MIMO system.

IA IN COGNITIVE RADIO NETWORK

5.1 INTRODUCTION

The Cognitive Radio (CR) technology provides various options for unlicensed wireless communication devices to adapt their spectrum use in response to their operating environment. This technology is known as one of the most promising techniques for an improvement of the spectrum efficiency in wireless communication networks [41, 73, 50]. Depending on how the spectrum reutilization being carried out, different CR strategies have been defined, e.g. interweave, underlay and overlay CR. The most common CR technique used in practice is the interweave CR, where unlicensed user (i.e. Secondary User (SU)) is allowed to access the radio spectrum if it is not occupied by a licensed user (i.e. Primary User (PU)) [2]. For this technique, a Spectrum Sensing (SS) process is required for the SUs to detect the spectrum holes and to acquire the radio environment knowledge before they access the licensed radio spectrum [119, 121]. In practice, this process can be complex and expensive, and has some disadvantages related to the PU detection. Interweave CR has been widely studied and is recommended to use in practical applications. Meanwhile, underlay CR, which provides higher SE in comparison to interweave CR, still poses a challenge that deserves to be studied. More specifically, there is an obvious room for improvement regarding the data transmission efficiency and coexistence of multiple SUs in underlay CR.

In underlay CR, a SU can use the same spectrum simultaneously with a PU as long as the QoS of the PU remains unaffected. Condition thereon is that the interference caused from a SU to the PU should not exceed the maximum tolerable level of the PU receiver [57, 61]. In this case, a spectrum sensing process is not required for the SU, but the SU transmit power has to be controlled steadily to guarantee a given QoS of the PU. The main drawback of this approach is that the throughput of the SU is limited and it is very difficult to detect the SU signal at the SU receiver in some application scenarios when its transmit power is extremely low. In addition, this CR technique requires the knowledge of the maximum "tolerable level" of interference at the PU for SU transmissions and also the effects of the SU transmissions have to be known at the PU receiver. Consequently, underlay CR has so far not been widely used in practice. Moreover, the traditional underlay CR might not work in case of multiple SUs, where the interference at the primary receiver is the sum of all interferences from all SUs (i.e. the transmit power of the SU must be extremely low) and the SUs cause interference to each other.

In order to remove the constraints on the SU transmit power and to make the underlay CR technique more applicable and more efficient in using the licensed frequency bands, additional signal processing techniques such as interference mitigation techniques and beamforming have been proposed in literature to be applied at the SUs [116]. Moreover, exploiting the MIMO technique at both transmitter and receiver sides in both links can also support the secondary transmissions without affecting the performance of the PU system. In other words, the use of the MIMO technique at both primary and secondary links allows multiple SUs to transmit their signals into the orthogonal complement of the PU transmission. In the primary link, assuming perfect CSI at both transmitter and receiver sides, the maximum capacity can be achieved by using the WF power allocation scheme over the spatial directions [29, 27, 108, 55]. Using the WF approach, the primary MIMO channel is divided into several parallel sub-channels so-called eigenmodes. It can be noted that even if the PU achieves the maximum transmission rate, some of its spatial directions (eigenmodes) may be unused due to a power limitation on each eigenmode. Therefore, these unused eigenmodes can be reused by another SU operating in the same frequency band and at the same time in an opportunistic way.

It has to be mentioned that in CR, the PU has generally high priority to access the licensed radio band, and hence the primary system must operate free of any additional interference caused by the secondary systems. Since the PU has normally no information about the SUs and does not care about the presence of the SUs or quality of the secondary transmissions, any additional signal processing at the PU regarding interference rejection is not required. In this context, a secondary transmitter is therefore allowed to send its own data to its respective receiver without any power constraints on the SUs by processing its signal in such a way that the secondary transmission is aligned to unused spatial dimensions of the primary link. As a result of this, the SU does not cause any interference to the PU. Nevertheless, the conventional WF pre-coding cannot guarantee any secondary transmission at high SNRs, as the number of unused primary eigenmodes is limited [58, 55]. In this case, an efficient pre-coding technique namely modified WF has been proposed in [58] for the uplink, so that even the QoS of the primary link is guaranteed, some primary eigenmodes are always available for the secondary transmissions. In that work, a coexistence scenario consisting of three nodes: one primary transmitter, one SU and one receiver, has been considered, where the secondary pre-coding matrix was designed to align the secondary transmission to the unused eigenmodes of the PU. It seems that this pre-coding approach delivers good system performance, but it cannot deal with the MAI in the secondary link, which is the major problem of a multi-user MIMO system in underlay CR networks.

In multiple SUs scenarios, the radio spectrum is used more efficiently due to the fact that multiple SUs can access the licensed radio spectrum at the same time with the PU. However, this coexistence requires an efficient interference management technique in the secondary link to deal with all generated interferences. A combination of the WF and IA approaches has been proposed in [5], which can guarantee a perfect coexistence of multiple SUs with a PU without laying constraints on the transmit power of the SUs. This method has been implemented using the

MIMO technique at both links. However, the assumption of at least one free primary eigenmode for the secondary transmission by utilizing the conventional WF does not hold, and thus is not realistic. This remains an open issue for practical realization of multiple SUs transmission to improve the spectrum efficiency in underlay CR, and thus, it is the scope of the investigations in this chapter.

In this chapter, a novel adaptive transmission is proposed for a multi-user underlay CR system, where multiple SUs try to coexist with each others and with one PU. Based on the number of unused eigenmodes of the primary link, the SUs can adapt their transmission to achieve higher data rates. Applying the modified WF algorithm at the primary link ensures that at least one primary eigenmode free for the secondary transmission for all cases. In the cognitive link, transmit and receive filters are jointly designed based on IA and the modified WF approach, so that the secondary transmissions are aligned to the unused eigenmodes of the primary link. By doing so, each SU does not receive any interference from the PU transmission and from the other SUs.

The proposed transmission scheme is discussed in detail in the rest of this chapter. The practical application scenarios and the general system model for a multi-user MIMO broadcast channel in underlay CR are described in section 5.2. In section 5.3 and 5.4, the modified WF algorithms applied in the primary network and the linear precoding based on the IA used in the secondary network are briefly derived, respectively. In section 5.5, the simulation results are presented and finally a conclusion is drawn in section 5.6.

5.2 APPLICATION SCENARIOS AND SYSTEM MODEL

5.2.1 Macro-Small Cell Coexistences

One approach to boost the throughput and to improve the coverage in wireless cellular networks is the deployment of Smallcell Base Station (SBS) in cellular networks. Using this approach, the user density can be improved by increasing the base station density. Thereby, the distance between users and their serving base stations is reduced, and hence the capacity of wireless communication systems can be significantly increased [78, 120, 96, 115]. In this context, the small cells can be developed in both indoor and outdoor scenarios such as in houses, shopping malls, airports or in any public place, where the small base stations have normally low costs and low-power consumption. In heterogeneous networks, there are several kinds of small cells such as picocells, microcells, metrocells and femtocells as well as relay nodes (see Fig. 5.1). Although the deployment of small cells provides an enhancement in terms of energy efficiency and data rate for short-range communication, additional spectrum is required for high user density networks. Due to the limited spectrum availability and the expensive spectrum resource, small cell users have to share the existing frequency resource or to coexist with macro cell users in some applications. Even though this coexistence approach yields higher SE, it requires an efficient interference management scheme due to the interferences caused by co-channel base stations. In such coexistence of two-tier networks, it is possible that a macro cell user coexists with one or multiple small cell users, where the SBS uses the spectrum assigned to the macro cell base station to com-

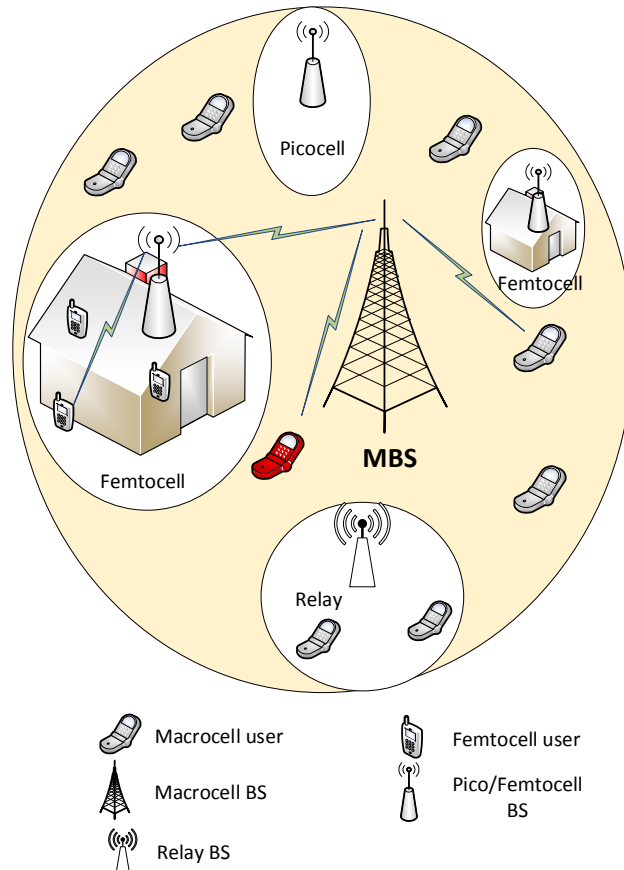


Figure 5.1: Heterogeneous networks-coexistence of macro and small cells

municate with its users in an efficient way such as by using the CR technique [22]. In case of using the CR technique, the communication between the macro base station and its users is referred as the primary link and the communications in small cells correspond to the cognitive links. In this context, researchers have recently proposed some approaches such as dynamic spectrum access [68, 45], interference coordination and power control [21, 109, 64] to deal with the cross-tier and co-tier interference. Additionally, IA can be efficiently used to guarantee an interference-free transmission in multi-tier heterogeneous networks by using linear pre-coding technique and by exploiting the advance of the MIMO technique [44].

5.2.2 Macrocell-Femtocell Coexistences

As mentioned in the previous subsections, a small cell in cellular networks is called femtocell, which typically has a coverage of 10 – 50m and is served by a Femtocell Access Point (FAP) to support stationary or low-mobility users in indoor scenarios [9]. A FAP, the so-called home base station has low power, low cost, and it can be considered as a short range, small and inexpensive cellular BS deployed in home area or small office. In practice, the femtocell base station is normally user-installed and it is connected to the cellular operator network through a backhaul provided by a broadband access network such as Digital Subscriber Line (DSL) or

cable modem [9]. Femtocells are usually deployed in unplanned way in cellular networks. They can be moved or switched on/off at any time, and hence it is difficult to control either the number or the location of femtocells. As a result, an optimal network planning can not be achieved. This leads to other problems such as resource allocation and interference management techniques for femtocells in multi-tier heterogeneous networks. In practice, the traditional frequency allocation technique OFDMA can be used for femtocells in two-tier networks to minimize the cross-tier interference [20, 69, 104, 97]. However, the OFDMA technique has low frequency reuse efficiency. Another approach of the frequency resource allocation for femtocells is by sharing the spectrum with a macro cell user, and it is known as underlay femtocells. Using this method, multiple femtocell users can use the same frequency band allocated to a macro cell user at the same time with the macro cell user, leading to an increase in SE [1]. The unplanned nature of femtocells development motivates researchers to develop efficient decentralized interference management techniques, which can independently be used in each small cell by using only local information if these small cells coexist with each other and with the macro cell. Base on this idea, IA can be used to handle the interference in femtocell and macro cell coexistence scenarios.

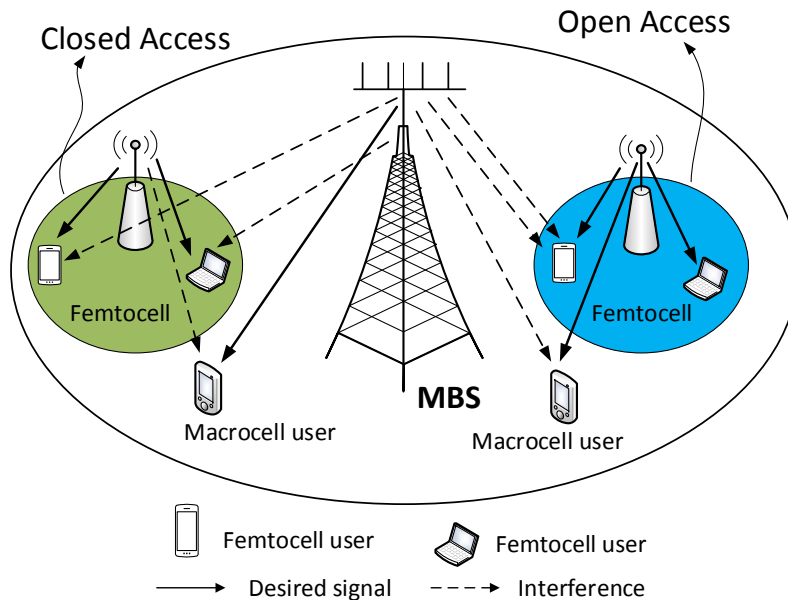


Figure 5.2: Open vs. Closed Access of femtocell in two-tier networks

Normally, a femtocell can choose the set of users allowed to access the femtocell base station. In practice, the femtocell access can be classified into two schemes: closed or open access (see Fig. 5.2) [7]. In open access scheme, any users closed to the femtocell are allowed to use this femtocell. In contrast, in closed access scheme only registered users can use the femtocell. In this chapter, the open access scheme is considered.

It is assumed that for a given time slot the macro cell and femtocell base stations transmit their signals simultaneously over a common set of frequencies to their users. In this case, the Macro-cell Base Station (MBS) uses its assigned frequency

band to support only one macro cell user, which is located close to the femtocell, and the Femtocell Base station (FBS) reuses this frequency band to support multiple femtocell users. In this coexistence scenario, the macro cell system acts as a single user primary system and the femtocell system is considered as a multiple secondary user system. The macro cell system operates in the licensed radio frequency band without information about femtocell users and the FBS is allowed to transmit its data over this radio frequency band if the interference caused by the FBS can be avoided at the macro user without additional signal processing in the primary link. In order to handle the interference between femtocell and macro cell users, the FBS does not need to have knowledge of the primary transmission but the CSI is required to be available at both transmitter and receiver sides in the femtocell network. The CSI can be obtained through the backhaul connection between the FAP and its associative MBS. By exploiting the CSI, a joint pre-coding technique based on IA can be applied in the femtocell network to guarantee an underlay CR coexistence.

5.2.3 System Model

The system model illustrated in Fig. 5.3 describes the coexistence scenario proposed in Fig. 5.2 for the open access scheme, where the macro cell system is denoted by index 0. In the primary link, the licensed MBS (PU transmitter) communicates directly with a macro cell user (PU receiver). The PU does not care about the presence and the system performance of a Femtocell User (FU). In the secondary link, the FBS (secondary transmitter) accesses the spectrum which is licensed to the PU to support K femtocell users (secondary receiver or SUs).

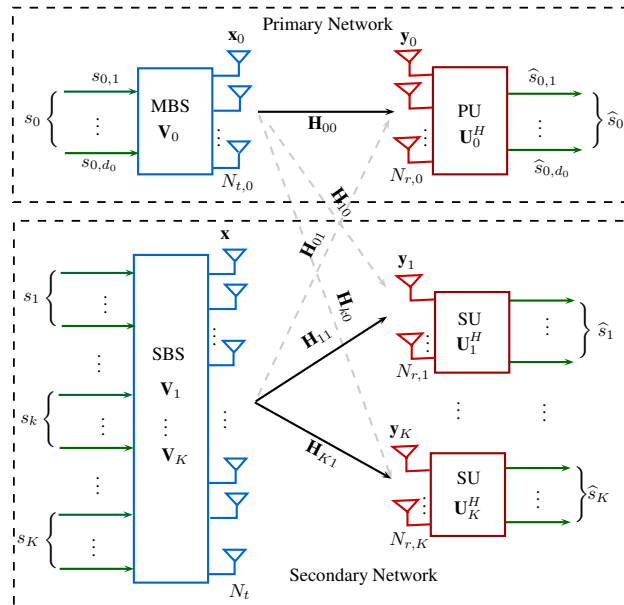


Figure 5.3: General system model of multi-user MIMO broadcast channel in underlay CR

In this system model, the MBS and the PU receiver are equipped with $N_{t,0}$ and $N_{r,0}$ antennas. Denote that N_t and $N_{r,k}$ are the number of antennas at the FBS and

the k -th femtocell SU, respectively. It is assumed that the FBS sends d_k independent data streams, i.e. $\mathbf{s}_k = [\mathbf{s}_{k,1}, \mathbf{s}_{k,2}, \dots, \mathbf{s}_{k,d_k}]^T$ to the k -th femtocell user. Thus, the total data streams to be supported by the FBS is $d = \sum_{k=1}^K d_k$. The number of independent transmitted data streams d_k supported by user k is also known as the achieved degree of freedom for user k . In Fig. 5.3, \mathbf{y}_k represents the $N_{r,k} \times 1$ received signal vector at the k -th femtocell user, which is expressed as

$$\mathbf{y}_k = \mathbf{H}_{k1}\mathbf{x} + \mathbf{H}_{k0}\mathbf{x}_0 + \mathbf{n}_k, \tag{5.1}$$

where $\mathbf{x} = \mathbf{V}\mathbf{s}$ is the $N_t \times 1$ transmitted signal vector at the FBS and \mathbf{n}_k is the $N_{r,k} \times 1$ noise signal vector at the k -th femtocell user. Additionally, $\mathbf{s} = [\mathbf{s}_1^T, \mathbf{s}_2^T, \dots, \mathbf{s}_K^T]^T$ and the block diagonal matrix $\mathbf{V} = \text{diag}\{\mathbf{V}_1, \mathbf{V}_2, \dots, \mathbf{V}_k\}$ stand for the transmitted data symbol vector and the pre-coding matrix at the FBS, respectively. The pre-coding matrix for the k -th femtocell user is represented as \mathbf{V}_k . The additive noise \mathbf{n}_k is assumed to be a zero mean circularly symmetric AWGN vector with covariance matrix $\mathbf{R}_{n,n} = \mathbb{E}\{\mathbf{n}_k\mathbf{n}_k^H\} = \sigma_n^2\mathbf{I}$, where σ_n^2 is the covariance of the noise or the noise power. The $N_{r,k} \times N_t$ channel matrix \mathbf{H}_{k1} and the $N_{k0} \times N_{r,k}$ channel matrix \mathbf{H}_{k0} contain the channel coefficients from the FBS and the MBS to the k -th femtocell user, respectively. Here, it is assumed that the macro cell user has no information about the femtocell users, i.e. for the pre-coding in the primary network only knowledge on the channel matrix \mathbf{H}_{00} is required. In the secondary network, the local CSI is available at the FBS and at each femtocell user, i.e. each node has perfect knowledge of local channel coefficients. The received signal at femtocell user k is linearly processed by the receive filter \mathbf{U}_k to reconstruct d_k transmitted streams. The estimated data streams $\hat{\mathbf{s}}_k \forall k \in \{1, \dots, K\}$ at the k -th femtocell user are given by

$$\hat{\mathbf{s}}_k = \underbrace{\mathbf{U}_k^H \mathbf{H}_{k1} \mathbf{V}_k \mathbf{s}_k}_{\text{Desired signal}} + \underbrace{\sum_{l=1, l \neq k}^K \mathbf{U}_k^H \mathbf{H}_{k1} \mathbf{V}_l \mathbf{s}_l}_{\text{Interference from other SUs}} + \underbrace{\mathbf{U}_k^H \mathbf{H}_{k0} \mathbf{x}_0}_{\text{Interference from PU}} + \underbrace{\mathbf{U}_k^H \mathbf{n}_k}_{\text{Noise}}. \tag{5.2}$$

Similarly, the estimated data streams \mathbf{s}_0 at the macro cell user can be expressed as follows:

$$\hat{\mathbf{s}}_0 = \underbrace{\mathbf{U}_0^H \mathbf{H}_{00} \mathbf{V}_0 \mathbf{s}_0}_{\text{Desired signal}} + \underbrace{\mathbf{U}_0^H \mathbf{H}_{01} \mathbf{V} \mathbf{s}}_{\text{Interference from SUs}} + \underbrace{\mathbf{U}_0^H \mathbf{n}_0}_{\text{Noise}}, \tag{5.3}$$

where \mathbf{V}_0 , \mathbf{H}_{01} and \mathbf{U}_0^H are the $N_{t,0} \times d_0$ pre-coding matrix at the MBS, the $N_{r,0} \times N_t$ channel matrix from the FBS to the macro cell user and the $N_{r,0} \times d_0$ post-processing matrix at the macro cell user, respectively. In this work, it is assumed that the transmitters send independent data streams, e.g. $\mathbb{E}\{\mathbf{s}_k \mathbf{s}_l^T\} = 0$ for $k \neq l$. In addition, all transmitted data streams and noise are statistically independent having $\mathbb{E}\{\mathbf{s}_k \mathbf{n}_l^T\} = 0$, for $\forall(k, l) \in \{1, 2, \dots, K\}$. As discussed before, the SUs are allowed to transmit their data, only if they do not cause any interference to the PU. Hence, each secondary transmitter has to adjust the pre-coding filter \mathbf{V}_k , in order to satisfy the condition

$$\mathbf{U}_0^H \mathbf{H}_{01} \mathbf{V} = 0. \tag{5.4}$$

Furthermore, each femtocell user shall not receive any interference from the MBS and from other femtocell users. Thus, each femtocell user has to suppress all interferences by multiplying the received signal with a post-processing filter \mathbf{U}_k . For this, the following conditions have to be fulfilled

$$\begin{aligned} \text{rank}(\mathbf{U}_k^H \mathbf{H}_{k1} \mathbf{V}_k) &= d_k, \\ \mathbf{U}_k^H \mathbf{H}_{k0} \mathbf{V}_0 &= 0, \\ \sum_{l=1, l \neq k}^K \mathbf{U}_k^H \mathbf{H}_{kl} \mathbf{V}_l &= 0 \quad \forall l, k = 1, \dots, K, l \neq k. \end{aligned} \quad (5.5)$$

Since a secondary transmission is only ensured if at least one unused primary eigenmode is available, the number of independent transmitted data streams d_k for the k -th femtocell user has to fulfill the following condition

$$d_k \leq \min((N_t - d_0)^+, (N_{r,k} - d_0)^+), \quad (5.6)$$

where $(N_t - d_0)^+$ and $(N_{r,k} - d_0)^+$ are known as equivalent transmit and receive antennas at the FBS and the k -th SU in the presence of the PU, respectively.

Here, the transmit/receive filters \mathbf{V} and \mathbf{U} are jointly designed to satisfy the conditions given in (5.4), (5.5) and (5.6).

5.3 MODIFIED WF ALGORITHM IN PRIMARY NETWORK

As mentioned above, the primary network tries to maximize its capacity using the WF approach based on the SVD technique, irrespective of whether the SUs use or do not use the radio frequency band allocated to the PU. In this section, it is assumed that the MIMO channel is a time-invariant channel. Using the WF approach, the primary transmitter sends parallel independent data streams along the eigenmodes (sub-channels) of the MIMO channel. The main purpose of the WF approach is to allocate different power to the sub-channels depending on the quality of each sub-channel, in order to achieve the maximal channel capacity. According to the WF approach, more power is allocated to "better" sub-channels having greater gain, and less or no power to "worse" sub-channels having more attenuation. In this case, the "worse" sub-channels are not used for the primary transmission, and thus can be reused by the secondary transmissions without interference to the PU. In the following, the fundamentals necessary to understand the concept of the WF technique will be explained.

The maximum spatial multiplexing gain or the number of eigenmodes of the primary MIMO channels is given as $d_0 = \min(N_{r,0}, N_{t,0})$. The aim of this section is to design the pre-coding filter \mathbf{V}_0 and post-processing filter \mathbf{U}_0 by exploiting the CSI in the primary link, so that maximum capacity can be achieved. Using the SVD technique, the channel matrix \mathbf{H}_{00} and the desired pre-coding matrix \mathbf{V}_0 can be factorized into

$$\begin{aligned} \mathbf{H}_{00} &= \mathbf{U}_{\mathbf{H}_{00}} \boldsymbol{\Sigma}_{\mathbf{H}_{00}} \mathbf{V}_{\mathbf{H}_{00}}^H, \\ \mathbf{V}_0 &= \mathbf{U}_{\mathbf{V}_0} \boldsymbol{\Sigma}_{\mathbf{V}_0} \mathbf{V}_{\mathbf{V}_0}^H, \end{aligned} \quad (5.7)$$

where the matrices $\mathbf{U}_{\mathbf{H}_{00}}$ and $\mathbf{V}_{\mathbf{H}_{00}}$ have dimensions of $N_{r,0} \times N_{r,0}$ and $N_{t,0} \times N_{t,0}$, respectively, and they are unitary matrix. The matrix $\mathbf{\Sigma}_{\mathbf{H}_{00}}$ is a $N_{r,0} \times N_{t,0}$ diagonal matrix of diagonal elements $\lambda_{\mathbf{H}_{00},i}$ being the singular values of the matrix \mathbf{H}_{00} , i.e. $\mathbf{\Sigma}_{\mathbf{H}_{00}} = \text{diag}\{\lambda_{\mathbf{H}_{00},1}, \dots, \lambda_{\mathbf{H}_{00},d_0}\}$. Here, $\lambda_{\mathbf{H}_{00},i}^2$ is the i -th diagonal element of the matrix \mathbf{T} with $\mathbf{T} = \mathbf{H}_{00}\mathbf{H}_{00}^H$ (for $N_t > N_r$) or $\mathbf{T} = \mathbf{H}_{00}^H\mathbf{H}_{00}$ (for $N_t < N_r$). Since the CSI is available at the PU transmitter, the system capacity of the primary link can be determined as [14, 28]

$$\mathbf{C} = \max_{\mathbf{Q}_{00}: \text{Tr}(\mathbf{Q}_{00}) \leq P_0} \mathbb{E} \{ \log_2 \det (\mathbf{I}_{N_r} + \rho \mathbf{H}_{00} \mathbf{Q}_{00} \mathbf{H}_{00}^H) \}, \quad (5.8)$$

where $\rho = 1/\sigma_n^2$ with σ_n^2 being the covariance of the noise. The matrix \mathbf{Q}_{00} stands for the covariance matrix of the transmitted signal \mathbf{x}_0 and is given by

$$\begin{aligned} \mathbf{Q}_{00} &= \mathbb{E} \{ \mathbf{V}_0 \mathbf{s}_0 (\mathbf{V}_0 \mathbf{s}_0)^H \}, \\ &= \mathbf{V}_0 \mathbf{V}_0^H. \end{aligned} \quad (5.9)$$

Inserting \mathbf{V}_0 in (5.7) into (5.9), we obtain

$$\begin{aligned} \mathbf{Q}_{00} &= (\mathbf{U}_{\mathbf{V}_0} \mathbf{\Sigma}_{\mathbf{V}_0} \mathbf{V}_{\mathbf{V}_0}^H) (\mathbf{U}_{\mathbf{V}_0} \mathbf{\Sigma}_{\mathbf{V}_0} \mathbf{V}_{\mathbf{V}_0}^H)^H, \\ &= \mathbf{\Sigma}_{\mathbf{V}_0}^2. \end{aligned} \quad (5.10)$$

The diagonal elements of $\mathbf{\Sigma}_{\mathbf{V}_0}^2$ are the square of the singular values of \mathbf{V}_0 , which are denoted by $\lambda_{\mathbf{V}_0,i}^2$. Here, the parameter $\lambda_{\mathbf{V}_0,i}^2$ corresponds to the allocated power to the i -th sub-channel and it is determined by using the WF technique. Accordingly, the capacity in (5.8) can be reformulated as [32]

$$\mathbf{C} = \sum_{i=1}^m \mathbb{E} \{ \log_2 (1 + p_i \lambda_{\mathbf{H}_{00},i}^2) \} \quad (5.11)$$

with $p_i = \lambda_{\mathbf{V}_0,i}^2$. Using the WF technique, the optimal power allocated to the i -th eigenmode is defined as [32]

$$p_i = \left[\zeta - \frac{\sigma_n^2}{\lambda_{\mathbf{H}_{00},i}^2} \right]_+, \quad (5.12)$$

with σ_n^2 the noise power. The parameter ζ is the water level, which is chosen in order to satisfy the following power constraints

$$\sum_{i=1}^m p_i = P_0, \quad (5.13)$$

where P_0 represents the total transmit power of the PU, and it is here assumed to be 1.

In a MIMO system, the "better" and "worse" sub-channels correspond to the eigenmodes with greater and smaller singular values, respectively. Therefore, the value of $\sigma_n^2/\lambda_{\mathbf{H}_{00},i}^2$ can be considered as the channel attenuation for the i -th sub-channel, which denotes as the sub-channel damping in Fig. 5.4. This figure illustrates the principle of the WF technique described in (5.12). Furthermore, it is

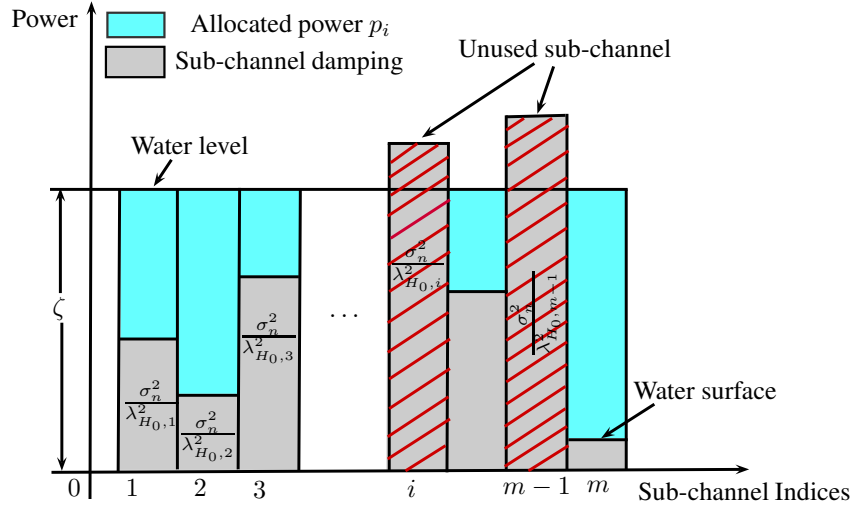


Figure 5.4: The Waterfilling concept

assumed that the eigenvalues of the MIMO channel \mathbf{H}_{00} , $\lambda_{\mathbf{H}_{00},i}^2$, are ordered in decreasing order of magnitude. It can be seen that in each sub-channel with $\sigma_n^2/\lambda_{\mathbf{H}_{00},i}^2$ smaller than ζ , the "pool" is filled up to the water level ζ and the "water" between the "water surface" and the water level determines the power that is assigned to this sub-channel. The sub-channel, for which the channel attenuation is greater than the water level ζ , i.e. $\sigma_n^2/\lambda_{\mathbf{H}_{00},i}^2 > \zeta$, receives no power allocation and it is unoccupied for the primary transmission. As a result, this unused eigenmode can be reused for the secondary transmissions. However, in high SNR regime, where all sub-channel attenuations are smaller than the water level, the primary link releases no eigenmode for the secondary transmission. In this case, if any secondary user wants to access the spectrum simultaneously with the primary link, the SUs have to limit its transmitted power.

To overcome aforementioned problem in underlay CR using the conventional WF approach, the modified WF approach has been proposed in [58]. Employing the modified WF approach in the primary link enables the PU to release some eigenmodes for the secondary transmission for all SNR values. Using the modified WF approach, the power allocation to each sub-channel is performed as follow

$$p_i = \begin{cases} (\zeta - \frac{\sigma_n^2}{\lambda_{\mathbf{H}_{00},i}^2}) & \text{if } (\zeta - \frac{\sigma_n^2}{\lambda_{\mathbf{H}_{00},i}^2}) \geq \delta, \quad i = 1, 2, \dots, m_s \\ 0 & \text{elsewhere,} \end{cases} \quad (5.14)$$

where m_s is the number of active primary eigenmodes. The parameter δ is denoted as the power level, and in case of $\delta = 0$ the modified WF corresponds to the conventional WF approach. The study in [58] shows that in contrast to the conventional WF approach, the modified WF approach allows the PU to flexibly control the transmitted power allocated at each eigenmode. Based on the system parameter δ the primary link can release some sub-channels without having any substantial loss in performance in terms of QoS. More specifically, a parameter δ with $\delta = P_0/m$ ensures that at least one eigenmode is always available for the secondary transmis-

sion at the high SNR regime. In order to maximize the system capacity, the solution for the pre-coding matrix \mathbf{V}_0 can be defined as follows:

$$\mathbf{U}_{\mathbf{V}_0} = \mathbf{V}_{\mathbf{H}_{00}}. \quad (5.15)$$

On the other hand, according to (5.8) and (5.10), it can be seen that the matrix $\mathbf{V}_{\mathbf{V}_0}$ does not affect the channel capacity. Thus, we can choose any unitary matrix as $\mathbf{V}_{\mathbf{V}_0} = \mathbf{I}$. Consequently, the pre-coding matrix \mathbf{V}_0 can be simplified as $\mathbf{V}_0 = \mathbf{V}_{\mathbf{H}_{00}} \boldsymbol{\Sigma}_{\mathbf{V}_0} \mathbf{I}$. If we sort the squares of singular values of \mathbf{H}_{00} in descending order, i.e. $\lambda_{\mathbf{H}_{00},1}^2 \geq \lambda_{\mathbf{H}_{00},2}^2 \geq \dots \geq \lambda_{\mathbf{H}_{00},m_s}^2$, we obtain

$$\begin{aligned} \lambda_{\mathbf{V}_0,i}^2 &= \left(\zeta - \frac{\sigma_n^2}{\lambda_{\mathbf{H}_{00},i}^2} \right), \quad i = 1, 2, \dots, m_s \\ \lambda_{\mathbf{V}_0,i}^2 &= 0 \quad i = m_s + 1, \dots, m \end{aligned} \quad (5.16)$$

Thus, the water level ζ can then be specified as

$$\zeta = \frac{1}{m_s} \left(P_0 + \sigma_n^2 \sum_{i=1}^{m_s} \frac{1}{\lambda_{\mathbf{H}_{00},i}^2} \right). \quad (5.17)$$

The post-processing filter matrix \mathbf{U}_0 is determined as the left-singular vectors of \mathbf{H}_{00} according to (5.7), also $\mathbf{U}_0 = \mathbf{U}_{\mathbf{H}_{00}}$.

5.4 LINEAR PRE-CODING BASED ON IA IN SECONDARY NETWORK

As mentioned in subsection 5.2.1, each secondary receiver suffers not only the interferences from another secondary users, but also the interference from the primary transmitter. In order to ensure an interference-free coexistence between one PU and multiple SUs, the pre-coding technique based on the IA and null-steering technique is proposed for the secondary link. IA ensures that all secondary multi-user interferences are suppressed at each SU. By employing the nullsteering approach, the secondary transmissions are aligned to the unused primary eigenmodes, so that the PU and the SUs do not interfere with each other. In the following, the proposed schemes are described in depth.

5.4.1 Beamforming for Coexistence Between PU and SUs

In this work, it is assumed that multiple SUs coexist with only one PU, which sends d_0 independent streams. Since the PU has priority to use the licensed frequency band and has no information about the SUs, the SBS has to transmit its signal within the null space of the primary receiver by premultiplying the transmitted signal with a transmit beamformer matrix \mathbf{G} . Due to a lack of information on the primary transmission, the SUs cannot decode the primary signal. As a result, the k -th SU tries to nullify the primary transmission by multiplying the received signal with a receive beamformer matrix \mathbf{B}_k . As a result of this, the following condition needs to be fulfilled:

$$\mathbf{U}_0^H \mathbf{H}_{01} \mathbf{G} = 0,$$

$$\mathbf{B}_k^H \mathbf{H}_{k0} \mathbf{V}_0 = 0, \quad (5.18)$$

where \mathbf{G} and \mathbf{B}_k span the null space of the matrix $\mathbf{U}_0^H \mathbf{H}_{0k}$ and $\mathbf{V}_0^H \mathbf{H}_{k0}$, respectively. By doing this, on the one hand, the SUs do not receive any interference from the primary transmission; on the other hand, the primary transmission does not interfere with the secondary transmissions. This approach is called the null-steering method. The study in [5] shows that the matrix dimensions of \mathbf{G} and \mathbf{B}_k can be chosen as $N_t \times (N_t - d_0)$ and $N_{r,k} \times (N_{r,k} - d_0)$ respectively, so that we can convert the considered cognitive system into two equivalent interference-free parallel systems, which are depicted in Fig. 5.5.

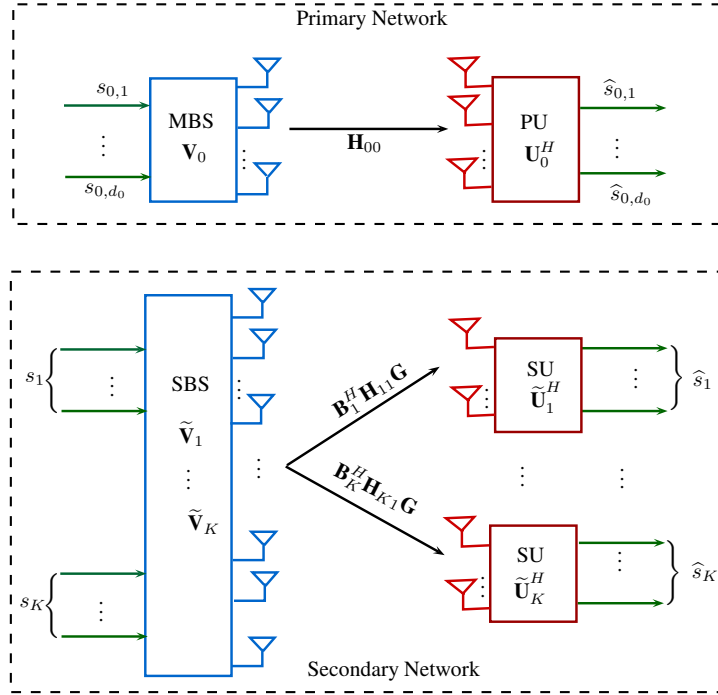


Figure 5.5: Equivalent two interference-free systems

The first system is a single user MIMO channel with d_0 transmit and receive antennas. The second system is a K -user broadcast channel having $N_t - d_0$ transmit and $N_{r,k} - d_0$ receive antennas. A combiner pre-coding based on IA and the null-steering method results in a definition of the pre-coding and post-processing filter in the secondary link to guarantee a coexistence in underlay CR as: $\mathbf{V}_1 = \mathbf{G} \tilde{\mathbf{V}}_1$ and $\mathbf{U}_1 = \mathbf{B}_1 \tilde{\mathbf{U}}_1$. Here, $\tilde{\mathbf{V}}_1$ and $\tilde{\mathbf{U}}_1$ are the pre-coding and post-processing matrix, respectively, which are determined by using the IA technique to mitigate the interference caused by the SUs in the secondary network. In other words, after applying the null-steering method the equivalent channel between the BS and the k -th SU is given by

$$\tilde{\mathbf{H}}_{k1} = \mathbf{B}_k^H \mathbf{H}_{k1} \mathbf{G}. \quad (5.19)$$

In this context, the condition in (5.5) is reformulated as:

$$\begin{aligned} \text{rank} \left(\tilde{\mathbf{U}}_k^H \mathbf{B}_k^H \mathbf{H}_{k1} \mathbf{G} \tilde{\mathbf{V}}_k \right) &= d_k \\ \sum_{l=1, l \neq k}^K \tilde{\mathbf{U}}_k^H \mathbf{B}_k^H \mathbf{H}_{kl} \mathbf{G} \tilde{\mathbf{V}}_l &= 0 \quad \forall l, k = 1, \dots, K. \end{aligned} \quad (5.20)$$

(5.20) can be considered as a standard condition for the conventional IA problem. In the presence of the PU, the matrices $\tilde{\mathbf{V}}_k$ and $\tilde{\mathbf{U}}_k$ in the secondary network have new dimensions of $(N_t - d_0) \times d_k$ and $(N_r - d_0) \times d_k$, respectively. This means that some antennas from both the transmitter and the receiver of the SU are used to eliminate the co-channel interference between the primary and secondary links, and the remaining antennas are used for the secondary transmissions. This is equivalent to a K-user MIMO broadcast channel system depicted in Fig. 5.5, where the equivalent channel from the SBS to the k-th SU is given by $\mathbf{B}_k^H \mathbf{H}_{k1} \mathbf{G}$.

5.4.2 Beamforming for Coexistence Between SUs

Here, only the secondary link is considered. For this, in order to cancel all interferences between the SUs, the IA filters can be determined based on the ZF or MMSE optimization problems, which are described in subsections 4.4.2 and 4.4.3, respectively. In this chapter, a dual network for a multi-user MIMO broadcast channel having the reciprocity principle is considered to solve the MUI problem. Therefore, the IA filter matrices $\tilde{\mathbf{V}}_l$ and $\tilde{\mathbf{U}}_l$ are determined by using the IA approach described in subsection 4.4.2. In this regard, in the downlink/original link the estimated signal at user k is given by:

$$\hat{\mathbf{s}}_k = \tilde{\mathbf{U}}_k^H \tilde{\mathbf{H}}_{k1} \tilde{\mathbf{V}}_k \tilde{\mathbf{s}}_k + \sum_{l=1, l \neq k}^K \tilde{\mathbf{U}}_k^H \tilde{\mathbf{H}}_{kl} \tilde{\mathbf{V}}_l \tilde{\mathbf{s}}_l + \tilde{\mathbf{U}}_k^H \tilde{\mathbf{n}}_k, \quad (5.21)$$

where $\tilde{\mathbf{H}}_{k1}$ is the equivalent channel matrix between the SBS and the k-th SU, and it is given by (5.19). The matrices $\tilde{\mathbf{V}}_k$ and $\tilde{\mathbf{U}}_k$ represent the IA transmit and receiver filters, respectively. Due to the role reversal between the transmitters and receivers in the reciprocal link, the estimated signal for the k-th user at the SBS can be defined as follows:

$$\hat{\mathbf{s}}_k = \bar{\mathbf{U}}_k^H \bar{\mathbf{H}}_{1k} \bar{\mathbf{V}}_k \bar{\mathbf{s}}_k + \sum_{l=1, l \neq k}^K \bar{\mathbf{U}}_k^H \bar{\mathbf{H}}_{1l} \bar{\mathbf{V}}_l \bar{\mathbf{s}}_l + \bar{\mathbf{U}}_k^H \bar{\mathbf{n}}_k, \quad (5.22)$$

where $\bar{\mathbf{U}} = \tilde{\mathbf{V}}$, $\bar{\mathbf{V}} = \tilde{\mathbf{U}}$ and $\bar{\mathbf{H}}_{1k} = \tilde{\mathbf{H}}_{k1}^H$ are the transmit and receive filter matrices as well as the channel matrix from the k-th user to the BS in the virtual uplink/reverse link, respectively. The transmitted signal for the k-th user in the reverse link is denoted by $\bar{\mathbf{s}}_k$. Note that the IA conditions are equal for both links. Due to the reciprocity principle in the uplink, the pre-coding filter in the downlink is updated in the uplink with $\tilde{\mathbf{V}}_k = \bar{\mathbf{U}}_k$. The iterative procedure for solving the optimization problem of the considered system model by exploiting the duality relationships enabled by the reciprocity of the propagation channel is described in subsection

4.4.2. Here, the filters $\tilde{\mathbf{V}}_l$ and $\tilde{\mathbf{U}}_k$ are determined by minimizing the interference leakage in the reciprocal and the original link, respectively. According to this, the IA filters are optimized using following steps:

1. initialize arbitrarily the pre-coding filter matrices $\tilde{\mathbf{V}}_1, \tilde{\mathbf{V}}_2, \dots, \tilde{\mathbf{V}}_K$
2. compute the interference suppression filter matrix $\tilde{\mathbf{U}}_k$ at each receiver k in the original link
3. reverse the communication direction and set $\bar{\mathbf{V}}_k = \tilde{\mathbf{U}}_k$
4. compute the interference suppression matrix $\bar{\mathbf{U}}_l$ at each receiver l in the reciprocal link
5. reverse the communication direction and set $\tilde{\mathbf{V}}_l = \bar{\mathbf{U}}_l$
6. repeat from step 2 until convergence.

5.4.3 Feasibility of IA Condition for Multi-user Broadcast Channel in Underlay CR

The feasibility of IA condition for a multi-user MIMO system in the absence of the PU is already reported in [117, 76]. In underlay CR radio, due to the presence of PU, the DoF of the k -th user cannot exceed the maximum DoF, which is achieved in a conventional K secondary user MIMO system when PU is absent. However, the study in [5] shows that we can remove the effect of PU with d_0 DoF by removing d_0 antennas from both transmitter and receiver sides of the SU system. As a result, the considered underlay CR system can be converted into two parallel systems, which do not cause interference to each other. In this case, a K user cognitive MIMO system with N_t and $N_{r,k}$ at the transmitter and the receiver side can be considered as a standard K user MIMO system with $N_t - d_0$ transmit antennas and $N_r - d_0$ receive antennas. In addition, we assume that the SUs have the same number of receive antennas N_r and DoF \tilde{d} , i.e. $N_{r,k} = N_r$ and $d_k = \tilde{d}$. As a consequence, the following IA conditions are obtained for a multi-user MIMO broadcast channel in underlay CR:

$$\begin{aligned}
 N_t + N_r - 2d_0 &\geq (K + 1)d_k \\
 (N_t - d_0 - d_k) &\geq [Kd - N_r + d_0]_+ \\
 N_t &\geq Kd_k \\
 d_k &\leq \min(N_r - d_0, N_t - d_0) \\
 d_0 &\leq \min(N_{r0}, N_{t0}).
 \end{aligned} \tag{5.23}$$

5.5 SIMULATION RESULTS

To evaluate the system performance of the proposed transmission scheme, a multi-user MIMO broadcast channel in underlay CR is considered, where the primary transmitter and receiver are equipped with the same number of antennas. In the secondary link, the FBS supports two SUs and each receiver has the same number of

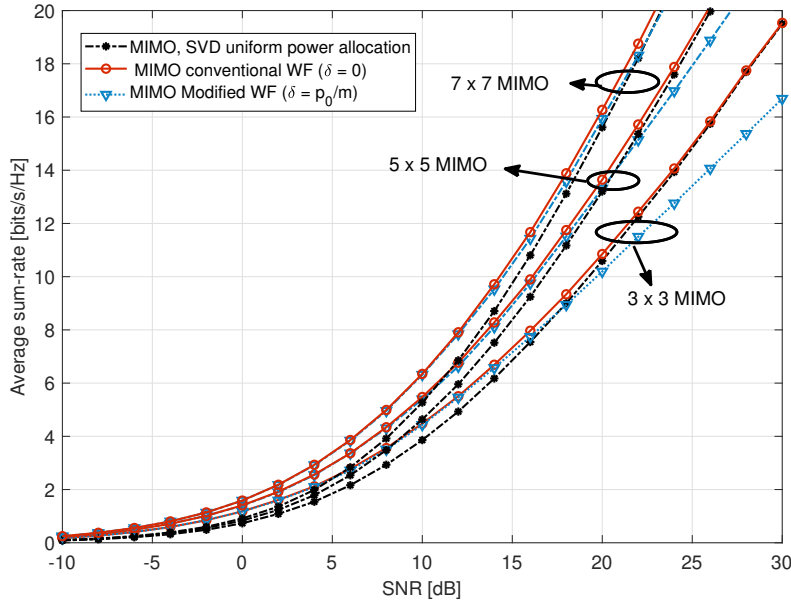


Figure 5.6: The capacity of the primary link with different number of antennas versus SNR by employing WF technique

antennas. All simulations were conducted using the 4-QAM modulation scheme and a statistical multi-path fading channel model.

For the primary link, the WF technique is employed to maximize the primary link capacity. The average sum-rate of the primary link is calculated according to (5.8). Fig. 5.6 shows the primary link capacity versus SNR for different numbers of antennas using the WF approaches (with $\delta = 0$ and $\delta = p_0/m$). The uniform power allocation using the SVD method is used as the reference. Using the uniform power allocation, all sub-channels are allocated with the same power independent on the quality of each sub-channel. In this case, the primary link releases no eigenmode free for the secondary transmissions. Consequently, the uniform power allocation method does not allow any secondary transmission without constraints on the secondary transmit power. However, it supports multiple data streams transmission at the primary link and by using this method, the maximum spatial diversity can be achieved. In Fig. 5.6, it can be seen that the conventional WF approach with $\delta = 0$ provides better capacity than the uniform power allocation for low SNRs due to the flexibility to allocate the transmit power based on the quality of each sub-channel. However, the capacity offered by both approaches is equal at high SNRs, where the allocated power is the same for all sub-channels. In addition, from low to intermediate SNRs, the modified WF $\delta = p_0/m$ offers the same capacity than the conventional WF $\delta = 0$. In high SNR regime, due to the release of some eigenmodes for the secondary transmissions, the system performance of the primary link in terms of capacity is deteriorated by using the modified WF approach. As was proven in [58], this performance degradation does not affect the primary system performance in terms of QoS. However, it can be seen that the system performance degradation decreases with increasing number of antennas.

The system performance of the secondary link is investigated for the case that the PU has three antennas at both transmitter and receiver sides and each sec-

ondary node is equipped with five antennas. Fig 5.7 and 5.8 show the number of DoF at the primary and secondary link depending on the quality of the primary channel by using the conventional and modified WF approach. The number of DoF at the primary link is the number of used eigenmodes, which corresponds to the eigenmodes with non-zero allocated power. It can be seen that at low SNRs (SNR < 7 dB) all sub-channels have large attenuation, and hence only one eigenmode is used for the primary transmission. The number of used eigenmodes increases with improvement of the channel quality. From an SNR value of around 15 dB, the conventional WF approach assigns uniformly the transmit power on the sub-channels. Thus, all eigenmodes are used for the primary transmission. In the presence of the PU, the DoF for the secondary link is determined according to (5.23). The results confirm that by using the conventional WF, the primary link releases no eigenmode for the secondary transmission at high SNR. In contrast to the conventional WF, using the modified WF approach with $\delta = p_0/m$ guarantees that at least one eigenmode is available for the secondary transmission for all SNR values. It can be concluded that based on the number of unused primary eigenmodes, the number of independent transmitted data streams supported by the SUs can be adjusted to improve the secondary data transmission rate.

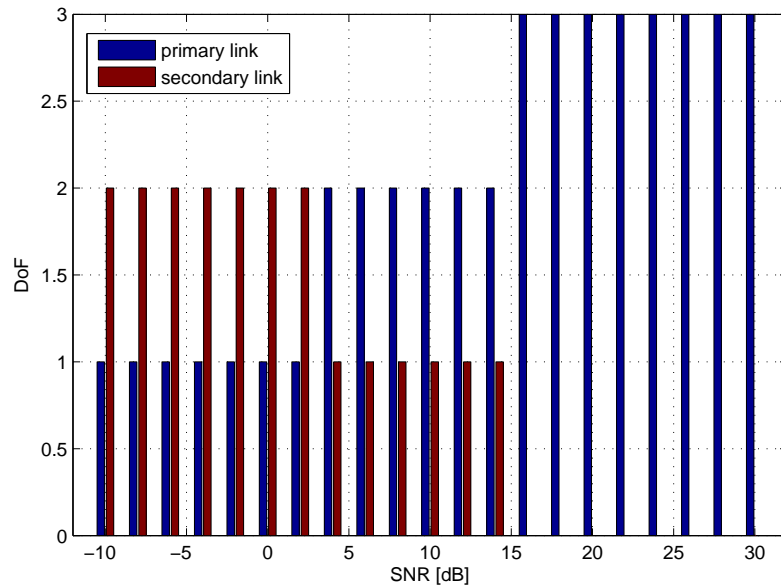


Figure 5.7: The DoF of the primary and secondary link versus SNR using the conventional WF for a 3×3 MIMO PU system.

As mentioned in subsection 5.4.1, the secondary link can be considered as a standard K-user IA scheme with $N_t - d_0$ and $N_r - d_0$ antennas at the transmitter and receiver sides, respectively. As a result, the maximum average sum-rate/sum-rate of the k-th SU can be determined according to [80]

$$\mathbf{R}_{IA,k} = \mathbb{E} \left\{ \log_2 \det \left(\mathbf{I}_{d_k} + \frac{P_k}{d_k} \mathbf{H}_{kk} \mathbf{H}_{kk}^H \right) \right\}, \quad (5.24)$$

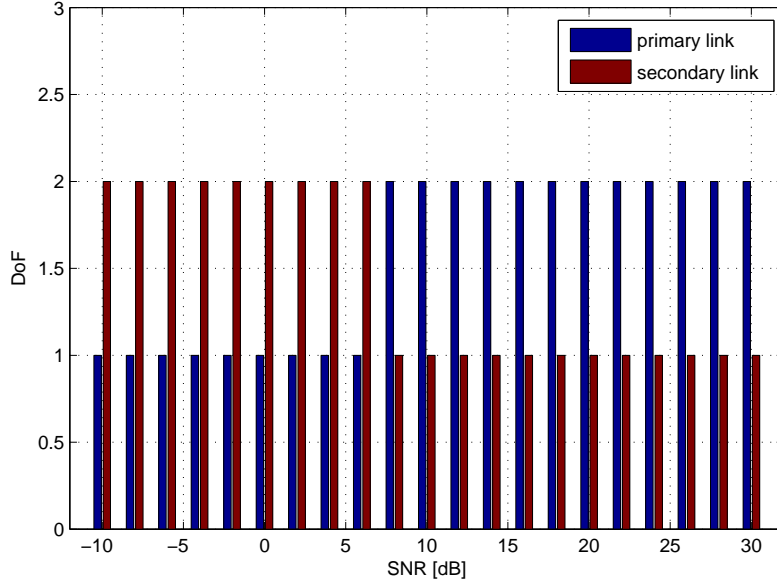


Figure 5.8: The DoF of the primary and secondary link versus SNR using the modified WF for a 3×3 MIMO PU system.

where P_k is the transmit power of user k . The effective channel $\underline{\mathbf{H}}_{kk}$ is defined as follows

$$\underline{\mathbf{H}}_{kk} = \tilde{\mathbf{U}}_k^H \mathbf{B}_k^H \mathbf{H}_k \mathbf{G} \tilde{\mathbf{V}}_k. \quad (5.25)$$

Fig. 5.9 illustrates the sum-rate/average sum-rate of the secondary link. Results show that by employing the conventional WF approach, the pre-coding technique based on IA and the null-steering method at the secondary link provides a positive cognitive rate at low SNRs. More specifically, the sum-rate achieves the maximum value at the SNR value of around 8 dB. At high SNRs where the primary sub-channel is good, the conventional WF approach spreads the transmit power symmetrically along the eigenmodes. Therefore, the cognitive sum-rate converges to zero, as no eigenmode is available for the secondary link. On the contrary, by employing the modified WF approach the cognitive rate does not converge to zero for high SNRs, but also increases with the increasing of SNR. Furthermore, it can be seen that at SNR values of 10 – 16 dB where the primary performance is not affected, that even though there is one available unused eigenmode for both cases of WF (with $\delta = 0$ and $\delta = p_0/m$), the cognitive rate significantly increases using the modified WF approach compared to the case using the conventional WF method. The system performance of the proposed approaches in terms of BER is depicted in Fig. 5.10, where the modified WF approach is employed at the primary link to ensure a secondary transmission for all SNR values. Here, the number of independent transmitted data streams is adaptive based on the quality of the sub-channels. It can be seen that since the PU does not care for the presence of the SUs, the modified WF supports multiple stream transmission and provides very good BER performance. The power level δ should not affect the BER performance. In the secondary link, the pre-coding technique based on IA and the null-steering method guarantees the coexistence in a multi-user underlay CR system. Although the BER performance of

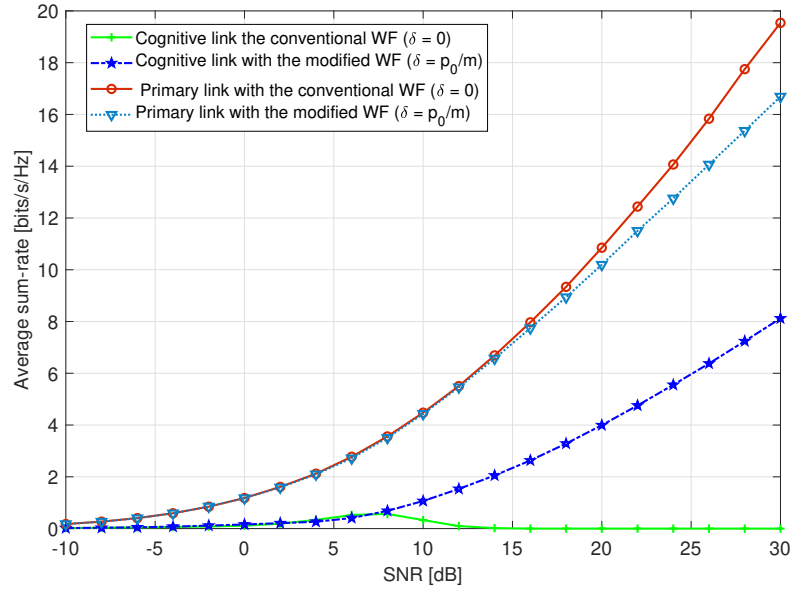


Figure 5.9: The sum-rate of the secondary link versus SNR using the conventional and modified WF algorithms at the primary link for a 3×3 MIMO PUs and 2-users 5×5 MIMO SU system

the secondary link is inferior to that of the primary link due to the interference from the PU and from other SUs, the proposed pre-coding technique still provides a good BER performance.

5.6 SUMMARY

In this chapter, an open issue concerning the transmission efficiency and interference-free coexistence in a multi-tier heterogeneous cellular network using the underlay CR technique is addressed. Here, a novel adaptive transmission scheme based on IA for a multi-user underlay CR system was proposed and discussed.

Section 5.1 illustrates the motivation of developing a new efficient transmission scheme to deal with the interference in a multi-user underlay CR system. In addition, an overview about related works is presented. It is shown that the main disadvantage of the conventional underlay CR technique is the limitation of the SU transmit power. In other words, using the conventional underlay CR technique, the SU has to control its transmit power, so that the interference caused from the SU to the PU lies in the noise floor of the PU. To overcome this problem, an additional signal processing issue such as interference mitigation technique can be applied in the secondary systems.

In section 5.2, a practical application scenario and the general system model for a multi-user MIMO broadcast channel in underlay CR are described. Literatures show that employing small base station in wireless cellular networks brings advantages regarding high network capacity and coverage improvement. However, the coexistence of two-tier networks (small and macro cells) represents a major challenge in regard to the network architecture, resource allocation and interference manage-

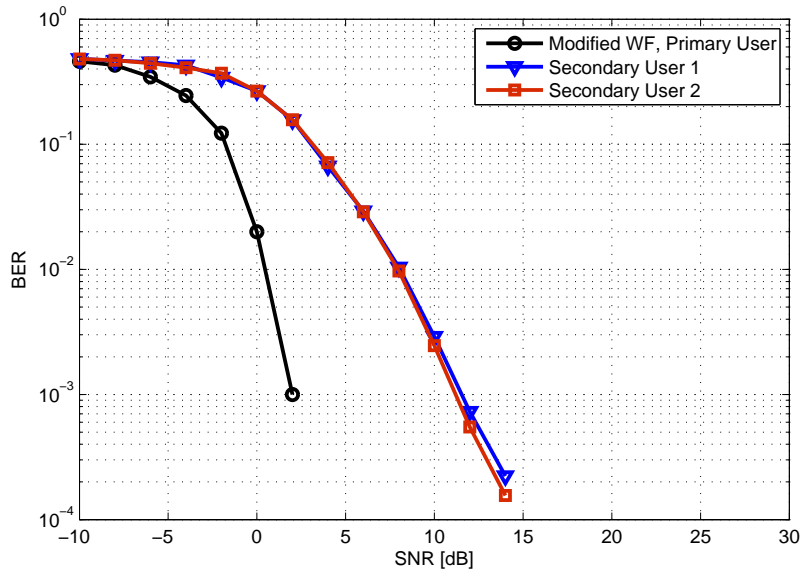


Figure 5.10: The BER performance of PU and SUs versus SNR a 3×3 MIMO PUs and 2-users 5×5 MIMO SU systems

ment. In order to improve SE in multi-tier heterogeneous networks, the underlay CR technique has been intensively discussed. Here, the communication between the macro base station and its users is considered as the primary link and the communications in small cells is referred as the cognitive links.

In sections 5.3 and 5.4, a novel pre-coding approach based on IA and the WF technique is proposed to deal with the MUI problem and to boost data rate as well as to improve SE. Using the proposed approach, on the one hand the power constraints on the SU is not required, and on the other hand, multiple SUs and one PU can access simultaneously the frequency band allocated to the PU. This leads to an increase of the data rate and the network capacity. The proposed scheme applies the modified WF approach in the primary link to ensure a steady transmission for the SUs and a pre-coding approach based on IA and the null-steering method in the secondary link to enable an interference-free coexistence between users.

In section 5.5, the results are presented and discussed. Simulation results show that utilizing this scheme both primary and secondary links can adapt their transmission to improve the spectral efficiency. Although this comes at the cost of capacity loss in the primary link at high SNRs, it is tolerable as long as a given quality of service for the primary link remains unaffected. A further achievement is that the proposed pre-coding technique provides a good performance in terms of BER.

IA IN MU-MIMO RELAY NETWORKS

6.1 INTRODUCTION

High throughput together with the energy efficiency and optimum coverage as well as SE is expected to be provided by the 5G of wireless communication networks. Recent studies have shown that HetNets offer promising solution to cope with this challenge. In this context, the concept by Relay Node (RN) densification within macro cells is seen as a reasonable candidate network architecture to improve the spectral and energy efficiency, due to the fact that the edge or indoor users can transmit at higher rate with lower transmission power, saving energy at the BS and battery life at the users. This in turn inspires new challenges particularly in terms of resource allocation, network architecture and interference mitigation technique, etc. For the resource allocation in HetNets, the traditional orthogonal scheme such as FDMA or TDMA and CR as well as the multi-user MIMO techniques have been discussed in literature [65]. Multi-user CR seems to be a promising solution for an SE improvement. This frequency reuse technique has been discussed in depth in chapter 5.

In this chapter, it is assumed that due to the limitation and cost of radio frequency resources multiple relays have to share the available radio frequency band to support their users. In this case, interference management issues become more challenging. *Therefore, two novel IA approaches based on both ZF and MMSE criteria are proposed to deal with co-tier interference in a multi-tier HetNets under different conditions of CSI.*

This chapter is structured as follows: Section 6.2 briefly introduces the application scenarios. Here, the mathematical description of the considered system model is presented, followed by a review on a multi-user relay system. In Section 6.3 and 6.4, two novel IA schemes namely a non-robust and a robust IA approach dealing with perfect and imperfect CSI are derived. The conditions required for the feasibility of the proposed IA approaches are presented in Section 6.5. Simulation results are discussed in Section 6.6 and finally a conclusion is presented in Section 6.7.

6.2 APPLICATION SCENARIOS AND SYSTEM MODEL

6.2.1 Relays in Wireless Communication Networks

Relaying to assist the data transmission in wireless communication systems has found widespread use for many decades. Oftentimes, due to the distance based at-

tenuation, shadowing, channel fading, etc., the link quality between a source and a destination in wireless networks is adversely deteriorated. A common approach to tackle this problem is the application of a RN between the source and the destination. It has been widely reported in literature that relay networks provide a major enhancement in coverage, reliability and throughput as well as an efficient utilization of the radio frequency bands in wireless communication networks [100, 12, 91, 92, 13]. By applying relay nodes in cellular wireless communication networks, not only the macro cell users at the edge cell can communicate well with the MBS without high transmit power at the MBS, but also the indoor coverage can be improved by the development of a femtorelay in an indoor environment [3]. In the femtorelay concept described in [3], a FAP located in the indoor serves not only as a FBS but also as an RN to support both femtocell and macro cell users within its coverage area.

Based on the signal processing operations, relays can mostly be classified in two groups: AF and Decode-and-Forward (DF) [63, 86]. In AF relay systems, the received signal at the relay is merely amplified, and then passed on to the destination without decoding. Whereas, in DF relay systems, the received signal is first decoded and then re-encoded before being forwarded to the destination [13]. In other words, a DF relay forwards only the desired signal while a AF relay amplifies both the desired signal and the interference plus noise. Thus, DF relays normally deliver better system performance compared to AF relays [63], [13]. However, the implementation cost and the complexity of a DF relay is significantly higher than that of an AF relay system. Generally, due to the requirement of full processing capability at the RN, a DF relay can be considered nearly as a complex basis station. In contrast, due to easy use and low implementation cost, the AF relay scheme is particularly popular and often preferred in practical applications.

Moreover, relays can generally operate in two different modes: (i) Time-Division-Transmit and Receive (TTR), and (ii) Simultaneous Transmit and Receive (STR). The description of both relay operating modes for the downlink is shown in Fig. 6.1. In TTR mode, both transmissions from the MBS to the RN and from the RN to its user will take place in different time t_1 and t_2 using the same frequency resource f_1 . Whereas in STR mode, the MBS transmits data to the RN and the RN retransmit its received signal to its supported user at the same time slots t_1 , but in different frequency resources f_1 and f_2 . By doing this, the transmission in both hops (MBS \rightarrow RN and RN \rightarrow UE) do not interfere with each other. These relay schemes are known as half- and full-duplex relay, respectively.

In HetNets with the high user density, due to the limited available and costly frequency resource, in some applications multiple RNs have to share the available radio frequency band to receive the signal from the MBSs and to transmit its received signal to its indicated destinations. This results in the MUI or cross-tier interference problem in multi-tier HetNets. A such multi-user relay system can be applied in cellular network as depicted in Fig. 6.2.

A HetNets architecture as illustrated in Fig. 6.2 is considered in this chapter, where the UEs at the edge of a macro cell are connected to an RN in the access link. The RNs are mainly utilized to extend the coverage of the MBS or to increase the user throughput in areas with high mobile traffic. It's often the case that the users are

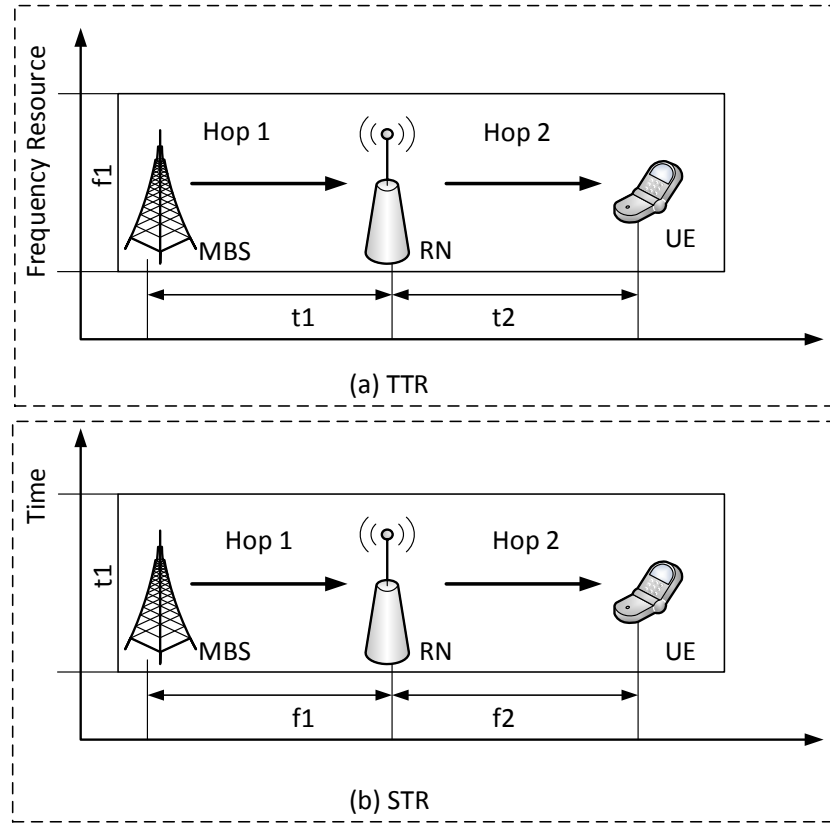


Figure 6.1: Two relay operating modes

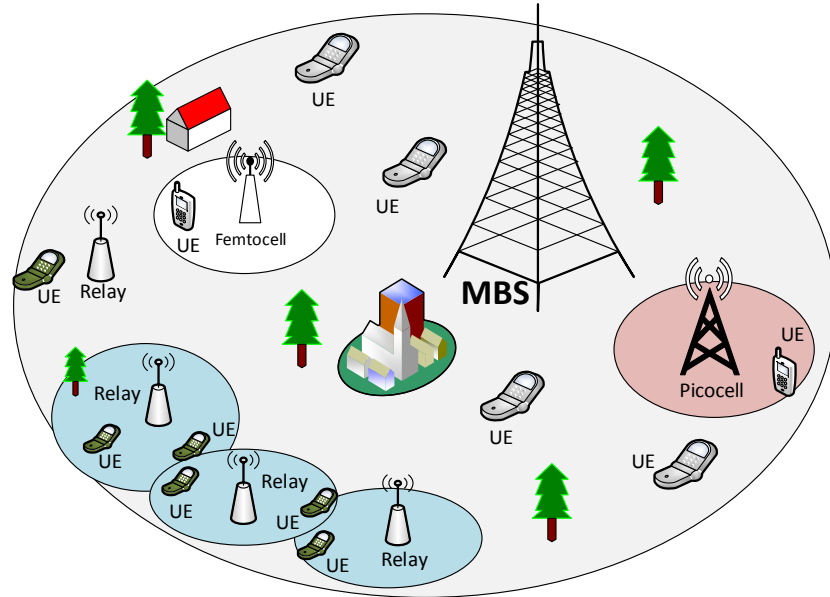


Figure 6.2: Relay based HetNets architecture.

in the edge or overlap area of the RNs and thus subject to interferences from neighboring users. As a result, the throughput decreases severely, unless an efficient interference management technique is deployed. In this regard, when each node is

equipped with multiple antenna, Interference Alignment (IA) can be deployed to overcome the MUI problem in multi-user MIMO relay networks.

6.2.2 *Related Works and Motivation*

As aforementioned, applying relays can increase the SE in a such manner that multiple relays share the available radio frequency band to support their users and to boost the network capacity. To this, interference management is one of the major issues and it has been investigated in numerous studies.

In many applications, the CSI is available at both transmitter and receiver sides. By exploiting the CSI, a relay beamforming technique can be applied at the RNs to establish the communication between the sources and their destinations and to suppress the interference at the receivers [49, 36]. In this regard, [36] extended the beamforming approach proposed in [49] for a multi-user SISO relay system. In [36], assuming that the second-order statistics of the channel coefficients are available at the RNs, the relay matrix is determined by minimizing the total relay transmit power while keeping the SINR at each destination above a certain pre-defined threshold. Compared to a single-antenna relay system, multiple antennas at the relay introduces additional DoF, which can be used to improve the system performance [81]. The study in [40] showed that, in comparison to a conventional K-users interference channel with the help of an RN having sufficient number of antennas, the multiplexing gain and the system capacity can be increased. Therefore, multiple antennas relay systems are mainly considered in literature. In [11, 43], a scenario of one source, one destination and multiple relay nodes, with each node having multiple antennas is considered. [11] proposed a relay beamforming approach based on the maximum of the transmission rate to determine the relay matrix. In [43], the relay matrix can be optimized by minimizing the MSE, so that the requirements on the QoS in terms of a given target SNR are fulfilled.

A multi-user MIMO AF half-duplex relay system is considered in [38, 77, 70, 110, 24]. In [77], assuming that relay nodes have a sufficient antennas, a transceive ZF can be performed at the relays in order to spatial separate the signal at each relay and to eliminate the interference at the destinations. Thus, all interferences can be suppressed at each destination node. In case that each relay node has not enough antennas to suppress the interference at the destinations, [38] proposed a suboptimal cooperative ZF approach to jointly determine the relay and pre-coding matrix. In this case, the sources cooperate with the relays in determining the pre-coding matrix and helping the relay to suppress the interference at the destinations. In contrast to that, in [70], the pre-coding, relay and post-processing matrices are jointly determined by minimizing the total MSE at the receivers under transmit power constraint at the sources and relays. In that study, the relay and post-processing matrices are determined using the KKT conditions while the optimal pre-coding matrix can be found by using numerical optimization tools such as CVX. In [110], three suboptimal solution approaches for optimization of the pre-coding, relay and post-processing matrices are proposed. The first approach is based on the total interference leakage minimization, where the receiver and transmit filters as well as the relay matrix are iteratively determined with the objective of minimizing the

total interference leakage under transmit power constraint at the source and relay nodes. The other two proposed approaches; one with and the other one without power control are based on the weighted MSE optimization problem. Using these approaches, the post-processing matrix is firstly determined, and then the weight matrix is chosen using a linear MMSE receiver. After having the post-processing and the optimal weight matrix, new cost functions regarding the objective of minimizing the weighted sum mean squared are defined to optimize the transmit and relay matrix. It has to be mentioned that there is no closed form solution for the transmit filter and relay matrix in [110]. They are optimized using the convex optimization toolbox CVX. In [24], the distributed IA approach proposed in [42] for a K-user MIMO interference channel is extended to a multi-user MIMO AF half-duplex relay system. Here, the reciprocity network is used to solve the IA problem and all filters are determined based on the minimization of the total interference leakage at users (ZF criterion).

In all these aforementioned works, the related matrices are determined under assumption that perfect CSI is available at each node, which does not hold in practice. In case of having imperfect CSI, the optimization of all filters should explicitly concern the CSI errors, leading to develop robust design approaches against the CSI errors. In such a relay network, relays first need to estimate the channels from sources to relays, which is usually done using pilot symbols. Next, the relays have to acquire the CSI of the channels from relay to destination either via feedback channels in FDD systems or using previous received signal by means of the channel reciprocity in TDD systems. Depending on the CSI acquisition method, the CSI error can be caused by different reasons such as the channel estimation and quantization errors as well as feedback delay etc. In this context, robust approaches to determine the relay matrix for AF-MIMO relay systems have been reported in [83, 113, 19, 18, 112]. In [83, 113], a relay system with one source, multiple relay nodes and one destination and each node equipped with single antenna is considered. For this, [113] proposed a robust distributed relay beamforming approach based on the minimization of the total transmit power at each relay under SNR constraints. Also in [113], a convex optimization problem is presented which can be solved efficiently using interior-point methods. Meanwhile, in [83], the optimization problems are formulated as a second-order cone program and a semi-definite program for the noncoherent and coherent AF relay networks, respectively. Furthermore, in [19, 18, 112], an AF relay system, where K single-antenna sources communicate with K single-antenna destinations via a multiple antennas relay node is considered. [19] proposed robust pre-coding concepts to handle the imperfection of CSI due to the channel estimation errors. In a later work, the study in [18] proposed robust pre-coding design approaches that are based on the assumption of having the knowledge of channel covariance matrices at the RNs and CSI errors caused by the feedback communication and the quantization of covariance estimation. Additionally, in [18], it was adopted that the uncertainty on the covariance matrices of channels from sources to relays is negligible, as the level of uncertainty on the covariance matrices of the channels from the relays to the destinations is higher than that of channels from sources to relays. In [112], a robust pre-coding concept is introduced for two kinds of the CSI errors, one is based on the stochastic error

model, where the imperfect CSI is mainly caused by the channel estimation errors, while the other is supported by the norm-bounded error model, where the CSI error is dominated by quantization errors. In that work, the relay matrices are determined by minimizing the sum of relay power, while requirements on the SINR for all destinations are met. However, the investigations in [83, 113, 19, 112] are limited to design of either a single source and destination or a single MIMO relay. Furthermore, all these studies have considered the scenarios, in which each source or destination is equipped only with a single-antenna and the related robust precoding algorithms are developed merely for frequency flat fading channels.

In this chapter, a multiple user half-duplex AF-MIMO relay system is considered, where the MBS communicates to the edge users through multiple relays and each node has multiple antennas. Due to the long distance from the MBS to the allocated edge users, the direct link between the MBS and the user is usually negligible. As previously mentioned, the major problem of such a transmission scheme is the MUI problem, thus the relay matrix has to be determined not only to maintain the communication link, but also to help the receivers by eliminating the MUI. In this context, two novel non-robust and robust IA schemes are proposed, for which a hybrid optimization approach based on the ZF and MMSE optimization criteria is developed to deal with the MUI under consideration of perfect and imperfect CSI. The main idea of the proposed approaches is that, first, the relay matrix is determined by minimizing the total interference leakage at the destinations, and then the pre-coder and post-processing matrices are optimized based on the MMSE criterion under the transmit power constraints at the sources. Here, the noises at the relay and destination nodes are considered in determining the pre-coding and post-processing matrix. This makes the proposed approach different from the existing approaches and efficient in terms of the system performance improvement in low to moderate SNRs. The proposed optimization approach is initially developed for the case of perfect CSI, and then is extended to the case of having CSI errors. For the performance evaluation, the system performance achieved by using the proposed approach is compared to that provided by the IA approach given in [24] in the case of having perfect CSI. For all investigations, a frequency selective channel is considered. In regard to the imperfect CSI, it is assumed that the CSI error is only caused by the channel estimation errors.

6.2.3 System Model

The system model considered for the above-mentioned HetNets architecture is illustrated in Fig. 6.3, where the MBS supports K dedicated edge users through M AF RNs. In a special case with $M = 1$, it corresponds to a scenario, in which one relay is used to support multi-users in the edge cell. Here, a two-hop transmission via half duplex relays is considered. In the first hop, the MBS sends signals to the relays, and in the second hop the relays forward the received signals to the users. It is considered that the MBS transmits signals to the associated edge users via relays to all users in the same frequency band and at the same time, and thus high efficiency in terms of spectrum usage can be achieved. It is assumed that the MBS and the k -th user are equipped with N_t and $N_{r,k}$ antennas, respectively, while each relay has $N_{r,e}$ antennas. The channel coefficient matrix from the MBS to relay m and from relay m to user k are denoted by \mathbf{F}_m and $\mathbf{G}_{k,m}$, respectively. It is supposed that the

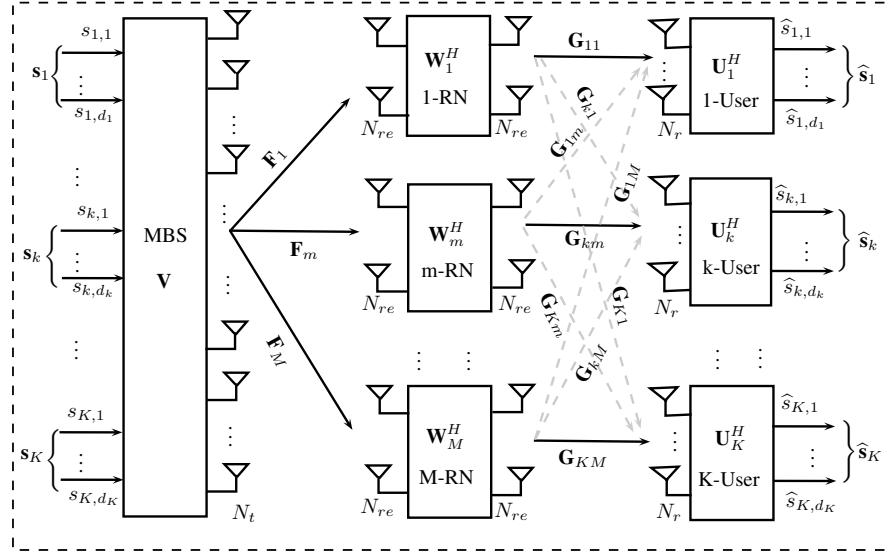


Figure 6.3: Multi-user relay MIMO system

MBS sends d_k independent data stream, $\mathbf{s}_k = [s_{k,1}, s_{k,2}, \dots, s_{k,d_k}]^T$ to the k -th user. Thus, the total number of data stream to be supported by the MBS is $d = \sum_{k=1}^K d_k$. The number of independent data streams d_k that can be transmitted to user k is also known as the achieved DoF for this user. For the maximum DoF of user k the following condition has to be fulfilled

$$d_k \leq \min(N_t, N_{r,k}). \quad (6.1)$$

As mentioned, the MBS broadcasts signals to the relays in the first hop, and thus the received signal at the m -th relay can be given by

$$\mathbf{z}_m = \sum_{k=1}^K \mathbf{F}_m \mathbf{V}_k \mathbf{s}_k + \mathbf{n}_m, \quad (6.2)$$

where $\mathbf{V}_k \in \mathbb{C}^{N_t \times d_k}$ denotes the linear pre-coding matrix at the MBS for user k and \mathbf{n}_m is the additive noise at relay m . The pre-coding \mathbf{V} at the MBS is defined as $\mathbf{V} = \text{diag}\{\mathbf{V}_1, \mathbf{V}_2, \dots, \mathbf{V}_K\}$. In the second hop, each relay amplifies the received signal with a matrix factor $\mathbf{W}_m \in \mathbb{C}^{N_{re} \times N_{re}}$, and then forwards it to the users. Therefore, the received signal at the k -th user can be expressed as

$$\mathbf{y}_k = \sum_{m=1}^M \mathbf{G}_{km} \mathbf{W}_m \mathbf{z}_m + \mathbf{n}_k, \quad (6.3)$$

where \mathbf{n}_k is the noise vector at user k . The additive noise is statistically independent and assumed to be white Gaussian with covariance matrix $\mathbf{R}_{\mathbf{n}_k \mathbf{n}_k} = \mathbb{E}[\mathbf{n}_k \mathbf{n}_k^H] = \sigma_n^2 \mathbf{I}$. By inserting (6.2) into (6.3), we obtain

$$\mathbf{y}_k = \sum_{m=1}^M \mathbf{G}_{km} \mathbf{W}_m \mathbf{F}_m \mathbf{V}_k \mathbf{s}_k + \sum_{l=1, l \neq k}^K \sum_{m=1}^M \mathbf{G}_{km} \mathbf{W}_m \mathbf{F}_m \mathbf{V}_l \mathbf{s}_l$$

$$\begin{aligned}
 & + \sum_{m=1}^M \mathbf{G}_{k,m} \mathbf{W}_m \mathbf{n}_m + \mathbf{n}_k \\
 & = \underbrace{\mathbf{H}_k \mathbf{V}_k \mathbf{s}_k}_{\text{Desired signal}} + \underbrace{\sum_{l=1, l \neq k}^K \mathbf{H}_k \mathbf{V}_l \mathbf{s}_l}_{\text{Interference}} + \underbrace{\sum_{m=1}^M \mathbf{G}_{k,m} \mathbf{W}_m \mathbf{n}_m + \mathbf{n}_k}_{\text{Noise}}, \tag{6.4}
 \end{aligned}$$

where \mathbf{H}_k is the equivalent channel matrix from the MBS to user k and is defined as

$$\mathbf{H}_k = \sum_{m=1}^M \mathbf{G}_{k,m} \mathbf{W}_m \mathbf{F}_m. \tag{6.5}$$

Denote the post-processing matrix at user k by $\mathbf{U}_k \in \mathbb{C}^{N_r \times d}$, the estimated data streams $\hat{\mathbf{s}}_k$ at the k -th user can be given as below:

$$\begin{aligned}
 \hat{\mathbf{s}}_k & = \underbrace{\mathbf{U}_k^H \mathbf{H}_k \mathbf{V}_k \mathbf{s}_k}_{\text{Desired signal}} + \underbrace{\sum_{l=1, l \neq k}^K \mathbf{U}_k^H \mathbf{H}_k \mathbf{V}_l \mathbf{s}_l}_{\text{Interfering signals}} \\
 & + \underbrace{\sum_{m=1}^M \mathbf{U}_k^H \mathbf{G}_{k,m} \mathbf{W}_m \mathbf{n}_m + \mathbf{U}_k^H \mathbf{n}_k}_{\text{Noise}}. \tag{6.6}
 \end{aligned}$$

With regard to the IA technique, the MBS and each user k have to adjust the pre-coder filter \mathbf{V}_k and post-processing filter \mathbf{U}_k , so that the following conditions are satisfied:

$$\sum_{l=1, l \neq k}^K \mathbf{U}_k^H \mathbf{H}_k \mathbf{V}_l = 0, \quad \forall l, k = 1, \dots, K, l \neq k, \tag{6.7}$$

$$\text{rank}(\mathbf{U}_k^H \mathbf{H}_k \mathbf{V}_k) = d_k, \quad \forall k. \tag{6.8}$$

The condition in (6.7) guarantees that all interference signals at user k are aligned in an interference subspace of $N_r - d_k$ dimension, and can be forced to have a value of zero by multiplying with the post-processing filter matrix \mathbf{U}_k . The condition in (6.8) ensures that after the post-processing at the receiver, the remaining signal space at user k has a space dimension of d_k . The maximum DoF can be achieved, if all these conditions are satisfied.

The IA approaches reported so far in the literature are based on the assumption of having perfect CSI knowledge at both transmitter and receiver sides. However, this assumption does not hold in practical applications, because of issues raised by the channel estimation and quantization errors and feedback delay, etc. This results in a deterioration of the IA system performance, which creates a need for developing robust IA approaches applicable to real systems. In the scope of this dissertation, the imperfect CSI due to the channel estimation error is taken into account. In this context, the actual channel matrices \mathbf{F}_m and $\mathbf{G}_{k,m}$ can be modeled as

$$\mathbf{F}_m = \hat{\mathbf{F}}_m + \mathbf{E}_m^F, \quad \forall m = 1, \dots, M, \tag{6.9}$$

$$\mathbf{G}_{km} = \widehat{\mathbf{G}}_{km} + \mathbf{E}_{km}^G, \quad \forall k, m, \quad (6.10)$$

where $\widehat{\mathbf{F}}_m, \widehat{\mathbf{G}}_{km}$ are the estimated channel matrices available at the relay and transmitter nodes, respectively. The matrices \mathbf{E}_m^F and \mathbf{E}_{km}^G are the additive estimation error matrices in the CSI imperfect model. Under the assumption that the channel estimation error matrices can be modeled as complex Gaussian distributed with zero mean and $\mathbb{E} \left\{ \text{vec}(\mathbf{E}_m^F) \text{vec}(\mathbf{E}_m^F)^H \right\} = \sigma_{\mathbf{E}_m^F}^2 \mathbf{I}_{N_{re}N_t}$, and $\mathbb{E} \left\{ \text{vec}(\mathbf{E}_{km}^G) \text{vec}(\mathbf{E}_{km}^G)^H \right\} = \sigma_{\mathbf{E}_{km}^G}^2 \mathbf{I}_{N_{re}N_{r,k}}$. In this case, the CSI at the transmitters and the RNs consists of the estimated channel and the related error covariance matrices. For the case of having perfect CSI, we have $\sigma_{\mathbf{E}_{km}^G}^2 = 0$ and $\sigma_{\mathbf{E}_m^F}^2 = 0, \forall k, m$.

6.3 JOINT ESTIMATION FOR PERFECT CSI

This section describes in detail the method proposed to jointly design the precoding filter matrix \mathbf{V}_l , the relay matrix \mathbf{W}_m and the post-processing filter matrix \mathbf{U}_k . The idea here is to jointly determine all matrices $\mathbf{V}_l, \mathbf{W}_m$ and \mathbf{U}_k , so that not only the total interference leakage, but also the mean square error are minimized for all users. Subsequently, the IA optimization problem is formulated, and followed by the description of the non-robust IA approach.

6.3.1 Optimization Problem

Because of neighboring transmitters, the total interference leakage at user k is defined as

$$I_k = \text{Tr}(\mathbf{U}_k^H \mathbf{Q}_k \mathbf{U}_k), \quad (6.11)$$

where \mathbf{Q}_k stands for the interference covariance matrix at user k and is given by

$$\mathbf{Q}_k = \sum_{l=1, l \neq k}^K \frac{1}{d_l} \mathbf{H}_k \mathbf{V}_l \mathbf{V}_l^H \mathbf{H}_k^H. \quad (6.12)$$

Note that if the total interference leakage is equal to zero, the conditions (6.7) is satisfied and the desired signal subspace is interference-free. In order to achieve this, one solution approach reported in [24] is applied to find a group of $\mathbf{V}_l, \mathbf{W}_m$ and \mathbf{U}_k to achieve a total interference leakage of zero at all users. However, by using this scheme, the aforementioned IA conditions can be achieved only at high SNRs. This solution method offers a simple realization but delivers inferior system performance in terms of throughput and BER in the low to moderate SNR regime. The reason for this is that the noise at the relay and the receiver nodes were not taken into account in design of the IA filters. *To resolve this shortcoming, we propose a method to determine the $\mathbf{V}_l, \mathbf{U}_k$ and \mathbf{W}_m matrices, so that not only the total interference leakage amounts to zero at high SNRs, but also the system performance is improved for low to moderate SNRs by minimizing both total interference leakage and MSE at each receiver.* By doing so, the condition in (6.7) is also fulfilled. It should be noted that

the condition in (6.8) has no direct connection to the optimization problem and it solely defines the maximal multiplexing gain (degree of freedom) achieved by using the IA technique. However, this condition can be achieved if the desired signal subspace is interference free. In general, d_k depends on K , M and the number of transmit and receive as well as relay antennas. As it is rather complicated to obtain a closed form solution for the IA problem, a suboptimal solution approach based on an iterative algorithm is proposed. The objective of an iterative algorithm is the instantaneous minimization of the cost function with respect to a certain variable group.

In the non-robust IA approach, the relay matrix \mathbf{W}_m at relay m is firstly optimized based on the zero-forcing optimization approach. In this context, the zero-forcing optimization problem to determine the relay matrix \mathbf{W}_m for a given set of $\{\mathbf{V}_l, \mathbf{U}_k\}$ can be formulated as

$$\begin{aligned} \mathbf{W}_m^{\text{opt}} = \underset{\mathbf{W}_m}{\operatorname{argmin}} \sum_{k=1}^K I_k, \\ \text{subject to: } \mathbf{w}^H \mathbf{w} = 1. \end{aligned} \quad (6.13)$$

Here $\mathbf{w} = [\operatorname{vec}\{\mathbf{W}_1\}^T, \dots, \operatorname{vec}\{\mathbf{W}_M\}^T]^T$, whereby $\operatorname{vec}\{\cdot\}$ indicates the vectorization of a matrix. Subsequently, provided that the relay matrix \mathbf{W}_m is determined by solving the optimization problem in (6.13), the pre-coding \mathbf{V}_l and post-processing \mathbf{U}_k filters can be determined by minimizing the MSE at each receiver. For a given relay matrix \mathbf{W}_m , $\forall m = 1, 2, \dots, M$, the MMSE optimization problem with respect to the transmit power constraints at the MBS can be described as follows:

$$\mathbf{V}_l^{\text{opt}}, \mathbf{U}_k^{\text{opt}} = \underset{\mathbf{V}_l, \mathbf{U}_k}{\operatorname{argmin}} \epsilon, \quad (6.14)$$

$$\text{subject to: } \operatorname{Tr}(\mathbf{V}_l \mathbf{V}_l^H) \leq P_0, \quad (6.15)$$

where P_0 is the transmit power. The cost function $\epsilon(\mathbf{V}_l, \mathbf{U}_k, \mathbf{W}_m)$ represents the sum MSE over all users and can be expressed by

$$\epsilon = \sum_{k=1}^K \epsilon_k = \sum_{k=1}^K \mathbb{E} \left\{ \|\hat{\mathbf{s}}_k - \mathbf{s}_k\|^2 \right\}. \quad (6.16)$$

with $\|\mathbf{X}\|^2$ the Frobenius norm of \mathbf{X} and $\|\mathbf{X}\|^2 = \operatorname{Tr}(\mathbf{X}\mathbf{X}^H)$. It has to be mentioned that the expectation (\mathbb{E}) is with respect to the distribution of the transmit and noise signals \mathbf{s} and \mathbf{n} . Here, ϵ_k is the MSE at user k and is defined as (see A.17 for the derivation)

$$\begin{aligned} \epsilon_k = & \left\| \mathbf{U}_k^H \mathbf{H}_k \mathbf{V}_k - \mathbf{I}_{d_k} \right\|^2 + \sum_{l=1, l \neq k}^K \left\| \mathbf{U}_k^H \mathbf{H}_k \mathbf{V}_l \right\|^2 \\ & + \operatorname{Tr}(\mathbf{U}_k^H \mathbf{R}_{\omega\omega} \mathbf{U}_k), \end{aligned} \quad (6.17)$$

whereas $\mathbf{R}_{\omega\omega} = \mathbb{E} \{ \omega_k \omega_k^H \}$ is the covariance matrix of the total effective noise ω_k at user k , which is given as follows:

$$\omega_k = \sum_{m=1}^M \mathbf{G}_{km} \mathbf{W}_m \mathbf{n}_m + \mathbf{n}_k. \quad (6.18)$$

Due to the noise vectors independency, it results in $\mathbb{E} \{n_m n_k^H\} = 0$ and

$$\mathbf{R}_{\omega\omega} = \sum_{m=1}^M \mathbf{G}_{km} \mathbf{W}_m \mathbf{W}_m^H \mathbf{G}_{km}^H \sigma_m^2 \mathbf{I}_{N_{r,k}} + \sigma_k^2 \mathbf{I}_{N_{r,k}}, \quad (6.19)$$

with $\mathbb{E} \{n_m n_m^H\} = \sigma_m^2 \mathbf{I}_{N_{re}}$, $\mathbb{E} \{n_k n_k^H\} = \sigma_k^2 \mathbf{I}_{N_{r,k}}$. It has to be mentioned that the IA conditions in (6.7) and (6.8) can only be achieved at high SNRs or without noise. In the proposed approaches, the pre-coding and post-processing filters \mathbf{V}_l , \mathbf{U}_k are defined according to the IA concept and they are optimized using the MMSE criterion. This means, each user tries to minimize the MSE, which is defined in (6.17). Since each term in (6.17) is positive, minimizing ϵ_k means that each term in (6.17) is minimized. Using the MMSE criterion, at the optimum point ϵ_k is very small (close to zero), leading to $\mathbf{U}_k^H \mathbf{H}_k \mathbf{V}_k \approx \mathbf{I}_{d_k}$, $\sum_{l=1, l \neq k}^K \|\mathbf{U}_k^H \mathbf{H}_k \mathbf{V}_l\|^2 \approx 0$, $\mathbf{U}_k^H \mathbf{R}_{\omega\omega} \mathbf{U}_k \approx 0$.

Consequently, it is to note that the first term in (6.17) implies that the MMSE criterion enforces condition (6.8). The second term in (6.17) indicates that multi-user interference is minimized, leading to the fulfilment of the IA condition in (6.7). The third term in (6.17) shows that MMSE criterion nulls out the noise. In other words, using the MMSE approach, the interference is aligned and minimized, and if the MSE in (6.17) is minimized that means the IA conditions are also fulfilled. To solve the optimization problem in (6.14) the method of Lagrange duality and the KKT is used, which is formulated as

$$L^{\text{non-robust}}(\lambda_l, \mathbf{U}_k, \mathbf{V}_l) = \epsilon + \lambda_l [\text{Tr}(\mathbf{V}_l \mathbf{V}_l^H) - P_0], \quad (6.20)$$

where the Lagrange multiplier $\lambda_l \geq 0$ is chosen so that the condition in terms of power constraints $\|\mathbf{V}_l\|^2 \leq P_0$ is fulfilled. Inserting (6.17) into (6.20) results in the Lagrange function as follows:

$$\begin{aligned} L^{\text{non-robust}}(\lambda_l, \mathbf{U}_k, \mathbf{V}_l) &= \sum_{k=1}^K \text{Tr} \left((\mathbf{U}_k^H \mathbf{H}_k \mathbf{V}_k - \mathbf{I}_{d_k}) (\mathbf{U}_k^H \mathbf{H}_k \mathbf{V}_k - \mathbf{I}_{d_k})^H \right) \\ &+ \sum_{k=1}^K \text{Tr} \left(\sum_{l=1, l \neq k}^K \mathbf{U}_k^H \mathbf{H}_k \mathbf{V}_l \mathbf{V}_l^H \mathbf{H}_k^H \mathbf{U}_k \right) \\ &+ \sum_{k=1}^K \text{Tr} (\mathbf{U}_k^H \mathbf{R}_{\omega\omega} \mathbf{U}_k) + \lambda_l [\text{Tr}(\mathbf{V}_l \mathbf{V}_l^H) - P_0]. \end{aligned} \quad (6.21)$$

According to the Lagrange and KKT method, the following KKT conditions are necessary and sufficient for solving the optimization problem described in (6.14):

$$\nabla_{\mathbf{U}_k} L^{\text{non-robust}}(\lambda_l, \mathbf{U}_k, \mathbf{V}_l) = 0, \quad (6.22)$$

$$\nabla_{\mathbf{V}_l} L^{\text{non-robust}}(\lambda_l, \mathbf{U}_k, \mathbf{V}_l) = 0, \quad (6.23)$$

$$\lambda_l \geq 0; \quad \text{Tr}(\mathbf{V}_l \mathbf{V}_l^H) - P_0 \leq 0, \quad (6.24)$$

$$\lambda_l [\text{Tr}(\mathbf{V}_l \mathbf{V}_l^H) - P_0] = 0. \quad (6.25)$$

In fact, an end-to-end system performance is of importance. In this regard, the aim of the design of the pre-coding and post-processing filters based on the MMSE

criterion has a two-aspects: a) to provide that the IA conditions are satisfied at the optimum point, specifically in the high SNR regime, b) to improve the system performance in the low to moderate SNR regimes.

6.3.2 Non-Robust IA Approach

6.3.2.1 Design of Relay Matrices based on the ZF Criteria

The sum interference leakage I of all users is given by

$$I = \sum_{k=1}^K I_k = \sum_{k=1}^K \sum_{l=1, l \neq k}^K \text{Tr} \{ \mathbf{U}_k^H \mathbf{H}_k \mathbf{V}_l \mathbf{V}_l^H \mathbf{H}_k^H \mathbf{U}_k \}. \quad (6.26)$$

Lemma I: Let \mathbf{X} be $L \times L$ random matrix, then $\text{Tr}\{\mathbf{X}\mathbf{A}\mathbf{X}^H\mathbf{B}\} = \text{vec}(\mathbf{X})^H (\mathbf{B}^T \otimes \mathbf{A}) \text{vec}(\mathbf{X})$, where \otimes denotes the Kronecker product of matrix \mathbf{A} and \mathbf{B} . Using the following properties of $\text{vec}(\cdot)$ and $\text{Tr}(\cdot)$ operations for matrices \mathbf{A} , \mathbf{B} and \mathbf{C}

1. $\text{Tr}(\mathbf{A}\mathbf{B}) = \text{vec}(\mathbf{A}^H)^H \text{vec}(\mathbf{B})$,
2. $\text{vec}(\mathbf{A}\mathbf{B}\mathbf{C}) = (\mathbf{C}^T \otimes \mathbf{A}) \text{vec}(\mathbf{B})$,

it results in

$$\begin{aligned} \text{Tr}(\mathbf{X}\mathbf{A}\mathbf{X}^H\mathbf{B}) &= \text{Tr}(\mathbf{X}^H\mathbf{B}\mathbf{X}\mathbf{A}) \\ &= \text{vec}(\mathbf{X})^H \text{vec}(\mathbf{B}\mathbf{X}\mathbf{A}) \\ &= \text{vec}(\mathbf{X})^H (\mathbf{A}^T \otimes \mathbf{B}) \text{vec}(\mathbf{X}). \end{aligned}$$

Inserting $\mathbf{H}_k = \sum_{m=1}^K \mathbf{G}_{km} \mathbf{W}_m \mathbf{F}_m$ into (6.26) and applying Lemma I leads to the following expression (see A.3.1 for the derivation):

$$I = \mathbf{w}^H \tilde{\mathbf{A}} \mathbf{w} \quad (6.27)$$

with

$$\tilde{\mathbf{A}} = \sum_{k=1}^K \sum_{l=1, l \neq k}^K \mathbf{A}_{kl} \quad (6.28)$$

and the matrix \mathbf{A}_{kl} is given in (6.29).

$$\mathbf{A}_{kl} = \begin{pmatrix} (\mathbf{F}_1^* \mathbf{V}_l^* \mathbf{V}_l^T \mathbf{F}_1^T) \otimes (\mathbf{G}_{k1}^H \mathbf{U}_k \mathbf{U}_k^H \mathbf{G}_{k1}) & \cdots & (\mathbf{F}_1^* \mathbf{V}_l^* \mathbf{V}_l^T \mathbf{F}_M^T) \otimes (\mathbf{G}_{k1}^H \mathbf{U}_k \mathbf{U}_k^H \mathbf{G}_{kM}) \\ \vdots & \ddots & \vdots \\ (\mathbf{F}_M^* \mathbf{V}_l^* \mathbf{V}_l^T \mathbf{F}_1^T) \otimes (\mathbf{G}_{kM}^H \mathbf{U}_k \mathbf{U}_k^H \mathbf{G}_{k1}) & \cdots & (\mathbf{F}_M^* \mathbf{V}_l^* \mathbf{V}_l^T \mathbf{F}_M^T) \otimes (\mathbf{G}_{kM}^H \mathbf{U}_k \mathbf{U}_k^H \mathbf{G}_{kM}) \end{pmatrix} \quad (6.29)$$

For given set of $\{\mathbf{U}_k, \mathbf{V}_l\}$, the optimization problem in (6.13) can be reformulated as

$$\mathbf{W}_m^{\text{non-robust}} = \underset{\mathbf{W}_m}{\text{argmin}} \left\{ \mathbf{w}^H \tilde{\mathbf{A}} \mathbf{w} \right\},$$

$$\text{subject to: } \mathbf{w}^H \mathbf{w} = 1. \quad (6.30)$$

It can be seen that the relay matrix $\mathbf{W}_m^{\text{non-robust}}$ can be determined by subtracting $N_{re} \times N_{re}$ coefficients of the optimal matrix \mathbf{w} starting from the index $((m - 1)N_{re} \times N_{re})$. Furthermore, the optimal \mathbf{w} corresponds to the least dominant eigenvector of $\tilde{\mathbf{A}}$ and the sum interference leakage is equal to the least dominant eigenvalue of $\tilde{\mathbf{A}}$.

6.3.2.2 Design of Post-processing and Pre-coding Matrices based on the MMSE Criteria

According to literature, to evaluate the derivation of the Lagrange function given in (6.22) and (6.23) matrices \mathbf{U}_k and \mathbf{U}_k^H are treated as independent variable. This also applies to \mathbf{V}_l^H and \mathbf{V}_l . Furthermore, using the mathematical properties $\frac{\partial \text{Tr}(\mathbf{A}\mathbf{X}\mathbf{B})}{\partial \mathbf{X}} = \mathbf{B}\mathbf{A}$ and $\frac{\partial \text{Tr}(\mathbf{A}\mathbf{X}^H\mathbf{B})}{\partial \mathbf{X}} = 0$ for a complex-valued matrix \mathbf{X} [87], the optimal post-processing filter for user k , \mathbf{U}_k , can be obtained as follow:

$$\mathbf{U}_k^{\text{non-robust}} = \left[\sum_{l=1}^K \mathbf{H}_k \mathbf{V}_l \mathbf{V}_l^H \mathbf{H}_k^H + \mathbf{R}_{\omega\omega} \right]^{-1} \mathbf{H}_k \mathbf{V}_k. \quad (6.31)$$

Optimizing the pre-coding filters via the derivation in (6.23) and concerning the transmit power constraints in (6.24) and (6.25) results in

$$\mathbf{V}_l^{\text{non-robust}} = \left[\sum_{k=1}^K \mathbf{H}_k^H \mathbf{U}_k \mathbf{U}_k^H \mathbf{H}_k + \lambda_l \mathbf{I}_{N_t} \right]^{-1} \mathbf{H}_l^H \mathbf{U}_l. \quad (6.32)$$

Note that for a given set of $\mathbf{U}_k, \forall k = 1, 2, \dots, K$ and $\mathbf{W}_m, \forall m = 1, 2, \dots, M$, the pre-coding filter of the particular user k does not depend on that of other users. Therefore, a close expression for λ_l cannot be given. An efficient approach to solve the Lagrange multiplier is based on the Newton approach [90].

The iterative procedure of the proposed algorithm, referred to as the non-robust IA approach, is summarized below:

Algorithm 1: Non-robust IA based on both MMSE and ZF criteria

- 1) initialize arbitrarily the filters $\{\mathbf{U}_k\}$ and $\{\mathbf{V}_l\}$
 - 2) compute the relay matrix \mathbf{W}_m according to the optimal matrix \mathbf{w} .
 - 3) update the equivalent channel \mathbf{H}_k .
 - 4) compute the post-processing filter matrix \mathbf{U}_k at each user according to (6.31).
 - 5) compute the pre-coding filter matrix \mathbf{V}_l at the MBS for each user according to (6.32).
 - 6) repeat from step 2 until convergence
-

6.4 JOINT ESTIMATION FOR IMPERFECT CSI

In this section, the above non-robust IA approach is extended for the case of having imperfect CSI. In this work, a stochastic model of the CSI error is considered. The proposed robust design approach is based on minimizing the expected values of the cost functions with respect to the estimated channels and CSI errors.

6.4.1 Optimization Problem

In this subsection, the optimization problem of the considered system model in the case of imperfect CSI is described. Assuming that the estimated channels $\hat{\mathbf{F}}_m$ and $\hat{\mathbf{G}}_{km}$ are available at the RNs, the actual channels \mathbf{F}_m and \mathbf{G}_{km} are modeled according to (6.9) and (6.10). In addition, the CSI error covariance $\sigma_{E_m^F}^2$ and $\sigma_{E_m^G}^2$ are also assumed to be available at the RNs. In the case of perfect CSI, the covariances of the channel estimation error amount zero. In this case, the pre-coding, relay and post-processing filter matrices are determined according to (6.31), (6.30) and (6.32), respectively, by using the non-robust IA approach.

For imperfect of CSI, a robust design of the relay matrix \mathbf{W}_m , pre-coding filter matrix \mathbf{V}_l and post-processing filter matrix \mathbf{U}_k is proposed by minimizing the expectation of the sum cost functions under constraints made on the MBS transmit powers with respect to the channel estimation errors. The relay matrix $\mathbf{W}_m, \forall m = 1, 2, \dots, M$ is determined based on the ZF criterion using the estimated channels $\hat{\mathbf{F}}_{ml}$ and $\hat{\mathbf{G}}_{km}$ as well as the CSI error covariances. Here, the noise at the RNs and the receivers are not taken into account in determining the relay matrix. In this case, the estimated equivalent channel $\hat{\mathbf{H}}_k$ is given by

$$\hat{\mathbf{H}}_k = \sum_{m=1}^M \hat{\mathbf{G}}_{km} \mathbf{W}_m \hat{\mathbf{F}}_m. \quad (6.33)$$

Accordingly, the optimization problem in (6.13) can be reformulated as

$$\mathbf{W}_m^{\text{opt}} = \underset{\mathbf{W}_m}{\text{argmin}} \mathbb{E}\{I\}. \quad (6.34)$$

$$\text{subject to: } \mathbf{w}^H \mathbf{w} = 1, \quad (6.35)$$

For a given relay filter \mathbf{W}_m , the robust design approach of \mathbf{V}_l and \mathbf{U}_k is based on the minimizing of the Mean Sum-of-Mean-Squared Error (MS-MSE) with respect to the channel estimated errors and the estimated channels. This leads to

$$\mathbf{V}_l^{\text{opt}}, \mathbf{U}_k^{\text{opt}} = \underset{\mathbf{V}_l, \mathbf{U}_k}{\text{argmin}} \mathbb{E}\{\epsilon\}, \quad (6.36)$$

$$\text{subject to: } \text{Tr}(\mathbf{V}_l \mathbf{V}_l^H) \leq P_0.$$

Lemma II: Let \mathbf{X} be $n \times n$ a random matrix with $\mathbb{E}\{\text{vec}(\mathbf{X})^H \text{vec}(\mathbf{X})\} = \sigma_X^2 \mathbf{I}_{nn}$, then $\mathbb{E}\{\text{Tr}\{\mathbf{X}^H \mathbf{B} \mathbf{X} \mathbf{A}\}\} = \sigma_X^2 \text{Tr}(\mathbf{A}) \text{Tr}(\mathbf{B})$. Utilizing Lemma I and the following properties of $\text{Tr}(\cdot)$ operations for both matrices \mathbf{A} and \mathbf{B}

- $\text{Tr}(\mathbf{A} \otimes \mathbf{B}) = \text{Tr}(\mathbf{A}) \text{Tr}(\mathbf{B})$,

- $\text{Tr}(\mathbf{A}^T) = \text{Tr}(\mathbf{A}),$

result in

$$\begin{aligned} \mathbb{E} \left\{ \text{Tr} \left(\mathbf{X}^H \mathbf{B} \mathbf{X} \mathbf{A} \right) \right\} &= \mathbb{E} \left\{ \text{vec}(\mathbf{X})^H (\mathbf{A}^T \otimes \mathbf{B}) \text{vec}(\mathbf{X}) \right\} \\ &= \text{Tr}(\mathbf{A}^T \otimes \mathbf{B}) \mathbb{E} \left\{ \text{vec}(\mathbf{X})^H \text{vec}(\mathbf{X}) \right\} \\ &= \sigma_{\mathbf{X}}^2 \text{Tr}(\mathbf{A}) \text{Tr}(\mathbf{B}). \end{aligned}$$

Utilizing the CSI error channel model in (6.9) and (6.10), and inserting (6.11) and (6.12) into (6.26) results in

$$\mathbb{E} \{I\} = \mathbb{E} \left\{ \text{Tr} \left(\sum_{k=1}^K \sum_{l=1, l \neq k}^K \mathbf{U}_k^H \mathbf{H}_k \mathbf{V}_l \mathbf{V}_l^H \mathbf{H}_k^H \mathbf{U}_k \right) \right\}, \quad (6.37)$$

with

$$\mathbf{H}_k = \sum_{m=1}^M \left(\hat{\mathbf{G}}_{km} + \mathbf{E}_{km}^G \right) \mathbf{W}_m \left(\hat{\mathbf{F}}_m + \mathbf{E}_m^F \right). \quad (6.38)$$

Here, the expectation (\mathbb{E}) is with respect to the distribution of the channel estimation errors. Applying Lemma I and Lemma II and the following properties

- $\mathbb{E} \left\{ \text{vec}(\mathbf{E}_{km}^G) \text{vec}(\mathbf{E}_{k'm'}^G)^H \right\} = 0, \forall k \neq k', m \neq m',$
- $\mathbb{E} \left\{ \text{vec}(\mathbf{E}_m^F) \text{vec}(\mathbf{E}_{m'}^F)^H \right\} = 0, \forall m \neq m',$
- $\mathbb{E} \left\{ \text{vec}(\mathbf{E}_{km}^G) \text{vec}(\mathbf{E}_{m'}^F)^H \right\} = 0,$
- $\sigma_{\mathbf{E}_{km}^G}^2 = \sigma_{\mathbf{E}^G}^2 \forall k, m,$
- $\sigma_{\mathbf{E}_m^F}^2 = \sigma_{\mathbf{E}^F}^2 \forall m,$

to (6.37), leads to the following expression for the expected value of the sum interference leakage:

$$\bar{I} = \mathbf{w}^H \Theta \mathbf{w}, \quad (6.39)$$

with

$$\begin{aligned} \Theta &= \sum_{k=1}^K \sum_{\substack{l=1 \\ l \neq k}}^K \left(\hat{\mathbf{A}}_{kl} + \sigma_{\mathbf{E}^G}^2 \sigma_{\mathbf{E}^F}^2 \text{Tr}(\mathbf{V}_l \mathbf{V}_l^H) \text{Tr}(\mathbf{U}_k \mathbf{U}_k^H) \mathbf{I}_{MN_{\text{re}}N_t} \right) \\ &\quad + \sum_{k=1}^K \sum_{\substack{l=1 \\ l \neq k}}^K \left(\sigma_{\mathbf{E}^G}^2 \text{Tr}(\mathbf{U}_k \mathbf{U}_k^H) \mathbf{B}_{kl} + \sigma_{\mathbf{E}^F}^2 \text{Tr}(\mathbf{V}_l \mathbf{V}_l^H) \mathbf{C}_{kl} \right), \end{aligned} \quad (6.40)$$

where $\hat{\mathbf{A}}_{kl}$ is given in (6.41). The matrices \mathbf{B}_{kl} and \mathbf{C}_{kl} are $(MN_{\text{re}}N_t \times MN_{\text{re}}N_t)$ block diagonal matrix, and their main diagonal block matrix $\mathbf{B}_{kl,m}$ and $\mathbf{C}_{kl,m}$ are

$(\hat{\mathbf{F}}_m^* \mathbf{V}_l^* \mathbf{V}_l^T \hat{\mathbf{F}}_m^T) \otimes \mathbf{I}_{N_{re}} \mathbf{I}_M$ and $(\mathbf{I}_{N_{r,k}} \otimes \hat{\mathbf{G}}_{km}^H \mathbf{U}_k \mathbf{U}_k^H \hat{\mathbf{G}}_{km}) \mathbf{I}_M, \forall m = 1, \dots, M$, respectively (see A.3.2 for the derivation).

$$\hat{\mathbf{A}}_{kl} = \begin{pmatrix} (\hat{\mathbf{F}}_1^* \mathbf{V}_l^* \mathbf{V}_l^T \hat{\mathbf{F}}_1^T) \otimes (\hat{\mathbf{G}}_{k1}^H \mathbf{U}_k \mathbf{U}_k^H \hat{\mathbf{G}}_{k1}) & \cdots & (\hat{\mathbf{F}}_1^* \mathbf{V}_l^* \mathbf{V}_l^T \hat{\mathbf{F}}_M^T) \otimes (\hat{\mathbf{G}}_{k1}^H \mathbf{U}_k \mathbf{U}_k^H \hat{\mathbf{G}}_{kM}) \\ \vdots & \ddots & \vdots \\ (\hat{\mathbf{F}}_M^* \mathbf{V}_l^* \mathbf{V}_l^T \hat{\mathbf{F}}_M^T) \otimes (\hat{\mathbf{G}}_{kM}^H \mathbf{U}_k \mathbf{U}_k^H \hat{\mathbf{G}}_{k1}) & \cdots & (\hat{\mathbf{F}}_M^* \mathbf{V}_l^* \mathbf{V}_l^T \hat{\mathbf{F}}_M^T) \otimes (\hat{\mathbf{G}}_{kM}^H \mathbf{U}_k \mathbf{U}_k^H \hat{\mathbf{G}}_{kM}) \end{pmatrix} \quad (6.41)$$

Similarly, inserting (6.38) into (6.17) and applying Lemma I and II to (6.17), we obtain the following expression for the expected value of the sum MSE

$$\begin{aligned} \bar{\epsilon} &= \sum_{k=1}^K \left\| \mathbf{U}_k^H \hat{\mathbf{H}}_k \mathbf{V}_k - \mathbf{I}_{d_k} \right\|^2 + \sum_{k=1}^K \sum_{l=1, l \neq k}^K \text{Tr} \left(\mathbf{U}_k^H \hat{\mathbf{H}}_k \mathbf{V}_l \mathbf{V}_l^H \hat{\mathbf{H}}_k^H \mathbf{U}_k \right) \\ &+ \sigma_{\text{EF}}^2 \sum_{k=1}^K \sum_{l=1}^K \text{Tr} (\mathbf{V}_l \mathbf{V}_l^H) \sum_{m=1}^M \text{Tr} \left(\mathbf{U}_k^H \hat{\mathbf{G}}_{km} \mathbf{W}_m \mathbf{W}_m^H \hat{\mathbf{G}}_{km}^H \mathbf{U}_k \right) \\ &+ \sigma_{\text{EF}}^2 \sigma_{\text{EG}}^2 \sum_{k=1}^K \text{Tr} (\mathbf{U}_k \mathbf{U}_k^H) \sum_{m=1}^M \text{Tr} (\mathbf{W}_m \mathbf{W}_m^H) \sum_{l=1}^K \text{Tr} (\mathbf{V}_l \mathbf{V}_l^H) \\ &+ \sigma_{\text{EG}}^2 \sum_{k=1}^K \text{Tr} (\mathbf{U}_k \mathbf{U}_k^H) \sum_{m=1}^M \sum_{l=1}^K \text{Tr} \left(\mathbf{W}_m \hat{\mathbf{F}}_m \mathbf{V}_l \mathbf{V}_l^H \hat{\mathbf{F}}_m^H \mathbf{W}_m^H \right) \\ &+ \sigma_m^2 \sum_{k=1}^K \sum_{m=1}^M \text{Tr} \left(\mathbf{U}_k^H \hat{\mathbf{G}}_{km} \mathbf{W}_m \mathbf{W}_m^H \hat{\mathbf{G}}_{km}^H \mathbf{U}_k \right) \\ &+ \sigma_{\text{EG}}^2 \sigma_m^2 \sum_{k=1}^K \sum_{m=1}^M \text{Tr} (\mathbf{W}_m \mathbf{W}_m^H) \text{Tr} (\mathbf{U}_k \mathbf{U}_k^H) \\ &+ \sigma_k^2 \sum_{k=1}^K \text{Tr} (\mathbf{U}_k \mathbf{U}_k^H), \end{aligned} \quad (6.42)$$

where $\hat{\mathbf{H}}_{kl}$ is given according to (6.33).

As already mentioned, the optimization problem in (6.36) can be solved by using the Lagrange duality and KKT method as

$$\mathcal{L}^{\text{robust}}(\lambda_l, \mathbf{U}_k, \mathbf{V}_l) = \bar{\epsilon} + \lambda_l [\text{Tr}(\mathbf{V}_l \mathbf{V}_l^H) - p_0]. \quad (6.43)$$

6.4.2 Robust IA Approach

6.4.2.1 Robust Design of Relay Matrix

The optimization problem in (6.39) can be reformulated as

$$\begin{aligned} \mathbf{W}_m^{\text{robust}} &= \underset{\mathbf{W}_m}{\text{argmin}} \mathbf{w}^H \Theta \mathbf{w}, \\ &\text{subject to: } \mathbf{w}^H \mathbf{w} = 1. \end{aligned} \quad (6.44)$$

Similar to subsection 6.3.2.1, the optimal relay matrix $\mathbf{W}_m^{\text{robust}}$ can be determined by subtracting $N_{re} \times N_{re}$ coefficients of the matrix \mathbf{w} starting from the row index $(m-1)N_{re}$. Here, the expected value of the sum interference leakage is equal to the least dominant eigenvalue of Θ . Consequently, the optimal \mathbf{w} corresponds to the least dominant eigenvector of Θ .

6.4.2.2 Robust Design of Post-processing and Pre-coding Matrices based on the MS-MSE Criteria

For a given set of $\{\mathbf{V}_l, \mathbf{W}_m\}$, applying KKT conditions given in (6.22), (6.23), (6.24) and (6.25) to the Lagrange function L^{robust} in (6.43) results in the following optimal post-processing filter for user k (see A.4 for the derivation)

$$\mathbf{U}_k^{\text{robust}} = \Upsilon^{-1} \hat{\mathbf{H}}_k \mathbf{V}_k, \quad (6.45)$$

where Υ is given by

$$\begin{aligned} \Upsilon = & \sum_{l=1}^K \hat{\mathbf{H}}_k \mathbf{V}_l \mathbf{V}_l^H \hat{\mathbf{H}}_k^H \\ & + \sigma_{\text{EF}}^2 \sum_{l=1}^K \text{Tr}(\mathbf{V}_l \mathbf{V}_l^H) \sum_{m=1}^M \left(\hat{\mathbf{G}}_{km} \mathbf{W}_m \mathbf{W}_m^H \hat{\mathbf{G}}_{km}^H \right) \\ & + \sigma_{\text{EF}}^2 \sigma_{\text{EG}}^2 \sum_{m=1}^M \text{Tr}(\mathbf{W}_m \mathbf{W}_m^H) \sum_{l=1}^K \text{Tr}(\mathbf{V}_l \mathbf{V}_l^H) \mathbf{I}_{N_{r,k}} \\ & + \sigma_{\text{EG}}^2 \sum_{m=1}^M \sum_{l=1}^K \text{Tr} \left(\mathbf{W}_m \hat{\mathbf{F}}_m \mathbf{V}_l \mathbf{V}_l^H \hat{\mathbf{F}}_m^H \mathbf{W}_m^H \right) \mathbf{I}_{N_{r,k}} \\ & + \sigma_m^2 \sum_{m=1}^M \left(\hat{\mathbf{G}}_{km} \mathbf{W}_m \mathbf{W}_m^H \hat{\mathbf{G}}_{km}^H \right) \\ & + \sigma_{\text{EG}}^2 \sigma_m^2 \sum_{m=1}^M \text{Tr}(\mathbf{W}_m \mathbf{W}_m^H) \mathbf{I}_{N_{r,k}} + \sigma_k^2 \mathbf{I}_{N_{r,k}}. \end{aligned} \quad (6.46)$$

Similarly, solving the optimization problem in (6.36) with the help of the Lagrange function leads to the following optimal pre-coding filter matrix as (see A.4 and A.5 for the derivation)

$$\mathbf{V}_l^{\text{robust}} = [\Gamma + \lambda_l \mathbf{I}_{N_t}]^{-1} \hat{\mathbf{H}}_l^H \mathbf{U}_l, \quad (6.47)$$

where Γ is defined by

$$\begin{aligned} \Gamma = & \sum_{k=1}^K \hat{\mathbf{H}}_k^H \mathbf{U}_k \mathbf{U}_k^H \hat{\mathbf{H}}_k \\ & + \sigma_{\text{EF}}^2 \sum_{k=1}^K \sum_{m=1}^M \text{Tr} \left(\mathbf{U}_k^H \hat{\mathbf{G}}_{km} \mathbf{W}_m \mathbf{W}_m^H \hat{\mathbf{G}}_{km}^H \mathbf{U}_k \right) \mathbf{I}_{N_t} \\ & + \sigma_{\text{EF}}^2 \sigma_{\text{EG}}^2 \sum_{k=1}^K \text{Tr}(\mathbf{U}_k \mathbf{U}_k^H) \sum_{m=1}^M \text{Tr}(\mathbf{W}_m \mathbf{W}_m^H) \mathbf{I}_{N_t} \\ & + \sigma_{\text{EG}}^2 \sum_{k=1}^K \text{Tr}(\mathbf{U}_k \mathbf{U}_k^H) \sum_{m=1}^M \hat{\mathbf{F}}_m^H \mathbf{W}_m^H \mathbf{W}_m \mathbf{F}_m \end{aligned} \quad (6.48)$$

The iterative procedure of the proposed algorithm, referred to as Robust IA, is summarized below:

Algorithm 2: Robust IA based on the MMSE and ZF criteria

- 1) initialize arbitrarily the filters $\{\mathbf{U}_k\}$ and $\{\mathbf{V}_l\}$
 - 2) compute the relay matrix \mathbf{W}_m according to the optimal matrix \mathbf{w} in (6.44).
 - 3) update the estimated equivalent channel $\hat{\mathbf{H}}_k$ according to (6.33).
 - 4) compute the post-processing filter matrix \mathbf{U}_k at each user according to (6.45).
 - 5) compute the pre-coding filter matrix \mathbf{V}_l at the MBS for each user according to (6.47).
 - 6) repeat from step 2 until convergence.
-

6.5 IA FEASIBILITY CONDITIONS

The feasibility of a IA solution for a $K \times M \times K$ two-hop MIMO interference channel, where K sources communicate with the K dedicated destinations through M AF RNs, is investigated in [23], [24] and [59]. According to these studies, the IA solutions for the system model described in subsection 6.2.3 is feasible if the following conditions are fulfilled:

$$\sum_{k=1}^K \sum_{\substack{l=1 \\ l \neq k}}^K d_k d_l \leq \sum_{k=1}^K d_k (N_{r,k} + N_t - 2d_k) + \left(\sum_{m=1}^M N_{re,m}^2 - 1 \right), \quad (6.49)$$

$$\sum_{k=1}^K d_k \leq \sum_{m=1}^M N_{re,m}, \quad (6.50)$$

$$d_k \leq \min\{N_t, N_{r,k}\}, \quad \forall k, \quad (6.51)$$

$$N_t \geq \sum_{k=1}^K d_k, \quad \forall k, \quad (6.52)$$

where the left term in (6.49) represents the number of equations and the right term stands for the number of variables. The condition in (6.50) states that the sum DoF should not exceed the number of antenna over all RNs, whereas (6.51) implies that the DoF of each user is not transcend the maximum DoF of the MIMO channels. Based on these conditions, the required number of relays and relay antennas can be specified for the system configuration.

6.5.1 Required Number of Relay Nodes

The minimum required number of relays for a given set of $\{N_{r,k}, N_t, d_k, N_{re,m}\}$ can be obtained by combining the conditions (6.49) and (6.50). Assuming that all relay

has the same number of antennas, i.e. $N_{re,m} = N_{re} \forall k$, the required number of relays is given by (6.53).

$$M \geq \max \left\{ \frac{d^2 K(K-1) + \sum_{k=1}^K d_k (N_{r,k} + N_t - 2d_k) + 1}{N_{re}^2}, \frac{Kd}{N_{re}} \right\} \quad (6.53)$$

Specifically, for the case that $d_k = N_{r,k} = N_{re,m}$ and $N_t = d$, $\forall k = 1, \dots, K$ and $\forall m = 1, \dots, M$, (6.53) can be simplified as

$$M \geq K(K-1) + 1. \quad (6.54)$$

Accordingly, it can be concluded that to achieve maximum DoF for each user, the considered system requires at least $K(K-1) + 1$ relays.

6.5.2 Required Number of Relay Antennas

Similar to subsection 6.5.1, for a given set of $\{N_{r,k}, N_t, d_k, K, M\}$ the required number of antennas at each relay can be determined from (6.49) and (6.50). More specifically, for the case $d_k = N_{r,k}$ and $Kd_k = N_t$, $\forall k = 1, \dots, K$ and $M = 1$, we obtain the following simplified formulation for the number of relay antennas.

$$\begin{aligned} N_{relay,m} &= \max \left\{ KM, \sqrt{K(K-1)M^2 + 1} \right\} \\ &= KM \end{aligned} \quad (6.55)$$

Moreover, (6.55) indicates that in areas of dense mobile traffic we can utilize a single relay with multiple antennas instead of deploying multiple relays, when $N_{re} = N_{r,k} = d_k$ and $N_t = Kd_k$.

6.6 SIMULATION RESULTS

This section provides numerical results to verify the analysis of the proposed IA approaches. To evaluate the system performance of two proposed IA approaches, a multi-user half-duplex AF MIMO relay system is considered, where the number of transmit and receive antennas are fixed, while the number of relay nodes and the number of antennas at each RN are varied. For a given set of $\{K, N_t, N_{r,k}\}$, the required number of relay nodes and the number of relay antennas can be determined to meet the conditions in (6.53) and (6.55). All simulations were conducted using the 4-QAM modulation scheme and a statistical multi-path fading channel model. The noise at each relay and receive node is assumed to be statistically independent, zero-mean complex Gaussian random variables. Moreover, the noise power and the CSI error are assumed to be the same for all nodes and hops, respectively.

First, the system performance of the proposed non-robust IA approach is compared with that of the reference approach introduced in [24] for the case of perfect CSI. In [24], all filter matrices are determined based on the minimization of the total

interference leakage at the receivers. In that study, the total interference leakage at receiver k is given by

$$I_k = \text{Tr} \{ \mathbf{U}_k^T \mathbf{Q}_k \mathbf{U}_k^* \}, \quad (6.56)$$

where \mathbf{Q}_k is the interference covariance matrix at user k . It should be mentioned that in [24] the noise at relays and receivers are not considered in determining the IA filters. Using an iterative approach, in which the cost function is minimized with respect to one variable while keeping other fixed, the filters \mathbf{U}_k , \mathbf{V}_l and \mathbf{W}_m can be optimized. By doing so, the zero-forcing post-processing filter matrix \mathbf{U}_k is determined according to the d_k least dominant eigenvectors of \mathbf{Q}_k . Here, the reciprocity principle of the channel is used to find the pre-coding filter \mathbf{V}_l , which is difficult to be obtained in practice. Because of the role reversal between transmitters and receivers in the reciprocal link, the interference, which a user receives from other users in original link, is the same as that caused by this user to other users in the reciprocal link. Therefore, the interference leakage is unchanged in both links. As a result, the pre-coding filter \mathbf{V}_l is the post-processing filter determined in the reciprocal link. Further on, the relay matrix is optimized having fixing both pre-coding and post-processing filter matrices.

Subsequently, the end-to-end system performance of the proposed robust IA approach is compared with that of the non-robust IA method. To assess the efficiency of the proposed IA approaches the system performance in terms of average sum-rate, BER and MSE is considered.

The end-to-end signal-to-interference-plus-noise ratio (SINR) at user k is determined by

$$\text{SINR}_k = \frac{\|\underline{\mathbf{H}}_{kk}\|^2}{\sum_{\substack{l=1 \\ l \neq k}}^K \|\underline{\mathbf{H}}_{kl}\|^2 + \sum_{m=1}^M \sigma_m^2 \|\mathbf{U}_k^H \mathbf{G}_{km} \mathbf{W}_m\|^2 + \sigma_k^2 \|\mathbf{U}_k\|^2}, \quad (6.57)$$

where the effective channel $\underline{\mathbf{H}}_{kl}$ is given as follows:

$$\underline{\mathbf{H}}_{kl} = \mathbf{U}_k^H \sum_{m=1}^M \mathbf{G}_{km} \mathbf{W}_m \mathbf{F}_m \mathbf{V}_l. \quad (6.58)$$

6.6.1 Convergence Analysis

Both iterative algorithms proposed above are based on the alternating minimization solution, i.e. the relay matrices are depending on the optimal pre-coder and post-processing filter matrix of all users, and vice versa. Although, \mathbf{W}_m and $\mathbf{V}_l, \mathbf{U}_k$ are determined based on two different object functions, we show that using our approach, reducing the interference leakage leads to the decreasing of MSE, and vice versa (see A.6 for the derivation). Alternating minimization solution used in this paper (first fixed $\{\mathbf{V}_l\}, \{\mathbf{U}_k\}$ to find \mathbf{W}_m then calculating $\{\mathbf{V}_l\}, \{\mathbf{U}_k\}$ for fixed $\{\mathbf{W}_m\}$) reduces not only the MSE, but also the interference leakage at each step of the iteration. Since the MMSE is lower bounded for the fixed transmit power constraint, the iterative algorithm based on the MMSE optimization problem is always convergent,

as shown in [94] and [75]. The convergence behavior with regard to both the MSE and interference leakage are shown via simulation results. However, it should be mentioned that due to the non-convex optimization problem of the cost function in (6.14) and (6.13), the convergence to a global minimum cannot be always ensured, and multiple local minima could be provided. However, the global minimum can be achieved by choosing an appropriate initialization as follow:

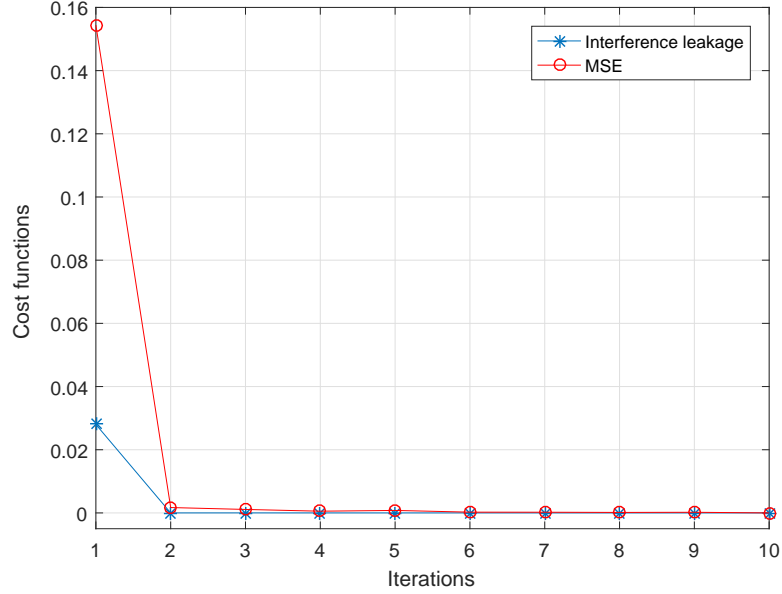


Figure 6.4: Convergence behavior of the non-robust IA approach for $\{K \times N_t \times N_{re} \times N_r\} = \{3 \times 6 \times 6 \times 2\}$.

$$\begin{aligned} \mathbf{V}_0 &= \sqrt{\frac{1}{d_k}} \mathbf{I}_{N_t \times d_k}, \\ \mathbf{U}_0 &= \sqrt{\frac{1}{d_k}} \mathbf{I}_{N_{r,k} \times d_k}, \\ \mathbf{W}_0 &= \sqrt{d_k} \mathbf{I}_{N_{re} \times N_{re}}. \end{aligned} \quad (6.59)$$

Fig. 6.4 illustrates the convergence analysis for the interference leakage and the MSE of the proposed method with the perfect CSI condition. It can be seen that in this case, both power of the interference leakage and the MSE are non-increasing functions over iteration. This is also valid for the case of imperfect CSI.

6.6.2 System Performance of the Non-Robust IA Approach

First of all, the system performance of the non-robust IA approach presented in 6.3.2 concerning perfect CSI is evaluated, where the estimated channels available at relay and transmitter nodes equal to the actual channels, i.e. $\hat{\mathbf{F}}_m = \mathbf{F}_m$ and $\hat{\mathbf{G}}_{kl} = \mathbf{G}_{kl}, \forall k, l = 1, \dots, K$ and $\forall m = 1, \dots, M$. In order to evaluate the system performance, two scenarios are considered. The first one is a single cell scenario, where the MBS communicates with 3 users ($K = 3$) at the edge cell via one RN

($M = 1$). In the second scenario (multi-cell scenario), where the MBS communicates with 3 users via 3 RNs ($M = 3$). Here, the MBS and each user node are equipped with 6 transmit and 2 receive antennas ($N_t = 6, N_{r,k} = 2$), respectively. In this case, each relay has 6 transmit and 6 receive antennas ($N_{re} = 6$). Here, the pre-coding and post-processing matrices \mathbf{V}_l , \mathbf{U}_k and the relay matrix \mathbf{W}_m are determined according to the **algorithm 1**. The system performance of two considered scenarios in terms of the effective SINR and the average sum-rate as a function of $1/\sigma_n^2$ was evaluated and shown in Fig. 6.5 and 6.6, respectively. To this, σ_n^2 stands for the noise power at each user.

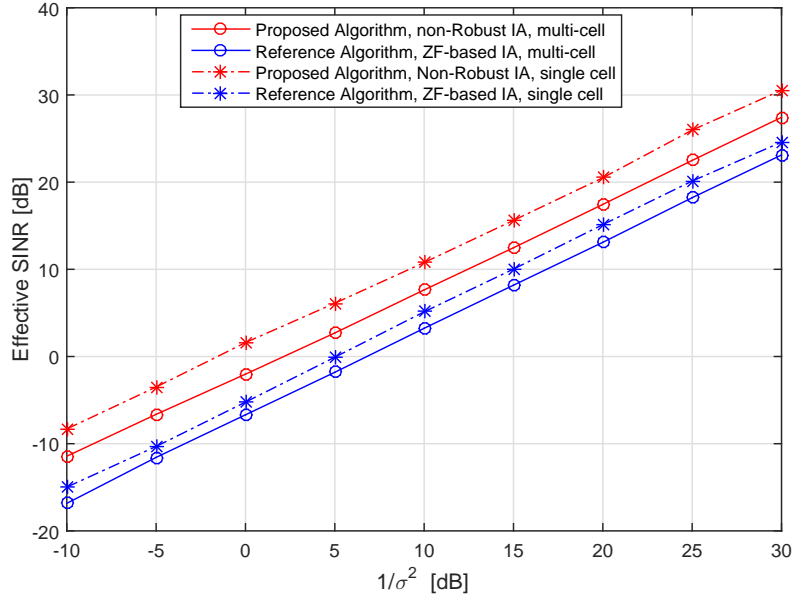


Figure 6.5: The effective end-to-end SINR for both single and multi-cell coexistence scenarios

Fig. 6.5 indicates that considering noise in IA filters design improves significantly the end-to-end effective SINR for all users. In this regard, an SINR gain of more than 5 dB can be achieved. Furthermore, it is seen in Fig. 6.6 that by using the proposed non-robust IA method, the average sum-rate is substantially higher than that achieved by the reference method.

Similarly, the system performance in terms of BER in Fig. 6.7 shows that by taking the total noise into consideration at the receiver to determine IA filters, the proposed IA approach provides better BER performance than that achieved by the reference method, (ZF-approach in [24]). In this regard, an SNR gain of about 4 dB can be achieved in the low and moderate SNR regimes. For high SNRs, both methods deliver the same BER performance. Moreover, the simulation results in Fig. 6.5, 6.6 and 6.7 confirm that the effective SINR and average sum-rate of the single cell scenario is higher than that of the multi-cell scenario.

In the next step, the system performance in terms of average sum-rate is investigated for the single cell scenario with different number of users and. Fig. 6.8 indicates that by increasing the number of user, the average sum-rate is raised significantly.

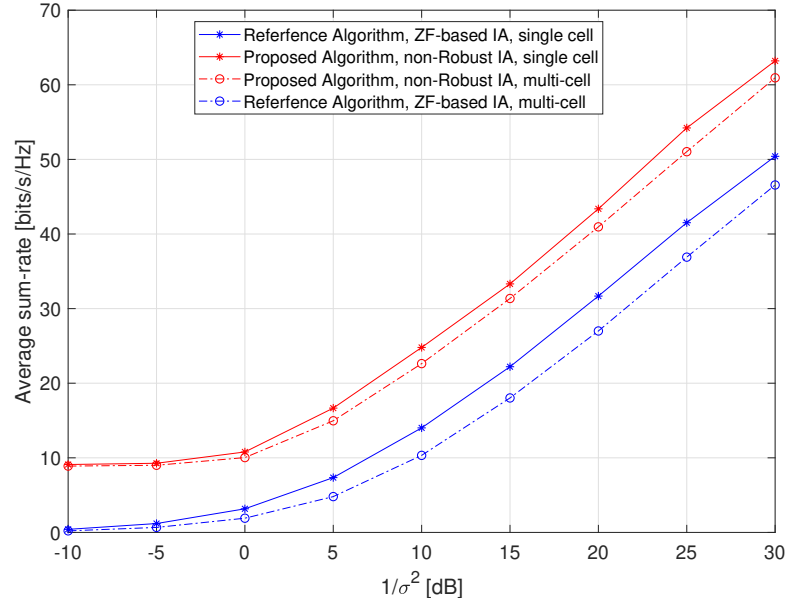


Figure 6.6: The average sum-rate for both single and multi-cell coexistence scenarios

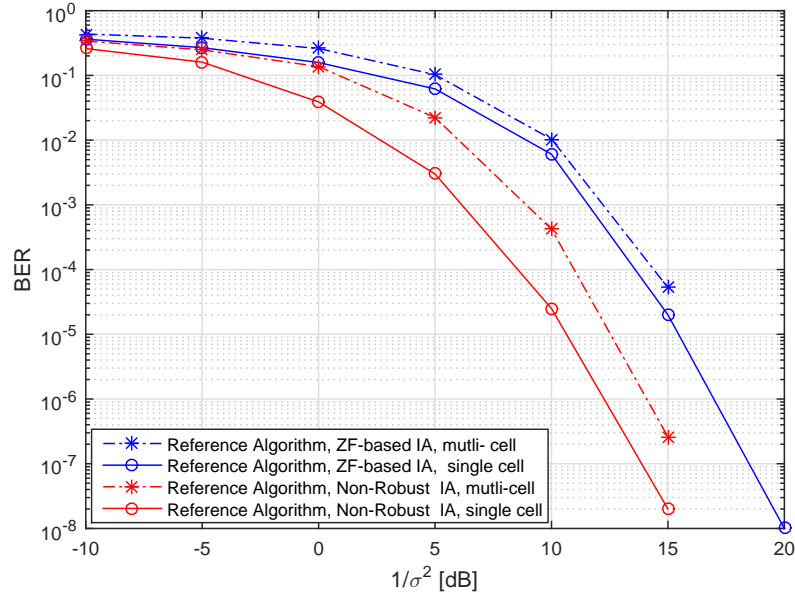


Figure 6.7: The BER performance comparison for both single and multi-cell coexistence scenarios

6.6.3 System Performance of the Robust IA Approach

This subsection covers the system performance of the robust IA approach presented in 6.4.2 for the imperfect CSI case. Here, the system performance of the non-robust IA design method serves as the reference system, where the IA and relay filters are determined using $\mathbf{F} = \hat{\mathbf{F}} + \mathbf{E}^F$, $\mathbf{G} = \hat{\mathbf{G}} + \mathbf{E}^G$ with $\sigma_{\mathbf{E}^F}^2 = 0$, $\sigma_{\mathbf{E}^G}^2 = 0$. In order to compare the efficiency of both proposed methods, the average MSE is investigated in the present of CSI error with different values of $\sigma_{\mathbf{E}^F}^2$ and $\sigma_{\mathbf{E}^G}^2$. For this purpose,

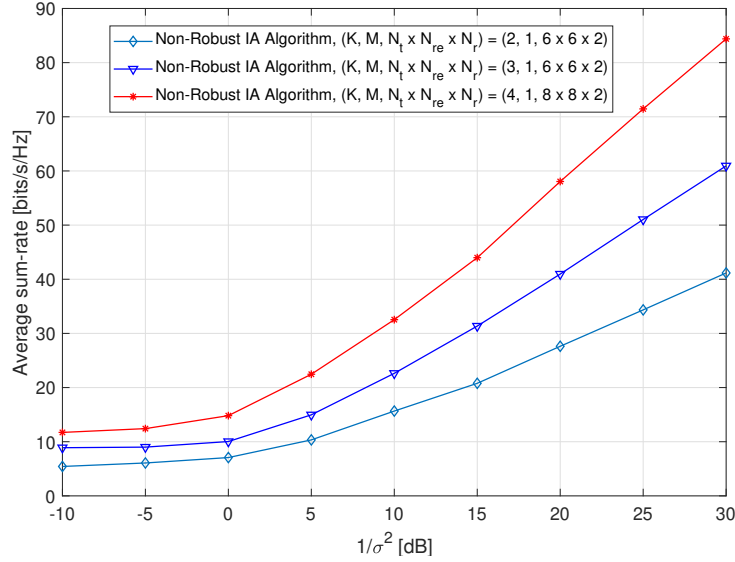


Figure 6.8: The average sum-rate of the non-robust IA design approach for different number of user in a single cell scenario

the average MSE as a function of $1/\sigma_n^2$ for a multi-cell scenario is illustrated in Fig. 6.9. According to simulation results, it can be seen that the non-robust IA performance is deteriorated due to the inaccuracy of CSI. This degradation is increased with the increasing of the CSI error. However, simulation results indicate that by concerning the CSI error to optimize all filters, the robust IA approach delivers better performance in comparison to the non-robust IA design approach. Here, the MSE is significantly reduced.

6.7 SUMMARY

In this chapter, a multi-user half-duplex AF MIMO relay system is considered, where a MBS communicates with edge cell users via relays and each node has multiple antennas. To improve the spectral efficiency, it is assumed that the MBS transmits signals to the associated users at the same time and in the same frequency band. In this regard, two novel IA approaches are proposed to deal with the MUI problem under different conditions of CSI. To this, a hybrid optimization approach based on both MMSE and ZF criteria to determine the IA filters was developed. This optimization approach was firstly developed for the case of having perfect CSI, and then was extended for the case of imperfect CSI.

In Section 6.2, a short introduction to the relay technique and the considered scenario are given. Furthermore, this section illustrates the motivation of our works. In addition, the mathematical description of a multi-user half-duplex AF MIMO relay system model is derived in Section 6.2.

In Section 6.3, the non-robust IA approach is proposed and analyzed in case of having perfect CSI. It is showed that the optimization problem can be solved using the method of Lagrange duality and the KKT conditions. Using the proposed non-robust IA approach, the relay matrix is firstly determined by minimizing the total interference leakage at the receivers. After that the pre-coding and post-processing

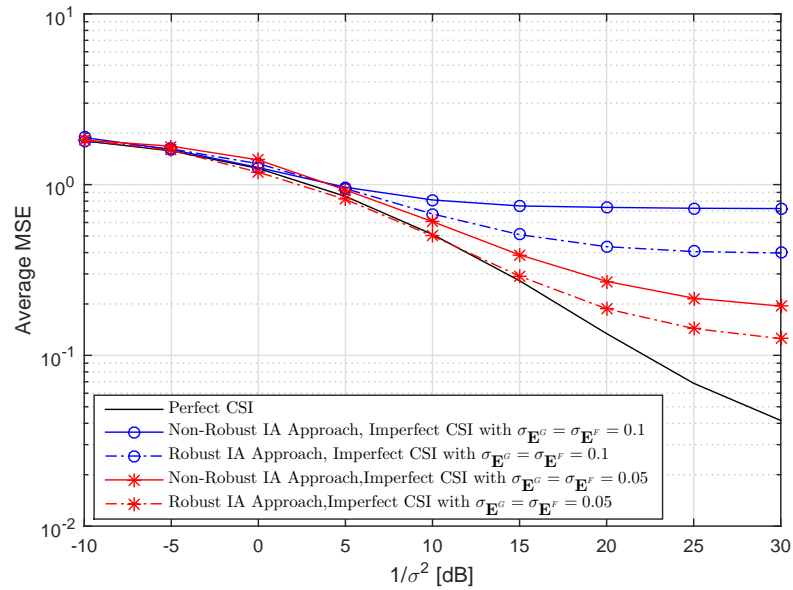


Figure 6.9: MSE performance comparison for a multi-cell scenario with $(N_t = 6, N_r = 2, N_{re} = 6$ and $d = 2)$

matrix are determined, so that the total MSE at the receivers is minimized. Here, the noises at the relay nodes and the receivers are considered in determining the pre-coding and post-processing matrix. This makes our approach different from the existing methods and efficient in low and moderate SNRs.

The proposed robust-IA approach is described and discussed in Section 6.4 for the case of imperfect CSI. Here, it is assumed that the CSI error is caused only by channel estimation error. To this, the expected values of the related cost functions dependent on the estimated channel are defined and used to optimize the IA filters.

Simulation results are shown in Section 6.6. Here, the system performance in terms of the effective SINR, the average sum-rate and BER was investigated. Simulation results indicate that, by considering the noises at the relays and the receivers in determining the IA filters, this approach delivers better performance in low to moderate SNR regimes compared to that achieved by the reference approach. For the case of having imperfect CSI, simulation results confirm that due to the inaccuracy of CSI using the non-robust IA, the system performance is deteriorated. This degradation is increased with with the increasing of CSI error. However, in this case, by using the robust IA approach, a significant performance improvement in terms of MSE can be achieved.

CONCLUSION AND FUTURE WORK

7.1 CONCLUSIONS

The raised question in this thesis was how the Spectral Efficiency (SE) can be improved for 5G/future wireless communication networks, particularly for massive device connectivity cases. To answer this question, novel approaches were developed and investigated.

First, the Faster-than Nyquist (FTN) signaling transmission scheme was investigated in Chapter 2 in order to achieve a SE improvement in a single user single carrier system. Using FTN, the data rate is significantly increased by reducing the symbol period below the Nyquist criteria. This results in Inter-symbol Interference (ISI). We showed that the FTN signaling delivers higher SE compared to the Nyquist signaling given that both systems have the same pulse shape and data rate. The reason for this is that the FTN signaling can also recover the loss of SE caused by the excess bandwidth of the used pulse shape by adjusting the symbol period and tolerating ISI. Furthermore, simulation results indicate that FTN allows for lower BER and PAPR compared to the Nyquist signaling, since a lower modulation order can be used in FTN signaling to achieve the same rate as the Nyquist signaling. In addition, a multiple-access channel, where a single-carrier system using the Nyquist or FTN signaling shares spectrum with a multi-carrier system was considered. The evaluation of the SE showed that FTN signaling can recover the loss of SE due to guard bands between these two systems by adjusting the FTN rate. The SE loss can completely be regained in high SNRs. For any other operational SNR, the spectral efficiency loss can be regained by choosing an appropriate FTN rate.

Subsequently, for an SE enhancement in multi-tier heterogeneous networks, multi-user cognitive radio and multi-user relay systems were studied. Here, the Interference Alignment (IA) technique was investigated to handle the multi-user interference problem. In Chapter 4, we proposed a novel IA scheme based on the average-sum minimum mean squared error to deal with the inaccuracy of the channel state information. We showed that using our approach the system performance in terms of MSE is significantly reduced compared to the MMSE-based IA approach in the presence of the channel state information error.

For multi-user underlay cognitive radio MIMO systems, where a macro cell user (licensed user-Primary Users (PUs)) coexists with multiple small cell/femtocell users (unlicensed users-Secondary Users (SUs)), an improvement of spectral efficiency is achieved not only through the high flexibility of frequency use for the SUs, but also by overlapping of multiple the SUs in both time and frequency dimen-

sions. A novel adaptive transmission scheme based on the Water-Filling (WF) and IA method was proposed in Chapter 5. Applying the modified Water-Filling (WF) algorithm at the primary link ensures the maximum capacity for the PU and at least one free primary eigenmode for secondary transmissions in all cases. In the secondary link, a linear pre-coding technique based on IA and null-steering algorithms is employed to align all secondary transmission into unused eigenmode of the PU and deal with Multi-user Interference (MUI). Simulation results indicated that by utilizing the proposed scheme, both primary and secondary links can adapt their transmission to improve the spectrum efficiency. Another advantage of this scheme is ensuring an interference free coexistence of users without having a need for sensing process and the SU transmit power constraints .

For a multi-user half-duplex Amplify-and-Forward (AF)-MIMO relay system, two novel IA approaches with a hybrid optimization approach based on both ZF and MMSE optimization criteria was employed in Chapter 6 to deal with the multi-user interference for both perfect and imperfect CSI cases. Here, the relay matrix was firstly determined by minimizing the total interference leakage at users, and then the pre-coder and post-processing filters were optimized based on the MMSE criterion. In addition, the noise at the relay and destination nodes were taken into account in determining the pre-coding and post-processing matrix. This makes the proposed approach efficient in term the system performance improvement in low to moderate SNRs. The proposed IA approach was initially developed for the case of having perfect CSI, and then was extended to the case of having CSI errors. Simulation results showed that under consideration of the noise at the relay and destination nodes the non-robust IA approach delivers better BER performance in the low to moderate SNR regimes compared to the reference approach. Additionally, the system performance in terms of the average sum-rate and effective SINR can be significantly improved. For the case of having imperfect CSI, the system performance in terms of MSE is significantly reduced by using the robust IA approach.

7.2 FUTURE WORKS

Extension of the proposed transmission scheme in multi-user underlay cognitive radio systems for the case of imperfect CSI can be a subject for future studies. Here, the IA approach based on the MMSE criterion could be investigated to solve the CSI error problem and improve the system performance in low and moderate SNRs. Another research issue could be the mathematical analysis to specify the system parameter δ for the modified WF approach. Moreover, the overall efficiency of the proposed transmission scheme needs to be verified.

A further research topic with future potential is to extend the hybrid optimization approach in Chapter 6, so that the noise at the relay and receiver nodes is also considered in determining the relay matrix. By doing so, the system performance could be improved.

Part II

APPENDIX - PROOF OF EQUATIONS

A

APPENDIX

A.1 FEASIBILITY CONDITIONS FOR THE IA TECHNIQUE

Note that d_k and d_l are the number of independent data streams for user k and l , respectively. According to (4.3), the total number of equations in the system is given by

$$N_e = \sum_{l,k=1,k \neq l}^K d_k d_l \quad (\text{A.1})$$

[117] shows that the number of variables to be determined for the pre-coding filter \mathbf{V}_k and post-processing filter \mathbf{U}_k for user k are $d_k(N_t - d_k)$ and $d_k(N_r - d_k)$, respectively. Therefore, the total variables of the system can be expressed as below

$$N_v = \sum_{k=1}^K d_k (N_t + N_r - 2d_k) \quad (\text{A.2})$$

To guarantee an IA solution, the following condition has to be satisfied

$$N_e \geq N_v. \quad (\text{A.3})$$

With assumption of $d_l = d_k = d$ results in

$$N_t + N_r \geq (K + 1) d \quad (\text{A.4})$$

In IA technique, the interference at receiver k is grouped into a $(N_r \times \sum_{l=1, l \neq k}^K d_l)$ matrix $\mathbf{H}_{k,INT}$ with

$$\mathbf{H}_{k,INT} = [\mathbf{H}_{k1} \mathbf{V}_1, \dots, \mathbf{H}_{k(k-1)} \mathbf{V}_{(k-1)}, \mathbf{H}_{(k+1)(k+1)} \mathbf{V}_{(k+1)}, \dots, \mathbf{H}_{kK} \mathbf{V}_K]. \quad (\text{A.5})$$

This interference lies in $(N_r - d_k)$ interference subspace of receiver k . This leads to

$$\text{rank}(\mathbf{H}_{k,INT}) = r_k \leq N_r - d_k \quad (\text{A.6})$$

It is assumed that the columns of the $(N_r \times \sum_{l=1, l \neq k}^K d_l)$ matrix $\mathbf{H}_{k,INT}$ are partitioned into $\mathbf{H}_{k,INT} = [\mathbf{H}_{k,INT}^{(1)}; \mathbf{H}_{k,INT}^{(2)}]$, where $\mathbf{H}_{k,INT}^{(1)}$ is a $N_r \times r_k$ matrix and has

a rank of r_k . This mean that $\mathbf{H}_{k,INT}^{(2)}$ shares the same column space as $\mathbf{H}_{k,INT}^{(1)}$ [74]. The orthogonal complement of $\mathbf{H}_{k,INT}^{(1)}$, has a dimension of $(N_r \times (\sum_{l=1, l \neq k} d_l - r_k))$ with $\mathbf{H}_{k,INT}^{1\perp} \mathbf{H}_{k,INT}^{(2)} = 0$. Since $\mathbf{H}_{k,INT}^{(2)}$ has a dimension of $(N_r \times (N_t - r_k))$, the number of constraints needed for having $\text{rank}(\mathbf{H}_{k,INT}) = r_k$ is given by

$$N_{\text{const}} = (N_r - r_k) \left(\sum_{l=1, l \neq k} d_l - r_k \right) \quad (\text{A.7})$$

As reported in [74], we have

$$r_k = \min \left(\sum_{k=1}^K d_k, N_r - d_k \right) \quad (\text{A.8})$$

Inserting (A.8) into (A.7), we obtain

$$N_{\text{const}} = d_k \left[\sum_{l=1}^K d_k - N_r \right]_+ \quad (\text{A.9})$$

An IA solution is only possible if

$$d_k (N_t - d_k) \geq d_k \left(\left[\sum_{l=1}^K d_k - N_r \right]_+ \right). \quad (\text{A.10})$$

With $d_k = d_l = d$, (A.10) can be reformulated as

$$(N_t - d) \geq [Kd - N_r]_+ \quad (\text{A.11})$$

Now, the interference caused from transmitter l to receiver k is considered, which lies in an interference subspace r_{kl} with

$$\text{rank}(\mathbf{H}_{kl} \mathbf{V}_l) = r_{kl} \leq (N_r - d_l). \quad (\text{A.12})$$

In this case, $r_{kl} = 0$ when the signal from transmitter l is aligned to the orthogonal complement of the space spanned by \mathbf{H}_{kl} . $r_{kl} = d_l$ when none of signal from transmitter l is aligned to the orthogonal complement of \mathbf{H}_{kl} . Assuming that α_{kl} is the number of signal aligned to the orthogonal complement of \mathbf{H}_{kl} , results in $r_{kl} = d_l - \alpha_{kl}$ and $0 \leq \alpha_{kl} \leq [N_t - N_r]_+$. Consequently, we obtain

$$[d_l + d_k - N_r] \leq \alpha_{kl} \leq [N_t - N_r]_+, \quad \forall k \neq l. \quad (\text{A.13})$$

(A.13) can be reformulated as

$$[d_l + d_k - N_r] \leq [N_t - N_r]_+, \quad \forall k \neq l. \quad (\text{A.14})$$

Since the total number of signal aligned by transmitter l at all receiver $k \neq l$ has to be bounded by $\sum_{k=1, k \neq l} \alpha_{kl} \leq d_l$. This leads to

$$\sum_{k=1, k \neq l}^K [d_l + d_k - N_r] \leq d_l, \quad \forall l \quad (\text{A.15})$$

A.2 DERIVATION OF THE MSE AT USER k

Using (6.6), (6.16) can be reformulated as follows

$$\epsilon_k = \mathbb{E} \left\{ \text{Tr} \left\{ \left(\mathbf{A}\mathbf{s}_k + \sum_{l=1, l \neq k}^K \mathbf{B}\mathbf{s}_l + \sum_{m=1}^M \mathbf{C}\mathbf{n}_m + \mathbf{U}_k^H \mathbf{n}_k - \mathbf{s}_k \right) \left(\mathbf{A}\mathbf{s}_k + \sum_{l=1, l \neq k}^K \mathbf{B}\mathbf{s}_l + \sum_{m=1}^M \mathbf{C}\mathbf{n}_m + \mathbf{U}_k^H \mathbf{n}_k - \mathbf{s}_k \right)^H \right\} \right\} \quad (\text{A.16})$$

with

$$\begin{aligned} \mathbf{A} &= \mathbf{U}_k^H \mathbf{H}_k \mathbf{V}_k \\ \mathbf{B} &= \mathbf{U}_k^H \mathbf{H}_k \mathbf{V}_l \\ \mathbf{C} &= \mathbf{U}_k^H \mathbf{G}_{km} \mathbf{W}_m. \end{aligned}$$

Applying the following conditions

$$\begin{aligned} \mathbb{E} \{ \mathbf{s}_k \mathbf{s}_k^H \} &= \mathbf{I}_{N_t} \\ \mathbb{E} \{ \mathbf{s}_k \mathbf{s}_l^H \} &= 0, \quad \forall k \neq l \\ \mathbb{E} \{ \mathbf{n}_k \mathbf{n}_m^H \} &= 0, \quad \forall k \neq m \\ \mathbb{E} \{ \mathbf{s}_k \mathbf{n}_m^H \} &= 0, \quad \forall k, m \\ \mathbb{E} \{ \mathbf{n}_k \mathbf{n}_k^H \} &= \sigma_n^2 \mathbf{I}_{N_r}, \quad \forall k \end{aligned}$$

we obtain

$$\begin{aligned} \epsilon_k &= \mathbb{E} \left\{ \text{Tr} \left\{ \mathbf{A}\mathbf{I}_{d_k} \mathbf{A}^H - \mathbf{A}\mathbf{I}_{d_k} + \sum_{l=1, l \neq k}^K \mathbf{B}\mathbf{I}_{d_k} \mathbf{B}^H \right\} \right. \\ &\quad \left. - \sum_{m=1}^M \mathbf{C}\sigma_m^2 \mathbf{C}^H + \mathbf{U}_k^H \sigma_k^2 \mathbf{U}_k - \mathbf{I}_{d_k} \mathbf{A} + \mathbf{I}_{d_k} \right\} \\ &= \mathbb{E} \left\{ \text{Tr} \left\{ \left(\mathbf{A}\mathbf{I}_{d_k} \mathbf{A}^H - \mathbf{A}\mathbf{I}_{d_k} - \mathbf{I}_{d_k} \mathbf{A} + \mathbf{I}_{d_k} \right) + \sum_{l=1, l \neq k}^K \mathbf{B}\mathbf{I}_{d_k} \mathbf{B}^H + \mathbf{U}_k^H \mathbf{R}_{\omega\omega} \mathbf{U}_k \right\} \right\} \\ &= \mathbb{E} \left\{ \left\| \mathbf{A} - \mathbf{I}_{d_k} \right\|^2 \right\} + \mathbb{E} \left\{ \sum_{l=1, l \neq k}^K \left\| \mathbf{B} \right\|^2 \right\} + \mathbb{E} \left\{ \mathbf{U}_k^H \mathbf{R}_{\omega\omega} \mathbf{U}_k \right\} \\ &= \mathbb{E} \left\{ \left\| \mathbf{U}_k^H \mathbf{H}_k \mathbf{V}_k - \mathbf{I}_{d_k} \right\|^2 \right\} + \mathbb{E} \left\{ \sum_{l=1, l \neq k}^K \left\| \mathbf{U}_k^H \mathbf{H}_k \mathbf{V}_l \right\|^2 \right\} + \mathbb{E} \left\{ \mathbf{U}_k^H \mathbf{R}_{\omega\omega} \mathbf{U}_k \right\} \end{aligned} \quad (\text{A.17})$$

$$\text{with } \mathbf{R}_{\omega\omega} = \sum_{m=1}^M \mathbf{G}_{km} \mathbf{W}_m \mathbf{W}_m^H \mathbf{G}_{km}^H \sigma_m^2 \mathbf{I}_{N_r} + \sigma_n^2 \mathbf{I}_{d_k}.$$

A.3 THE SUM-INTERFERENCE LEAKAGE

A.3.1 Perfect CSI

Inserting (6.5) into (6.26) results in

$$I = \sum_{k=1}^K \sum_{\substack{l=1 \\ l \neq k}}^K \text{Tr} \left\{ \mathbf{U}_k^H \sum_{m=1}^M \mathbf{G}_{km} \mathbf{W}_m \mathbf{F}_m \mathbf{V}_l \mathbf{V}_l^H \sum_{m=1}^M \mathbf{F}_m^H \mathbf{W}_m^H \mathbf{G}_{km}^H \mathbf{U}_k \right\}. \quad (\text{A.18})$$

Using the property of $\text{Tr}(\mathbf{AB}) = \text{Tr}(\mathbf{BA})$, we obtain

$$I = \sum_{k=1}^K \sum_{\substack{l=1 \\ l \neq k}}^K \sum_{m=1}^M \sum_{m=1}^M \text{Tr} \left\{ \mathbf{W}_m^H \mathbf{G}_{km}^H \mathbf{U}_k \mathbf{U}_k^H \mathbf{G}_{km} \mathbf{W}_m \mathbf{F}_m \mathbf{V}_l \mathbf{V}_l^H \mathbf{F}_m^H \right\}. \quad (\text{A.19})$$

With $\mathbf{a}_{mm} = \sum_{k=1}^K \mathbf{G}_{km}^H \mathbf{U}_k \mathbf{U}_k^H \mathbf{G}_{km}$ and $\mathbf{b}_{mm} = \sum_{\substack{l=1 \\ l \neq k}}^K \mathbf{F}_m \mathbf{V}_l \mathbf{V}_l^H \mathbf{F}_m^H$, A.19 can be reformulated as

$$I = \text{Tr} \left\{ \sum_{m=1}^M \sum_{m=1}^M \mathbf{W}_m^H \mathbf{a}_{mm} \mathbf{W}_m \mathbf{b}_{mm} \right\}. \quad (\text{A.20})$$

Applying Lemma I, we obtain

$$I = \sum_{m=1}^M \sum_{m=1}^M \text{vec}(\mathbf{W}_m)^H \left(\mathbf{b}_{mm}^T \otimes \mathbf{a}_{mm} \right) \text{vec}(\mathbf{W}_m). \quad (\text{A.21})$$

Equation (A.21) can be written using matrix notation as follows:

$$I = \mathbf{w}^H \left(\sum_{k=1}^K \sum_{l=1, l \neq k}^K \mathbf{A}_{kl} \right) \mathbf{w}, \quad (\text{A.22})$$

where $\mathbf{w} = [\text{vec}\{\mathbf{W}_1\}^T, \dots, \text{vec}\{\mathbf{W}_M\}^T]^T$ and matrix \mathbf{A}_{kl} is given by (6.29).

A.3.2 Imperfect CSI

(6.37) can be reformulated as

$$\begin{aligned} \mathbb{E}\{I\} &= \sum_{k=1}^K \sum_{\substack{l=1 \\ l \neq k}}^K \text{Tr} \left\{ \mathbf{U}_k^H \sum_{m=1}^M \hat{\mathbf{G}}_{km} \mathbf{W}_m \hat{\mathbf{F}}_m \mathbf{V}_l \mathbf{V}_l^H \sum_{m=1}^M \hat{\mathbf{F}}_m^H \mathbf{W}_m^H \hat{\mathbf{G}}_{km}^H \mathbf{U}_k \right\} \\ &+ \mathbb{E} \left\{ \sum_{k=1}^K \sum_{\substack{l=1 \\ l \neq k}}^K \text{Tr} \left\{ \mathbf{U}_k^H \sum_{m=1}^M \hat{\mathbf{G}}_{km} \mathbf{W}_m \mathbf{E}_m^F \mathbf{V}_l \mathbf{V}_l^H \sum_{m=1}^M (\mathbf{E}_m^F)^H \mathbf{W}_m^H \hat{\mathbf{G}}_{km}^H \mathbf{U}_k \right\} \right\} \\ &+ \mathbb{E} \left\{ \sum_{k=1}^K \sum_{\substack{l=1 \\ l \neq k}}^K \text{Tr} \left\{ \mathbf{U}_k^H \sum_{m=1}^M \mathbf{E}_{km}^G \mathbf{W}_m \hat{\mathbf{F}}_m \mathbf{V}_l \mathbf{V}_l^H \sum_{m=1}^M \hat{\mathbf{F}}_m^H \mathbf{W}_m^H (\mathbf{E}_{km}^G)^H \mathbf{U}_k \right\} \right\} \end{aligned}$$

$$+ \mathbb{E} \left\{ \sum_{k=1}^K \sum_{\substack{l=1 \\ l \neq k}}^K \text{Tr} \left\{ \mathbf{U}_k^H \sum_{m=1}^M \mathbf{E}_{km}^G \mathbf{W}_m \mathbf{E}_m^F \mathbf{V}_l \mathbf{V}_l^H \sum_{m=1}^M (\mathbf{E}_m^F)^H \mathbf{W}_m^H (\mathbf{E}_m^G)^H \mathbf{U}_k \right\} \right\} \quad (\text{A.23})$$

Using Lemma II and results in A.3.1 , we obtain

$$\mathbb{E} \{I\} = \mathbf{w}^H \left\{ \sum_{k=1}^K \sum_{\substack{l=1 \\ l \neq k}}^K (\hat{\mathbf{A}}_{kl} + \sigma_{\text{EG}}^2 \sigma_{\text{EF}}^2 \text{Tr}(\mathbf{V}_l \mathbf{V}_l^H) \text{Tr}(\mathbf{U}_k \mathbf{U}_k^H) \mathbf{I}_{MN_t N_{\text{re}}}) \right. \\ \left. + \sigma_{\text{EF}}^2 \text{Tr}(\mathbf{V}_l \mathbf{V}_l^H) \mathbf{C}_{kl} + \sigma_{\text{EG}}^2 \text{Tr}(\mathbf{U}_k \mathbf{U}_k^H) \mathbf{B}_{kl} \right\} \mathbf{w}, \quad (\text{A.24})$$

where \mathbf{B}_{kl} and \mathbf{C}_{kl} are $(MN_t N_{\text{re}} \times MN_t N_{\text{re}})$ block diagonal matrices with the main diagonal block matrix of $((\hat{\mathbf{F}}_m^* \mathbf{V}_l^* \mathbf{V}_l^T \hat{\mathbf{F}}_m^T) \otimes \mathbf{I}_{N_{\text{re}}}) \mathbf{I}_M$ and $(\mathbf{I}_{N_t} \otimes \hat{\mathbf{G}}_{km}^H \mathbf{U}_k \mathbf{U}_k^H \hat{\mathbf{G}}_{km}) \mathbf{I}_M$, $\forall m = 1, \dots, M$, respectively.

A.4 DERIVATION OF THE POST-PROCESSING FILTER FOR USER k

(6.42) can be rewritten as

$$\bar{\epsilon} = \sum_{k=1}^K \sum_{l=1}^K \text{Tr} \left(\mathbf{U}_k^H \hat{\mathbf{H}}_k \mathbf{V}_l \mathbf{V}_l^H \hat{\mathbf{H}}_k^H \mathbf{U}_k \right) - \sum_{k=1}^K \text{Tr} \left(\mathbf{U}_k^H \hat{\mathbf{H}}_k \mathbf{V}_k \right) - \sum_{k=1}^K \text{Tr} \left(\mathbf{V}_k^H \hat{\mathbf{H}}_k^H \mathbf{U}_k \right) \\ + \sum_{k=1}^K \text{Tr} \left(\mathbf{I}_{d_k} \right) + \sigma_{\text{EF}}^2 \sum_{k=1}^K \sum_{l=1}^K \text{Tr} \left(\mathbf{V}_l \mathbf{V}_l^H \right) \sum_{m=1}^M \text{Tr} \left(\mathbf{U}_k^H \hat{\mathbf{G}}_{km} \mathbf{W}_m \mathbf{W}_m^H \hat{\mathbf{G}}_{km}^H \mathbf{U}_k \right) \\ + \sigma_{\text{EF}}^2 \sigma_{\text{EG}}^2 \sum_{k=1}^K \text{Tr} \left(\mathbf{U}_k \mathbf{U}_k^H \right) \sum_{m=1}^M \text{Tr} \left(\mathbf{W}_m \mathbf{W}_m^H \right) \sum_{l=1}^K \text{Tr} \left(\mathbf{V}_l \mathbf{V}_l^H \right) \\ + \sigma_{\text{EG}}^2 \sum_{k=1}^K \text{Tr} \left(\mathbf{U}_k \mathbf{U}_k^H \right) \sum_{m=1}^M \sum_{l=1}^K \text{Tr} \left(\mathbf{W}_m \hat{\mathbf{F}}_m \mathbf{V}_l \mathbf{V}_l^H \hat{\mathbf{F}}_m^H \mathbf{W}_m^H \right) \\ + \sigma_m^2 \sum_{k=1}^K \sum_{m=1}^M \text{Tr} \left(\mathbf{U}_k^H \hat{\mathbf{G}}_{km} \mathbf{W}_m \mathbf{W}_m^H \hat{\mathbf{G}}_{km}^H \mathbf{U}_k \right) \\ + \sigma_{\text{EG}}^2 \sigma_m^2 \sum_{k=1}^K \sum_{m=1}^M \text{Tr} \left(\mathbf{W}_m \mathbf{W}_m^H \right) \text{Tr} \left(\mathbf{U}_k \mathbf{U}_k^H \right) \\ + \sigma_k^2 \sum_{k=1}^K \text{Tr} \left(\mathbf{U}_k \mathbf{U}_k^H \right). \quad (\text{A.25})$$

Applying the mathematical properties of $\frac{\partial \text{Tr}(\mathbf{AXB})}{\partial \mathbf{X}} = \mathbf{BA}$ and $\frac{\partial \text{Tr}(\mathbf{AX}^H \mathbf{B})}{\partial \mathbf{X}} = 0$ [87], we obtain

$$\nabla_{\mathbf{U}_k} L(\lambda_l, \mathbf{U}_k, \mathbf{V}_l) = \sum_{l=1}^K \hat{\mathbf{H}}_k \mathbf{V}_l \mathbf{V}_l^H \hat{\mathbf{H}}_k^H \mathbf{U}_k - \hat{\mathbf{H}}_k \mathbf{V}_k$$

$$\begin{aligned}
& + \sigma_{\text{EF}}^2 \sum_{l=1}^K \text{Tr}(\mathbf{V}_l \mathbf{V}_l^H) \sum_{m=1}^M \widehat{\mathbf{G}}_{km} \mathbf{W}_m \mathbf{W}_m^H \widehat{\mathbf{G}}_{km}^H \mathbf{U}_k \\
& \sigma_{\text{EF}}^2 \sigma_{\text{EG}}^2 \sum_{m=1}^M \text{Tr}(\mathbf{W}_m \mathbf{W}_m^H) \sum_{l=1}^K \text{Tr}(\mathbf{V}_l \mathbf{V}_l^H) \mathbf{I}_{d_k} \mathbf{U}_k \\
& + \sigma_{\text{EG}}^2 \sum_{m=1}^M \sum_{l=1}^K \text{Tr}(\mathbf{W}_m \widehat{\mathbf{F}}_m \mathbf{V}_l \mathbf{V}_l^H \widehat{\mathbf{F}}_m^H \mathbf{W}_m^H) \mathbf{I}_{d_k} \mathbf{U}_k \\
& + \sigma_m^2 \sum_{m=1}^M \widehat{\mathbf{G}}_{km} \mathbf{W}_m \mathbf{W}_m^H \widehat{\mathbf{G}}_{km}^H \mathbf{U}_k \\
& + \sigma_{\text{EG}}^2 \sigma_m^2 \sum_{m=1}^M \text{Tr}(\mathbf{W}_m \mathbf{W}_m^H) \mathbf{I}_{d_k} \mathbf{U}_k + \sigma_k^2 \mathbf{I}_{d_k} \mathbf{U}_k. \tag{A.26}
\end{aligned}$$

Consequently, the KKT condition in (6.22) can be expressed by

$$\Upsilon \mathbf{U}_k - \widehat{\mathbf{H}}_k \mathbf{V}_k = 0, \tag{A.27}$$

with Υ given in (6.46). This leads to $\mathbf{U}_k = \Upsilon^{-1} \widehat{\mathbf{H}}_k \mathbf{V}_k$

A.5 DERIVATION OF THE PRE-CODING FILTER FOR USER l

Similar to A.4, the KKT condition in 6.23 for user l can be formulated as follows

$$\begin{aligned}
& \sum_{k=1}^K \widehat{\mathbf{H}}_k^H \mathbf{U}_k \mathbf{U}_k^H \widehat{\mathbf{H}}_k \mathbf{V}_l + \sigma_{\text{EF}}^2 \sum_{k=1}^K \sum_{m=1}^M \text{Tr}(\mathbf{U}_k^H \widehat{\mathbf{G}}_{km} \mathbf{W}_m \mathbf{W}_m^H \widehat{\mathbf{G}}_{km}^H \mathbf{V}_l \\
& + \sigma_{\text{EF}}^2 \sigma_{\text{EG}}^2 \sum_{k=1}^K \text{Tr}(\mathbf{U}_k \mathbf{U}_k^H) \sum_{m=1}^M \text{Tr}(\mathbf{W}_m \mathbf{W}_m^H) \mathbf{I}_{d_k} \mathbf{V}_l \\
& + \sigma_{\text{EG}}^2 \sum_{l=1}^H \text{Tr}(\mathbf{U}_k \mathbf{U}_k^H) \sum_{m=1}^M \widehat{\mathbf{F}}_m^H \mathbf{W}_m^H \mathbf{W}_m \widehat{\mathbf{F}}_m \mathbf{V}_l + \lambda_l \mathbf{I}_{N_t} \mathbf{V}_l - \widehat{\mathbf{H}}_l^H \mathbf{U}_k = 0, \tag{A.28}
\end{aligned}$$

which results in

$$\Gamma \mathbf{V}_l + \lambda_l \mathbf{I}_{N_t} \mathbf{V}_l = \widehat{\mathbf{H}}_l^H \mathbf{U}_l \tag{A.29}$$

Accordingly, we obtain $\mathbf{V}_l = \left(\Gamma + \lambda_l \mathbf{I}_{N_t} \right)^{-1} \widehat{\mathbf{H}}_l^H \mathbf{U}_l$

A.6 RELATION BETWEEN MMSE AND THE TOTAL INTERFERENCE LEAKAGE

It has to be noted that the relation between the total interference leakage and the MMSE is the same for both perfect and imperfect CSI cases. For the case of having perfect CSI, the relay matrix \mathbf{W}_m is optimized based on the minimization of the total interference leakage given by (6.26) and is determined according to (6.30). The pre-coder \mathbf{V}_l and post-processing \mathbf{U}_k filters are optimized using the MMSE criterion and KKT conditions and the filters can iteratively be adjusted according

to (6.31) and (6.32). According to (6.31), the covariance matrix of the total noise at user k can be expressed as follows:

$$\mathbf{R}_{\omega\omega} = (\mathbf{H}_k \mathbf{V}_k \mathbf{U}_k)^{-1} - \sum_{l=1}^K \mathbf{H}_k \mathbf{V}_l \mathbf{V}_l^H \mathbf{H}_k^H. \quad (\text{A.30})$$

Inserting $\mathbf{R}_{\omega\omega}$ into (6.17) results in

$$\epsilon_k = \text{Tr} (\mathbf{I}_{d_k} - \mathbf{V}_k^H \mathbf{H}_k^H \mathbf{U}_k). \quad (\text{A.31})$$

Inserting (6.32) into (A.31), we obtain

$$\epsilon_k = \text{Tr} \left(\mathbf{I}_{d_k} - \frac{\mathbf{H}_k^H \mathbf{U}_k \mathbf{U}_k^H \mathbf{H}_k}{\mathbf{H}_k^H \mathbf{U}_k \mathbf{U}_k^H \mathbf{H}_k + \sum_{l=1, l \neq k}^K \mathbf{H}_l^H \mathbf{U}_l \mathbf{U}_l^H \mathbf{H}_l + \lambda \mathbf{I}_{N_t}} \right). \quad (\text{A.32})$$

It is seen that by considering a dual network the term $\sum_{l=1, l \neq k}^K \mathbf{H}_l^H \mathbf{U}_l \mathbf{U}_l^H \mathbf{H}_l$ is the MUI in the reverse link and it is the same as the interference leakage at user k in the forward link. According to (A.32), it can be concluded that reducing the interference leakage leads to decreasing the MSE at user k and vice versa.

BIBLIOGRAPHY

- [1] Ansuman Adhikary and Giuseppe Caire. "On the coexistence of macrocell spatial multiplexing and cognitive femtocells." In: *2012 IEEE International Conference on Communications (ICC)*. 2012, 6830–6834.
- [2] Ian F Akyildiz et al. "A survey on spectrum management in cognitive radio networks." In: *IEEE Communications Magazine* 46.4 (2008), 40–48.
- [3] Ian F Akyildiz et al. "Enabling next generation small cells through femto-relays." In: *Physical Communication* 9 (2013), 1–15.
- [4] Siavash M Alamouti. "A simple transmit diversity technique for wireless communications." In: *IEEE Journal on selected areas in communications* 16.8 (1998), 1451–1458.
- [5] Mohamed Amir, Amr El-Keyi, and Mohammed Nafie. "Constrained interference alignment and the spatial degrees of freedom of MIMO cognitive networks." In: *IEEE Transactions on Information Theory* 57.5 (2011), 2994–3004.
- [6] V Sreekanth Annapureddy and Venugopal Veeravalli. "Gaussian interference networks: Sum capacity in the low-interference regime and new outer bounds on the capacity region." In: *IEEE Transactions on Information Theory* 55.7 (2009), 3032–3050.
- [7] Saied M Abd El-atty and ZM Gharseldien. "Analytical model for mobile user connectivity in coexisting femtocell/macrocell networks." In: *arXiv preprint arXiv:1301.1825* (2013).
- [8] O. El Ayach, S. W. Peters, and R. W. Heath. "The practical challenges of interference alignment." In: *IEEE Wireless Communications* 20.1 (Feb. 2013), 35–42.
- [9] Yong Bai and Lan Chen. "Hybrid spectrum arrangement and interference mitigation for coexistence between LTE macrocellular and femtocell networks." In: *EURASIP Journal on Wireless Communications and Networking* 2013.1 (2013), 1–15.
- [10] John R Barry, Edward A Lee, and David G Messerschmitt. *Digital communication*. Springer Science & Business Media, 2004.
- [11] Alireza Shahan Behbahani, Ricardo Merched, and Ahmed M Eltawil. "Optimizations of a MIMO relay network." In: *IEEE Transactions on Signal Processing* 56.10 (2008), 5062–5073.
- [12] Tommaso Beniero et al. "Effect of relaying on coverage in 3GPP LTE-advanced." In: *IEEE 69th Vehicular Technology Conference, 2009 (VTC Spring)*. 2009, 1–5.
- [13] S. Berger et al. "Recent advances in amplify-and-forward two-hop relaying." In: *IEEE Communications Magazine* 47.7 (July 2009), pp. 50–56.

- [14] Ezio Biglieri et al. *MIMO wireless communications*. Cambridge university press, 2007.
- [15] Rasmus Brandt, Per Zetterberg, and Martin Bengtsson. "Interference alignment over a combination of space and frequency." In: *IEEE International Conference on Communications Workshops (ICC)*. 2013, 149–153.
- [16] V. R. Cadambe and S. A. Jafar. "Can 100 speakers talk for 30-minutes each in one room within one hour and with zero interference to each other's audience?" In: *Proceedings of the 45th Annual Allerton Conference on Communication, Control, and Computing, Monticello, IL*. 2007.
- [17] V. R. Cadambe and S. A. Jafar. "Interference Alignment and Degrees of Freedom of the K -User Interference Channel." In: *IEEE Transactions on Information Theory* 54.8 (Aug. 2008), 3425–3441.
- [18] B.K. Chalise and L. Vandendorpe. "Optimization of MIMO Relays for Multipoint-to-Multipoint Communications: Nonrobust and Robust Designs." In: *IEEE Transactions on Signal Processing* 58.12 (Dec. 2010), 6355–6368.
- [19] Batu K Chalise and Luc Vandendorpe. "MIMO relay design for multipoint-to-multipoint communications with imperfect channel state information." In: *IEEE Transactions on Signal Processing* 57.7 (2009), 2785–2796.
- [20] Vikram Chandrasekhar and Jeffrey G Andrews. "Spectrum allocation in two-tier networks." In: *IEEE 42nd Asilomar Conference on Signals, Systems and Computers*. 2008, 1583–1587.
- [21] Vikram Chandrasekhar et al. "Power control in two-tier femtocell networks." In: *IEEE Transactions on Wireless Communications* 8.8 (2009), 4316–4328.
- [22] Symeon Chatzinotas and Björn Ottersten. "Cognitive interference alignment between small cells and a macrocell." In: *IEEE 19th International Conference on Telecommunications (ICT)*. 2012, 1–6.
- [23] Xiang Chen, SH Song, and Khaled Ben Letaief. "Interference alignment in MIMO interference relay channels." In: *IEEE Wireless Communications and Networking Conference (WCNC)*, 2012, 630–634.
- [24] Xiang Chen, SH Song, and Khaled Letaief. "Interference alignment in dual-hop MIMO interference channel." In: *IEEE Transactions on Wireless Communications* 13.3 (Mar. 2014), 1274–1283.
- [25] Yong Soo Cho et al. *MIMO-OFDM Wireless Communications with MATLAB*. Wiley Publishing, 2010.
- [26] Lai-U Choi and R. D. Murch. "A transmit preprocessing technique for multiuser MIMO systems using a decomposition approach." In: *IEEE Transactions on Wireless Communications* 3.1 (Jan. 2004), 20–24.
- [27] Chen-Nee Chuah, Joseph M Kahn, and David Tse. "Capacity of multi-antenna array systems in indoor wireless environment." In: *IEEE The Bridge to Global Integration, Global Telecommunications Conference, GLOBECOM*. Vol. 4. 1998, 1894–1899.

- [28] Bruno Clerckx and Claude Oestges. *MIMO wireless networks: Channels, techniques and standards for multi-antenna, multi-user and multi-cell systems*. Academic Press, 2013.
- [29] Thomas M Cover and Joy A Thomas. *Elements of information theory*. John Wiley & Sons, 2012.
- [30] Steredenn Daumont, Basel Rihawi, and Yves Lout. "Root-raised cosine filter influences on PAPR distribution of single carrier signals." In: *IEEE 3rd International Symposium on Communications, Control and Signal Processing, ISCCSP*. 2008, 841–845.
- [31] Ruben De Francisco et al. "Orthogonal linear beamforming in MIMO broadcast channels." In: *IEEE Wireless Communications and Networking Conference, WCNC*. 2007, 1210–1215.
- [32] Ming Ding and Hanwen Luo. *Multi-point Cooperative Communication Systems: Theory and Applications*. Springer, 2013.
- [33] Omar El Ayach, Steven W Peters, and Robert W Heath Jr. "The feasibility of interference alignment over measured MIMO-OFDM channels." In: *IEEE Transactions on Vehicular Technology* 59.9 (2010), 4309–4321.
- [34] Marwa El Hefnawy and Hidekazu Taoka. "Overview of Faster-than-Nyquist for future mobile communication systems." In: *IEEE 77th Vehicular Technology Conference (VTC Spring)*. 2013, 1–5.
- [35] Ericsson. *On CSI feedback for ITU requirement fulfilling CoMP schemes*. Tech. rep. R1-092024. 3GPP, 2009.
- [36] Siavash Fazeli-Dehkordy, Shahram Shahbazpanahi, and Saeed Gazor. "Multiple peer-to-peer communications using a network of relays." In: *IEEE Transactions on Signal Processing* 57.8 (2009), 3053–3062.
- [37] *Further advancements for E-UTRA physical layer aspects*. Tech. rep. TR 36.814. http://www.3gpp.org/ftp/Specs/archive/36_series/36.814/36814-900.zip.: 3GPP, 2010.
- [38] R. S. Ganesan et al. "Cooperative zero forcing in multi-pair multi-relay networks." In: *2012 IEEE 23rd International Symposium on Personal, Indoor and Mobile Radio Communications - (PIMRC)*. Sept. 2012, pp. 1740–1745.
- [39] Xiaohu Ge et al. "5G wireless backhaul networks: challenges and research advances." In: *IEEE Network* 28.6 (2014), 6–11.
- [40] Hassan Ghozlan et al. "The MIMO wireless switch: Relaying can increase the multiplexing gain." In: *IEEE International Symposium on Information Theory (ISIT)*. 2009, 1448–1452.
- [41] Andrea Goldsmith et al. "Breaking spectrum gridlock with cognitive radios: An information theoretic perspective." In: *Proceedings of the IEEE* 97.5 (2009), 894–914.
- [42] Krishna Gomadam, Viveck R Cadambe, Syed Jafar, et al. "A distributed numerical approach to interference alignment and applications to wireless interference networks." In: *IEEE Transactions on Information Theory* 57.6 (June 2011), 3309–3322.

- [43] Wei Guan, Hanwen Luo, and Wen Chen. "Linear relaying scheme for MIMO relay system with QoS requirements." In: *IEEE Signal Processing Letters* 15 (2008), 697–700.
- [44] Basak Guler and Aylin Yener. "Selective interference alignment for MIMO cognitive femtocell networks." In: *IEEE Journal on Selected Areas in Communications* 32.3 (2014), 439–450.
- [45] Ismail Güvenç et al. "A hybrid frequency assignment for femtocells and coverage area analysis for co-channel operation." In: *IEEE Communications Letters* 12.12 (2008), 880–882.
- [46] Ralf Haas and J-C Belfiore. "Multiple carrier transmission with time-frequency well-localized impulses." In: *IEEE Second Symposium on Communications and Vehicular Technology in the Benelux*. 1994, 187–193.
- [47] Lajos L Hanzo et al. *MIMO-OFDM for LTE, WiFi and WiMAX: Coherent versus non-coherent and cooperative turbo transceivers*. Vol. 9. John Wiley & Sons, 2010.
- [48] T. Haustein et al. "Performance of MIMO systems with channel inversion." In: *Vehicular Technology Conference. IEEE 55th Vehicular Technology Conference. VTC Spring 2002*. Vol. 1. 1. 2012, 35–39.
- [49] Veria Havary-Nassab et al. "Distributed beamforming for relay networks based on second-order statistics of the channel state information." In: *IEEE Transactions on Signal Processing* 56.9 (2008), 4306–4316.
- [50] Simon Haykin. "Cognitive radio: brain-empowered wireless communications." In: *IEEE Journal on Selected Areas in Communications* 23.2 (2005), 201–220.
- [51] Ekram Hossain and Monowar Hasan. "5G cellular: key enabling technologies and research challenges." In: *IEEE Instrumentation & Measurement Magazine* 18.3 (2015), 11–21.
- [52] Anders Host-Madsen and Aria Nosratinia. "The multiplexing gain of wireless networks." In: *Proceedings. International Symposium on Information Theory, ISIT*. 2005, 2065–2069.
- [53] Syed Ali Jafar and Maralle Jamal Fakhereddin. "Degrees of freedom for the MIMO interference channel." In: *IEEE Transactions on Information Theory* 53.7 (2007), 2637–2642.
- [54] R Karmakar, S Chattopadhyay, and S Chakraborty. "Impact of IEEE 802.11n/ac PHY/MAC High Throughput Enhancements on Transport and Application Protocols-A Survey." In: *IEEE Communications Surveys Tutorials* 19 (2017), 2050–2091.
- [55] Mohammad Ali Khalighi et al. "Water filling capacity of Rayleigh MIMO channels." In: *12th IEEE International Symposium on Personal, Indoor and Mobile Radio Communications*. Vol. 1. 2001, A–155.
- [56] Md Hashem Ali Khan et al. "A simple block diagonal precoding for multi-user MIMO broadcast channels." In: *EURASIP Journal on Wireless Communications and Networking* 2014.1 (June 2014), 95.

- [57] Mohsen Karimzadeh Kiskani and Babak Hossein Khalaj. "Novel power control algorithms for underlay cognitive radio networks." In: *IEEE 21th International Conference on Systems Engineering (ICSEng)*. 2011, 206–211.
- [58] Ioannis Krikidis. "Space alignment for cognitive transmission in MIMO uplink channels." In: *EURASIP Journal on Wireless Communications and Networking* (2010), 79.
- [59] C. Le, S. Moghaddamnia, and J. Peissig. "An adaptive transmission scheme for multiuser MIMO broadcast channel in Cognitive Radio." In: *IEEE 10th International Conference on Wireless and Mobile Computing, Networking and Communications (WiMob)*. Oct. 2014, 506–512.
- [60] C. Le et al. "Effect of spatial correlation on MMSE-based interference alignment in a multiuser MIMO MB-OFDM system." In: *IEEE 8th International Conference on Wireless and Mobile Computing, Networking and Communications (WiMob)*. Oct. 2012, 739–744.
- [61] Long Bao Le and Ekram Hossain. "Resource allocation for spectrum underlay in cognitive radio networks." In: *IEEE Transactions on Wireless Communications* 7.12 (2008), 5306–5315.
- [62] J. Lee and N. Jindal. "High SNR Analysis for MIMO Broadcast Channels: Dirty Paper Coding Versus Linear Precoding." In: *IEEE Transactions on Information Theory* 53.12 (Dec. 2007), 4787–4792.
- [63] Georgy Levin and Sergey Loyka. "Amplify-and-Forward Versus Decode-and-Forward Relaying: Which is Better?" In: *International Zurich Seminar on Communications*. 2012, 123.
- [64] Xiangfang Li, Lijun Qian, and Deepak Kataria. "Downlink power control in co-channel macrocell femtocell overlay." In: *IEEE 43rd Annual Conference on Information Sciences and Systems, CISS*. 2009, 383–388.
- [65] Min Liang et al. "A novel frequency reuse scheme for OFDMA based relay enhanced cellular networks." In: *IEEE 69th Vehicular Technology Conference, VTC Spring*. 2009, 1–5.
- [66] Angelos D Liveris and Costas N Georghiades. "Exploiting faster-than-Nyquist signaling." In: *IEEE transactions on communications* 51.9 (2003), 1502–1511.
- [67] Luo Fa-Long and Zhang Charlie (Jianzhong). *Signal Processing for 5G: Algorithms and Implementations*. Wiley-IEEE Press, Oct. 2016.
- [68] David Lopez-Perez et al. "Enhanced intercell interference coordination challenges in heterogeneous networks." In: *IEEE Wireless Communications* 18.3 (2011), 22–30.
- [69] David López-Pérez et al. "OFDMA femtocells: A roadmap on interference avoidance." In: *IEEE Communications Magazine* 47.9 (2009), 41–48.
- [70] S. Ma et al. "Iterative transceiver design for MIMO AF relay networks with multiple sources." In: *2010 - MILCOM 2010 MILITARY COMMUNICATIONS CONFERENCE*. Oct. 2010, pp. 369–374.

- [71] JE Mazo. "Faster-than-Nyquist signaling." In: *The Bell System Technical Journal* 54.8 (1975), 1451–1462.
- [72] Shahriar Mirabbasi and Ken Martin. "Design of prototype filter for near-perfect-reconstruction overlapped complex-modulated transmultiplexers." In: *IEEE International Symposium on Circuits and Systems ISCAS 2002*. Vol. 1. 2002, I–821.
- [73] Joseph Mitola III and Gerald Q Maguire Jr. "Cognitive radio: making software radios more personal." In: *IEEE Personal Communications* 6.4 (1999), 13–18.
- [74] F. Negro et al. "Interference alignment feasibility in constant coefficient MIMO interference channels." In: *IEEE 11th International Workshop on Signal Processing Advances in Wireless Communications (SPAWC)*. 2010, 1–5.
- [75] F. Negro et al. "On the MIMO interference channel." In: *Information Theory and Applications Workshop (ITA)*. 2010.
- [76] Francesco Negro et al. "Interference alignment limits for K-user frequency-flat MIMO interference channels." In: *17th European Signal Processing Conference*. 2009, 2445–2449.
- [77] O. Oyman and A. J. Paulraj. "Design and analysis of linear distributed MIMO relaying algorithms." In: *IEE Proceedings - Communications* 153.4 (Aug. 2006), pp. 565–572.
- [78] Francesco Pantisano et al. "Improving macrocell-small cell coexistence through adaptive interference draining." In: *IEEE Transactions on Wireless Communications* 13.2 (2014), 942–955.
- [79] Steven W Peters and Robert W Heath Jr. "Cooperative algorithms for MIMO interference channels." In: *IEEE Transactions on Vehicular Technology* 60.1 (2011), 206–218.
- [80] Steven W Peters and Robert W Heath Jr. "Interference alignment via alternating minimization." In: *IEEE International Conference on Acoustics, Speech and Signal Processing, ICASSP*. 2009, 2445–2448.
- [81] Steven W Peters et al. "Relay architectures for 3GPP LTE-advanced." In: *EURASIP Journal on Wireless Communications and Networking* (2009), 1.
- [82] *Physical channels and modulation*. Tech. rep. TS 36.211 V10.1.0. http://www.3gpp.org/ftp/Specs/archive/36_series/36.211/36211-a10.zip: 3GPP, 2011.
- [83] Tony QS Quek, Hyundong Shin, and Moe Z Win. "Robust wireless relay networks: Slow power allocation with guaranteed QoS." In: *IEEE Journal of Selected Topics in Signal Processing* 1.4 (2007), 700–713.
- [84] Srinivas Ramavath and Rakesh Singh Kshetrimayum. "Analytical calculations of CCDF for some common PAPR reduction techniques in OFDM systems." In: *International Conference on Communications, Devices and Intelligent Systems (CODIS)*. 2012, 393–396.

- [85] Fredrik Rusek and John B Anderson. "Constrained capacities for faster-than-Nyquist signaling." In: *IEEE Transactions on Information Theory* 55.2 (2009), 764–775.
- [86] Abdallah Bou Saleh et al. "Performance of amplify-and-forward and decode-and-forward relays in LTE-advanced." In: *IEEE 70th Vehicular Technology Conference Fall (VTC 2009-Fall)*. 2009, 1–5.
- [87] Hemanth Sampath, Petre Stoica, and Arogyaswami Paulraj. "Generalized linear precoder and decoder design for MIMO channels using the weighted MMSE criterion." In: *IEEE Transactions on Communications* 49.12 (2001), 2198–2206.
- [88] Wiroonsak Santipach and Michael L Honig. "Asymptotic capacity of beamforming with limited feedback." In: *IEEE International Symposium on Information Theory*. 2004, 290–290.
- [89] Hiroshi Sato. "The capacity of the Gaussian interference channel under strong interference (corresp.)." In: *IEEE Transactions on Information Theory* 27.6 (1981), 786–788.
- [90] David Schmidt et al. "Minimum mean squared error interference alignment." In: *Conference Record of the Forty-Third Asilomar Conference on Signals, Systems and Computers*. 2009, 1106–1110.
- [91] Rainer Schoenen, Ruediger Halfmann, and Bernhard H Walke. "An FDD multihop cellular network for 3GPP-LTE." In: *IEEE Vehicular Technology Conference, (VTC Spring)*. 2008, 1990–1994.
- [92] Rainer Schoenen, Wolfgang Zirwas, and Bernhard H Walke. "Capacity and coverage analysis of a 3GPP-LTE multihop deployment scenario." In: *IEEE International Conference on Communications Workshops, ICC Workshops' 08*. 2008, 31–36.
- [93] Martin Schubert and Holger Boche. "Iterative multiuser uplink and downlink beamforming under SINR constraints." In: *IEEE Transactions on Signal Processing* 53.7 (2005), 2324–2334.
- [94] S. Serbetli and A. Yener. "Transceiver optimization for multiuser MIMO systems." In: *IEEE Transactions on Signal Processing* 52 (2004), 214–226.
- [95] Xiaohu Shang, Gerhard Kramer, and Biao Chen. "A new outer bound and the noisy-interference sum-rate capacity for Gaussian interference channels." In: *IEEE Transactions on Information Theory* 55.2 (2009), 689–699.
- [96] Shree Krishna Sharma, Symeon Chatzinotas, and Björn Ottersten. "Interference alignment for spectral coexistence of heterogeneous networks." In: *EURASIP Journal on Wireless Communications and Networking* 1 (2013), 1–14.
- [97] Yongsheng Shi et al. "On resource reuse for cellular networks with Femto and Macrocell coexistence." In: *IEEE Global Telecommunications Conference (GLOBECOM 2010)*. 2010, 1–6.

- [98] Sanjay Singh, Sathish M Kumar, and HS Mruthyunjaya. "Effect of peak-to-average power ratio reduction on the multicarrier communication system performance parameters." In: *International Journal of Electrical and Computer Engineering* 4.12 (2009), 779–786.
- [99] Pierre Siohan and Christian Roche. "Cosine-modulated filterbanks based on extended Gaussian functions." In: *IEEE Transactions on Signal Processing* 48.11 (2000), 3052–3061.
- [100] Aaron So and Ben Liang. "Effect of relaying on capacity improvement in wireless local area networks." In: *IEEE Wireless Communications and Networking Conference*. Vol. 3. 2005, 1539–1544.
- [101] Bongyong Song, Rene L Cruz, and Bhaskar D Rao. "Network duality and its application to multi-user MIMO wireless networks with SINR constraints." In: *2005 IEEE International Conference on Communications (ICC 2005)*. Vol. 4. 2005, 2684–2689.
- [102] Q. H. Spencer, A. L. Swindlehurst, and M. Haardt. "Zero-forcing methods for downlink spatial multiplexing in multiuser MIMO channels." In: *IEEE Transactions on Signal Processing* 52.2 (Feb. 2004), 461–471.
- [103] Q. H. Spencer et al. "An introduction to the multi-user MIMO downlink." In: *IEEE Communications Magazine* 42.10 (Oct. 2004), 60–67.
- [104] Karthikeyan Sundaresan and Sampath Rangarajan. "Efficient resource management in OFDMA femto cells." In: *Proceedings of the tenth ACM international symposium on Mobile ad hoc networking and computing*. ACM. 2009, 33–42.
- [105] V. Tarokh, H. Jafarkhani, and A. R. Calderbank. "Space-time block coding for wireless communications: performance results." In: *IEEE Journal on Selected Areas in Communications* 17.3 (Mar. 1999), 451–460.
- [106] HAN Te Sun and Kingo Kobayashi. "A new achievable rate region for the interference channel." In: *IEEE transactions on information theory* 27.1 (1981), 49–60.
- [107] *Technical Specification Group Radio Access Network; Evolved Universal Terrestrial Radio Access (E-UTRA); User Equipment (UE) radio access capabilities*. Release 14. 3GPP TS 36.306 V14.6.0. Mar. 2018.
- [108] I Emre Telatar et al. "Capacity of multi-antenna Gaussian channels." In: *European transactions on telecommunications* 10.6 (1999), 585–595.
- [109] John Paul M Torregozza, Rentsen Enkhbat, and Won-Joo Hwang. "Joint power control, base station assignment, and channel assignment in cognitive femtocell networks." In: *EURASIP Journal on wireless communications and networking* (2010), 6.
- [110] Kien T Truong, Philippe Sartori, and Robert W Heath. "Cooperative algorithms for MIMO amplify-and-forward relay networks." In: *IEEE Transactions on Signal Processing* 61.5 (2013), 1272–1287.
- [111] David Tse and Pramod Viswanath. *Fundamentals of wireless communication*. Cambridge university press, 2005.

- [112] P Ubaidulla and Ananthanarayanan Chockalingam. "Relay precoder optimization in MIMO-relay networks with imperfect CSI." In: *IEEE Transactions on Signal Processing* 59.11 (2011), 5473–5484.
- [113] P Ubaidulla and Ananthanarayanan Chockalingam. "Robust distributed beamforming for wireless relay networks." In: *IEEE 20th International Symposium on Personal, Indoor and Mobile Radio Communications*. 2009, 2345–2349.
- [114] Sriram Vishwanath, Nihar Jindal, and Andrea Goldsmith. "Duality, achievable rates, and sum-rate capacity of Gaussian MIMO broadcast channels." In: *IEEE Transactions on Information Theory* 49.10 (2003), 2658–2668.
- [115] Su Wei et al. "Small Cell Deployment and Smart Cooperation Scheme in Dual-Layer Wireless Networks." In: *International Journal of Distributed Sensor Networks* (2014).
- [116] Uditha L Wijewardhana, Marian Codreanu, and Matti Latva-aho. "Robust beamformer design for underlay cognitive radio network using worst case optimization." In: *IEEE 11th International Symposium on Modeling & Optimization in Mobile, Ad Hoc & Wireless Networks (WiOpt)*. 2013, 404–411.
- [117] Cenk M Yetis et al. "Feasibility conditions for interference alignment." In: *IEEE Global Telecommunications Conference, GLOBECOM 2009*. 2009, 1–6.
- [118] Wei Yu. "Uplink-downlink duality via minimax duality." In: *IEEE Transactions on Information Theory* 52.2 (2006), 361–374.
- [119] Tevfik Yücek and Hüseyin Arslan. "A survey of spectrum sensing algorithms for cognitive radio applications." In: *IEEE Communications Surveys & Tutorials* 11.1 (2009), 116–130.
- [120] Haijun Zhang et al. "Coexistence of Wi-Fi and heterogeneous small cell networks sharing unlicensed spectrum." In: *IEEE Communications Magazine* 53.3 (2015), 158–164.
- [121] Qing Zhao and Brian M Sadler. "A survey of dynamic spectrum access." In: *IEEE Signal Processing Magazine* 24.3 (2007), 79–89.

INDEX

- Complementary Cumulative
 - Distribution Function (CCDF),
12
- Cognitive Radio (CR), 59
 - Primary User (PU), 59
 - Secondary User (SU), 59
 - Underlay CR, 59–61
- Channel State Information (CSI), 31
- Faster-than Nyquist (FTN) signaling,
6
 - Spectral Efficiency (SE), 17–24
 - BER, 14–17
 - FTN factor, 6
 - FTN mapper, 6
 - FTN rate, 6
 - PAPR, 10–13
 - Bit rate, 7
 - Mazo limit, 5
- Interference Alignment (IA), 41–44
 - AS-MMSE IA approach, 52–54
 - DoF, 45–46
 - IA via reciprocity, 47–50
 - KKT conditions, 51
 - MMSE-based IA approach, 50–52
 - Closed-form Solution, 46–47
 - Dual network, 48
- Multiple-Input and
 - Multiple-Output (MIMO), 27
 - Space-time Block Coding (STBC),
29
 - Alamouti scheme, 29, 30
 - Array gain, 28
 - Channel capacity, 28
 - Spatial diversity, 29
 - Spatial multiplexing gain, 28
- Singular Value Decomposition (SVD),
33
- Water-Filling (WF), 60, 66–68
 - MU-MIMO, 34–37
 - OFDM, 38–39
 - OQAM/OFDM, 19–22
 - Modified WF, 60, 68–69
- Multi-user MIMO AF relay, 83–86
- Null-steering approach, 69
- Nyquist pulse, 8
 - EGF, 8, 9, 13
 - rRC, 8
 - Excess bandwidth, 8
 - Excess bandwidth factor, 8, 13, 17
 - Hermite, 8, 9, 13
 - Nyquist bandwidth, 8
 - PHYDYAS, 8, 9, 13
- Nyquist signaling, 5, 7
 - Orthogonal transmission scheme,
7
- Reciprocity, 32
- Relay, 78–79
 - Amplify-and-Forward (AF), 79
 - Decode-and-Forward (DF), 79
 - Half-duplex relay, 79
 - Non-robust IA approach, 89–90
 - Robust IA approach, 93–95

SCIENTIFIC CAREER

Name	Chung Le Thi
Date of birth	10.10.1984
Education	
Oct. 2005 – Feb. 2009	Master of Science in electrical engineering and information technology at Leibniz Universität Hannover
Oct. 2002 – Jun. 2005	Bachelor of Science in electrical engineering and telecommunications technology at Hanoi University of Science and Technology, Vietnam
Working Experience	
Mai 2011 – present	Research assistant and PhD student: Institute of Communications Technology at Leibniz Universität Hannover Research in the field of digital signal processing, multiuser MIMO system, cognitive radio and relay technology, interference mitigation/cancellation/alignment technique
Mai. 2007 – Apr. 2011	Graduate assistant: Institute of Communications Technology at Leibniz Universität Hannover Research in the field of signal processing, filter design, audio signal processing/blind source separation, channel modeling
Jun. 2008 – Aug. 2008	Working student: IMST GmbH Channel modeling, MATLAB Programming, MATLAB (GUI) programming, Visual C++.Net programming, simulation (Wave Transmission)
Feb. 2008 – Mai. 2008	Intern: IMST GmbH

Antenna modeling (Ray Tracing), channel modeling, MATLAB programming, MATLAB (GUI) programming, Visual C++.Net programming

Teaching Experience

Oct. 2015 – Apr. 2016

Exercises on "Signals and systems"

Oct. 2012 – Apr. 2016

Exercises on "Digital Communications"

Oct. 2011 – present

Lab exercises on "Physical layer transmission techniques"

Supervision of 4 student thesis (Master, Bachelor)

Publications

2 journals, 9 conference publications

PUBLICATIONS

JOURNAL ARTICLES

- [J1] C. Le, S. Moghaddamnia, and J. K. Peissig. "A Hybrid Optimization Approach for Interference Alignment in Multi-User MIMO Relay Networks Under Different CSI." In: *IEEE Transactions on Wireless Communications* 16.12 (Dec. 2017), 7834–7847.
- [J2] Sanam Moghaddamnia et al. "On the efficiency of PAPR reduction schemes deployed for DRM systems." In: *EURASIP Journal on Wireless Communications and Networking* 2016.1 (Oct. 2016), 255.

CONFERENCE PAPERS

- [C1] C. Le, S. Moghaddamnia, and J. Peissig. "On the Performance of Alamouti Scheme in 2×2 MIMO-FBMC Systems." In: *19th International Conference on OFDM and Frequency Domain Techniques (ICOF 2016)*. Aug. 2016, 1–6.
- [C2] C. Le et al. "Faster than Nyquist-An enabler for achieving maximum spectral efficiency in coexistence scenarios?" In: *2015 23rd European Signal Processing Conference (EUSIPCO)*. 2142-2146. 2015.
- [C3] C. Le et al. "On the practical benefits of faster-than-Nyquist signaling." In: *2014 International Conference on Advanced Technologies for Communications (ATC)*. 208-213. Oct. 2014.
- [C4] C. Le, S. Moghaddamnia, and J. Peissig. "An adaptive transmission scheme for multiuser MIMO broadcast channel in Cognitive Radio." In: *IEEE 10th International Conference on Wireless and Mobile Computing, Networking and Communications (WiMob)*. Oct. 2014, 506–512.
- [C5] C. Le et al. "Effect of spatial correlation on MMSE-based interference alignment in a multiuser MIMO MB-OFDM system." In: *IEEE 8th International Conference on Wireless and Mobile Computing, Networking and Communications (WiMob)*. Oct. 2012, 739–744.
- [C6] A. Anggraini et al. "MIMO multi-user relay system." In: *2012 International Symposium on Signals, Systems, and Electronics (ISSSE)*. 1-4. Oct. 2012.
- [C7] Chung Le et al. "Performance investigation of MMSE-based interference alignment for multiuser MIMO UWB." In: *2011 IEEE International Conference on Ultra-Wideband (ICUWB)*. Sept. 2011, 170–174.
- [C8] C. T. Le et al. "Performance evaluation of blind source separation algorithms base on source signal statistics in convolutive mixtures." In: *International Conference on Communications and Electronics (ICCE)*. Aug. 2010, 268–272.

- [C9] A. Ayadi - Miessen et al. "Investigation of Doppler effect in UWB-based rotor-telemetry system." In: *The 2010 International Conference on Advanced Technologies for Communications*. 99-103. Oct. 2010.